Dissertation

submitted to the

Combined Faculties for the Natural Sciences and

for Mathematics

of the Ruperto Carola University of Heidelberg,

Germany

for the degree of

Doctor of Natural Sciences

Presented by

M.Sc. Lisa Neuner

born in Heidelberg

oral examination: 16th December 2020

Fluorescence based recognition elements for glucose sensing using the glucose-galactose binding protein from Escherichia coli

Referees: Prof. Dr. Stefan Wölfl

Prof. Dr. Tobias Werner

In memory of

Mario

23rd september 2018

†

“Der Weg ist das Ziel.“

~ Konfuzius

Abstract

The biotechnology industry is growing rapidly and is embedded in a highly regulated and dynamic environment. Under the regulations and guidelines of the Food and Drug Association, short FDA, a pharmaceutical company must ensure the quality of biotechnological products. Within the last few years so called in-line technologies revolutionized the batch production procedure in the biopharmaceutical industry towards continuous manufacturing and real-time monitoring of critical vitality parameters in a bioreactor. As a key benefit, it is expected that with this technology, final product deviations can be reduced by up to 50%. Furthermore, studies have been shown that regulating vitality parameters such as glucose can improve overall product quality. Despite the increasing adoption and expected doubling of the market in the next years, there are challenges. Continuous manufacturing methods are not yet well characterized for therapeutic proteins due to a lack of (bio-)analytical in-line technology.

The overall objective of this work was to develop optical glucose biosensor recognition elements that can measure ‘in-line’ physiological glucose concentrations. For that purpose, the well-researched glucose-galactose binding protein in E. coli (GGBP) was genetically and chemically modified to enhance the spectral properties of the biosensing element. Several single-labelled as well as self-calibrated dual-labelled systems were developed. The candidate proteins were designed, synthesized, and labelled with commercially available fluorophores. The best result for the single-labelled glucose sensing system was achieved with the combination of GGBP variant H152C/A213R/L238S labelled with the newly developed commercially available dye Atto 465. A linear dependency between 1-75 mM glucose with a total fluorescence increase of +48% could be demonstrated.

Furthermore, this work presents for the first time, selective labeling of FRET-based biosensor recognition elements based on the recently discovered π-clamp strategy (Nature Chem., 2016). For this purpose, a chemical synthesis of perfluoro arylated fluorophore (XC113) has been developed. It could be shown that dual labeling of a FRET pair was highly accurate and selective. GGBP variant H152C/A213R/L238S_DGTN280-283FCPF labeled with XC113 and DY585 proved the idea of the concept and a successful labeling of the pi-clamp. A fluorescence transfer rate of 18% was obtained and a maximal fluorescence intensity change by 12% upon binding of glucose was observed. In a future experiment, this mutant can be further improved by using Atto 495 and DY585 as a FRET pair and an overly sensitive ratiometric glucose biosensor could be developed for bioreactor environments.

Zusammenfassung

Die Biotechnologie Industrie erfährt in den letzten Jahren ein starkes Wachstum und befindet sich in einem hoch regulierten Umfeld welches durch die FDA, die amerikanische Arzneimittelzulassungsbehörde, kontrolliert wird, um die Qualität von Arzneimitteln zu gewährleisten. In den letzten Jahren haben integrierte analytische Verfahren die Batch Produktion revolutioniert und den Weg zu kontinuierlichen Produktionsverfahren mit Echtzeitanalytik geebnet. Dabei stellt sich die Reduktion der Produktabweichungen um potenziell fast 50% als einer die größten Vorteile heraus. Des Weiteren konnte durch Studien gezeigt werden, dass das Regulieren wichtiger Vitalstoffe während des Prozesses wie z.B. der Glukose die gesamte Produktqualität positiv beeinflussen kann. Obwohl das kontinuierliche Verfahren viel Zuspruch findet und sich stark entwickeln wird gibt es dennoch Rückschläge. Für viele therapeutische Proteine ist das kontinuierliche Verfahren noch nicht ausgereift genug, denn es fehlt an integrierbaren (bio-)analytischen Sensorikmethoden.

Das Ziel dieser Arbeit war es integrierbare optische Biosensorerkennungselemente zu entwickeln, die es erlauben Glukosekonzentrationen in physiologischen Konzentrationen zu messen. Hierfür wurde das Glucose-Galactose Bindeprotein in E. coli. (GGBP) genetisch verändert und sowohl mit einzelnen umgebungssensitiven Fluoreszenzfarbstoffen als auch mit jeweils einem FRET Paar (zwei selektiv markierte Fluoreszenzfarbstoffe) markiert. Das beste Ergebnis für einen umgebungssensitives Sensorelement wurde durch die GGBP Variante H152C/A213R/L238S und dem neu entwickelten Farbstoff Atto 465 erzielt. Ein linearer Zusammenhang (R^2=0.98) konnte für Glucosekonzentration von 1-75 mM mit einer Gesamtfluoreszenzerhöhung von +48% gezeigt werden.

Im zweiten Teil dieser Arbeit konnte zum ersten Mal gezeigt werden, dass sich Biosensorelemente mit FRET Paaren mithilfe der kürzlich entdeckten ‚Pi-Clamp Methode' (Nature Chem., 2016) sehr einfach hoch selektiv markieren lassen. Dafür wurde eine einfache Syntheseroute entwickelt, um kommerzielle Fluoreszenzfarbstoffe mit perfluorarylierten Linkermolekülen zu koppeln. Die, mit den Farbstoffen XC113 und DY585 markierte GGBP Variante H152C/A213R/L238S_DGTN280-283FCPF konnte eine Glucosesensitivität bis 100 mM mit einer FRET Übertragungsrate von 18% bei einer absoluten Fluoreszenzänderung von +12% beweisen. Aufgrund dieser Ergebnisse könnte gezeigt werden, dass mithilfe von diesem FRET System in einem weiteren Experiment mit dem umgebungssensitiven Farbstoff Atto 495 und dem Fluorophor DY 585 ein noch sensitiveres ratiometrisches Biosensorelement entwickelt werden könnte.

Table of content

Abstract I

Zusammenfassung II

1 Introduction 1

1.1 Modernizing the biotechnological industry – towards continuous manufacturing and real-time quality control of pharmaceuticals 1

1.2 Real-time monitoring of glucose in bioreactors 3

1.3 Definition of a biosensor 3

1.4 Biosensor Classifications and Past Glucose Systems & Developments 4

1.4.1 Enzymes in glucose biosensors 6

1.4.2 Boronic acids 9

1.4.3 Glucose Binding Proteins 10

1.4.4 Glucose-Galactose binding protein in E. coli 12

1.5 Half a Century of intense glucose monitoring research – A critical comparison of current continuous glucose monitoring developments and learnings 16

1.6 Fluorescence spectroscopy 17

1.6.1 Underlying Basics of Fluorescence Spectroscopy 17

1.6.2 Fluorescence Detection Principles 19

1.6.3 Environmental factors that can influence fluorescence spectroscopy 20

1.7 Environmental-Sensitive Sensing 20

1.7.1 Site-selective labeling of proteins with environmental-sensitive dyes 21

1.8 Förster-Resonance-Energy-Transfer used as a strategy in biosensors 23

1.8.1 Site-selective labeling of proteins: introduction of a recently discovered peptide tag 'π-Clamp' 25

1.8.2 Choice of FRET pairs 27

2 Objectives 29

3 Results & Discussion Part 1 30

3.1 Terminology of gene and protein variants 30

3.2 Design and cloning of GGBP analogues 31

3.3 Expression of GGBP-variants 32

3.4 Purification of GGBP_wt and GGBP_mut_H152C/A213R/L238S 33

3.5 Environmentally sensitive glucose sensors based on the Glucose-Galactose Binding Protein 35
3.5.1 Cysteine labeling of GGBP_mut_H152C/A213R/L238S 36
3.5.2 Labeling efficiency 37
3.6 BADAN used for optimization of glucose sensing & validation system 37
3.7 Dyomics Dyes have optimized environmental sensitive fluorescence properties when bound to proteins 41
3.7.1 Spectral Characteristics of DYV11 and GGBP-DYV11 42
3.7.2 Spectral Characteristics of DY 610 and GGBP-DY610 45
3.7.3 Spectral Characteristics of DY490 and GGBP-DY490 48
3.8 Atto Dyes are highly effective environmental sensitive dyes in aqueous solutions 51
3.8.1 Spectral characteristics of Atto 425 and GGBP-Atto 425 52
3.8.2 Spectral characteristics of Atto 465 and GGBP-Atto 465 54
3.8.3 Spectral characteristics of Atto 495 and GGBP-Atto 495 57
3.9 Discussion environmentally sensitive fluorescent labels for GGBP 61

4 Results & Discussion Part 2 63

4.1 Using the Pi-Clamp strategy for FRET-based glucose biosensors based on GGBP 63
4.2 Sequence Alignments 64
4.3 Identification of suitable FRET positions in GGBP using Swiss Model 65
4.4 Cloning, Expression and Purification of GGBP variant with the encoded pi-clamp 73
4.5 Synthesis of 5/6-Carboxyfluoresceine in conjugation with a perfluoro-biphenyl linker as pi-clamp reactive FRET donor molecule 77
4.6 ^{1}H-NMR chemical analysis of XC113 and its synthesis precursors 79
4.7 Spectral characterization of XC113 and suitable FRET pair combinations 81
4.8 Labelling of GGBP pi-clamp variants XC113 and DY585 82
4.9 Glucose Sensitivity of FRET labelled GGBP 83
4.10 Discussion 84

5 Conclusion & Outlook 87

6 Experimental Part 88

6.1 Material 88
6.1.1 Technical Equipment and Software 88
6.1.2 Chemicals 89
6.1.3 Bacteria strains, plasmids, restriction enzymes 90

Sequence Alignments 91

6.2 Methods and Protocols *93*

6.2.1 Cloning 93

6.2.2 Expression 95

6.2.3 Expression Profiling by SDS-PAGE 95

6.2.4 Protein Purification 97

6.2.5 Labeling of Solvatochromic Thiol-Reactive Fluorophores 100

6.2.6 Labeling Purification 100

6.2.7 Protein Determination with Bradford Reagent 101

6.2.8 Labeling Efficiency (DOL) 101

6.2.9 **F**örster-**R**esonance-**E**nergy-**T**ransfer Determination 102

6.2.10 Synthesis 102

List of Abbreviations **IV**

List of Tables **V**

List of Figures **VI**

List of Publications **XI**

Acknowledgement **XVIII**

1 Introduction

1.1 Modernizing the biotechnological industry – towards continuous manufacturing and real-time quality control of pharmaceuticals

The biotechnological production of biopharmaceuticals has nowadays become immensely popular in the pharmaceutical industry. The german association for pharmaceutical research companies (vfa) stated that currently 194 recombinant produced drugs are registered in Germany (April 2018) and almost 30% of recombinant drugs enter the market every year.(1) Biotechnological products like regulatory proteins, enzymes or monoclonal antibodies (mABs) act as the active pharmaceutical ingredient in drugs for diverse indications such as cancer, diabetes, inflammatory diseases or as vaccinations against viruses.(2)

Since drug products can always be a risk for patients the quality of the manufactured drug products is highly regulated by the Food and Drug Association's (FDA) regulations and guidelines. To ensure a high product quality and minimize risks for patients, the FDA advices pharmaceutical companies to continuously improve pharmaceutical development, manufacturing and quality assurance through innovative process development, process analysis and process control.(3, 4) Therefore, the FDA's initiative published guidelines for 'Quality by Design' (QbD) and Process Analytical Technology (PAT) which are provided as internationally harmonized guidelines for Quality Systems and Risk Management (Q8, 9, 10). The goal of QbD and PAT is to enhance the understanding, consistency and control of the manufacturing process, as "Quality cannot be tested into products; it should be built-in or should be by design" (5). Continuous manufacturing has the potential to increase quality of the products, to improve product yield and to save time and money for the biopharmaceutical industry. Moreover, with the help of on-line, at-line or in-line measurements, a good understanding of a process and the respective parameters can be achieved and countermeasures can be taken early to keep the production line within the acceptable quality thresholds.

Even though continuous manufacturing provides lots of opportunities for biopharmaceutical companies, a few challenges keep the industry cautious in adopting continuous methods. One critical aspect is predominant. Continuous manufacturing methods are not yet well characterized for therapeutic proteins due to a lack of analytical methods. The biopharmaceutical industry is used to produce in batches which is a well characterized and widely accepted method. Manufacturing of pharmaceutical products in batches, however, can be a time-intensive and disconnected process which lacks the flexibility to

changes in supply and demand that this industry is facing.(6) The conventional at-line (off-line) approach in biopharmaceutical manufacturing uses analytical technology that is taken manually or automatically through a sampler within the bioreactor. When analyzing substrates in cultivation media in an off-line approach, it is necessary to collect a sample at sterile conditions to ensure neither contaminating the bioreactor nor the sample. Off-line analytics is the most time-consuming process as the samples must be taken manually and will be analyzed between a few of minutes or up to a few hours (**see Figure 1**). A real-time monitoring of the reactor is not possible with this approach; action can be taken only after obtaining analysis results, but the actual value of the parameter might have changed significantly during analysis time. Immediate intervention into the process is often delayed by several hours which can result in a non-acceptable quality of the product and the discard and restart of a whole process.

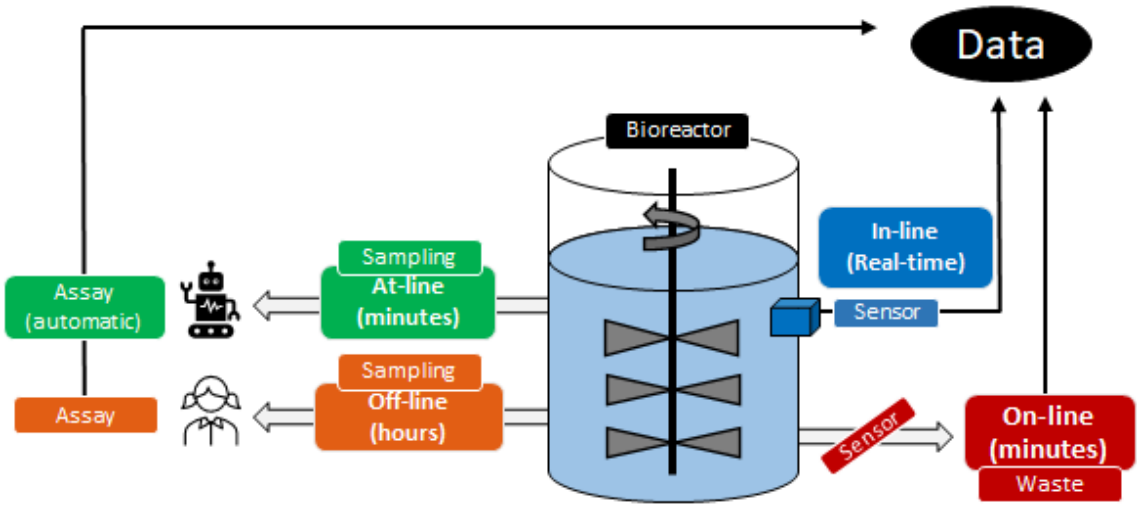

Figure 1: Process analytical technologies.
Off-line, at-line, on-line and in-line monitoring of bioprocesses.(7)

To minimize the risk of contamination of a whole batch, on-line systems are more likely used that are directly connected to the process and can automatically take samples and analyze them. A prominent example is the TRACE C2 control device that can either collect a sample through filters or through dialysis depending on the volume of the bioreactor and therefore cleaning already the sample from cells and residues. The samples of an on-line measurement are usually discarded and not returned to the process. Monitoring a bioreactor in real time is considered as being the most efficient approach in continuous manufacturing using an in-line technology. In-line process analytical technology systems are incorporated into the bioreactor and produce continuous data. Both procedures, on-line & in-line monitoring enable a fast and sterile analysis of the sample from the bioreactor. There are several potential sensing approaches whereas optical sensing might be the easiest in terms of non-invasive signal

readout which can be directly integrated into steered tanks or disposable plastic bags. However, analytical technologies for on-line or in-line systems must meet certain requirements. They need to be sensitive, sterilizable and have an operation time of at least two weeks up to 60 days. Therefore, innovative approaches are highly needed to face these challenges and advance this important field. Regarding the billions of dollars that the pharmaceutical industry loses every year due to rejected batches forces the manufacturers to constantly improve their processes.

1.2 Real-time monitoring of glucose in bioreactors

The most widely used expression organism to produce recombinant proteins is the from chinese hamster ovary (CHO) mammalian cell line. Mammalian cell lines have similar post-translational modifications compared to humans which are important for their function in the human body and can therefore be used in the production of recombinant proteins for therapeutic use. Several studies indicate that nutrient regulation plays a crucial role in cell growth, product yield and the glycosylation pattern of mammalian cell culture products with can result in a direct impact on their biological activity (8-11) Consequently, biological drugs produced by cell lines can become ineffective, even harmful. A few sensors already exist for the most important chemical and physical parameters such as the partial pressure of gaseous molecules (oxygen, carbon dioxide, and nitrogen), pH and temperature. Another important parameter in a fermentation process is glucose, the main carbon source for mammalian cells.

1.3 Definition of a biosensor

A biosensor is a functional biological system integrated into a device that is capable of measuring chemical or biological molecules, also called analytes, in a qualitatively as well as quantitatively manner. In general, a device that can specifically detect an analyte is called a biosensor, but also the biomolecule itself that acts as a recognition element of an analyte can be called a biosensor. In this work, both terms are used equally as the objective of this work was to find a new designed recognition element for an analyte that could be later used in a biosensor device.

The goal of using biosensors is to measure certain molecules in specific environments and matrices in a point-of care application or outside where no laboratory. As an example, in the medical diagnostics field biosensors are of special interest for the detection of various biomarkers, such as proteins, peptides and small molecules or nucleic acids such as DNA or miRNAs that occur in the blood streams and that can give information about the current status of physiological processes in the body of a patient.

Moreover, disease-specific biomarkers enable physicians to diagnose diseases earlier and to monitor the disease in a controlled manner to minimize the risk of complications. Biosensors are manifold and are distinguished by the biochemical receptor they use, which analytes they measure and how this analyte-receptor interaction works. The various kinds of biosensors are listed in table 1.

Table 1: Analyte-receptor interactions of a biosensor.

biochemical receptor	**analytes**	**mechanism**
enzymes	metabolites	substrate conversion
apo-enzymes	metabolites	binding affinity
antibodies	proteins	irreversible binding
nucleic acids	ssDNA, RNA	irreversible binding
peptides & proteins	proteins	protein-protein interaction
chemicals	small molecules	binding affinity
cells	various	various

bioreceptor can selectively recognize the analyte in a solution by a reversible or irreversible binding event (e.g. binding to a protein), by conversion to a substrate (e.g. substrate conversion of an enzyme). A biosensor device consists of a bioreceptor, a transducer and an amplifier (see Figure 2).

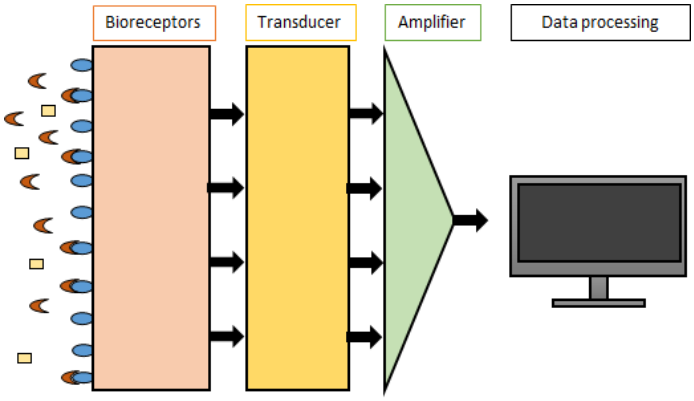

Figure 2: Schematic draw of a biosensor.
A biosensor consists of a bioreceptor, a transducer and an amplifier that enhances the signal

1.4 Biosensor Classifications and Past Glucose Systems & Developments

In the last half decade, more than 200 concepts of a glucose sensor have been published and were presented in a review from Steiner et al. as of May 2011 in which optical sensors are considered only. These efforts clearly reflect the need for a continuous system for applications mainly in diabetes. For most researchers and companies, the

'holy grail' lies within the diabetes market and is displayed by an implantable, continuous and stable glucose sensor that can be coupled to an artificial pancreas in order to enable automatic dosing of insulin.(12, 13) However, only the minority of studies had the ultimate goal to develop a glucose monitoring system for biotechnological applications.

Continuous glucose biosensors can be mainly divided into two main classes, electrochemical and optical sensors which is referred to their readout. The bioreceptor component can be either label-free which comprise electrochemical approaches such as amperometric, potentiometric and conductometric sensors but also optical approaches such as colorimetric, surface plasmon resonance (SPR) or intrinsic fluorescence of the bioreceptor component.

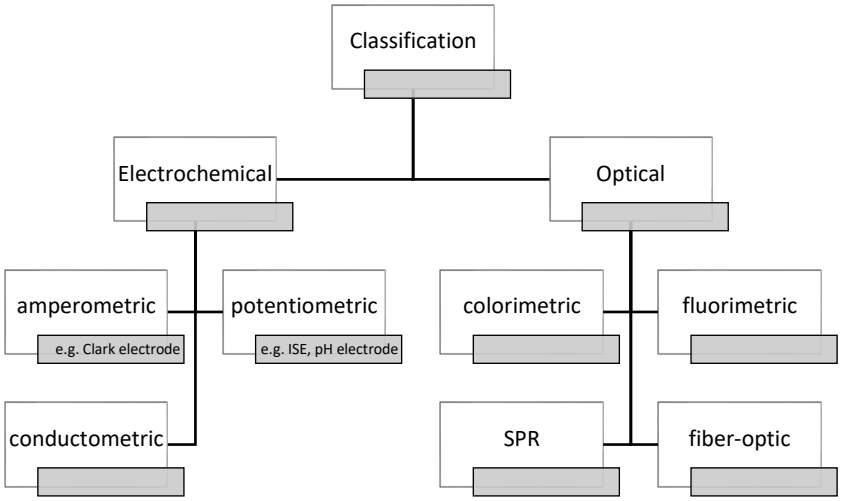

Figure 3: Biosensor classifications.
Biosensors can be classified by electrochemical and optical readout, each of which can be subclassified even further. The most prominent sensor systems are from the electrochemical type such as the Clark-, Ion-selective- or pH electrode. The optical biosensors comprise colorimetric, fluorometric, fiber-optic as well as surface plasmon resonance (SPR) measurements as detection methods. Optical sensors have obvious advantages in continuous sensing and are therefore currently under extensive research.

Former glucose sensor developments differ mainly in the bioreceptor component, the readout and the immobilization strategy. In this work the four main glucose bioreceptors, namely enzymes, apo-enzymes, boronic acids and glucose-binding proteins will be discussed as they turned out to be the most promising recognition elements for glucose. Electrochemical sensors caught attention very early in the development of continuous glucose biosensors when Clark and Lyons invented the very first glucose biosensor back in 1962 based on the Clark oxygen electrode.(14) This platin electrode was comprised of a reference and a sensing electrode. The latter was covered with a layer of glucose oxidase and an oxygen-permeable membrane. When glucose is present in a solution, oxygen will be consumed by the enzyme and less oxygen can be reduced which results

in a reduction of the current that is inversely proportional to the glucose concentration in solution. The reaction of glucose oxidase is represented in figure 5.

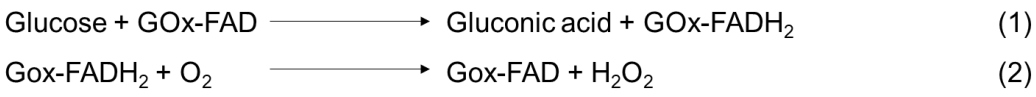

Figure 4: Chemical reaction of the enzyme glucose oxidase.

Electrochemical sensors are still the state-of the art technology in the few continuous and discontinuous sensors that are on the market.(15-18) However, the electrochemical approach has certain disadvantages for monitoring in a bioreactor and especially in a cell culture environment which will be discussed in chapter 1.7.1. Since the focus of this work lies on optical sensors, electrochemical sensor will not be further discussed in detail. The different sensor technologies will be discussed regarding their recognition elements for glucose which comprise enzymes, boronic acids and glucose binding proteins (GBP) such as apo-enzymes and glucose transporter proteins (Concanavalin A and glucose-galactose binding proteins (GGBP)). Since several hundreds of sensor concepts have been studied, only some examples will be presented for the different readout possibilities that were used for the above-mentioned recognition elements.

1.4.1 Enzymes in glucose biosensors

Enzymes have naturally specific functions in organisms in almost all metabolic processes. In general, they are reaction catalysts that accelerate the conversion of substrates to certain products. Enzymes are used in biosensors because of their high specificity towards their natural substrates. Naturally, only a certain substrate can bind to its respective enzyme in an induced fit mechanism. This allows for highly specific applications in biosensor developments. An enzyme can be identified by its name and the common ending -ace. They can be divided into several classes according to their specific functions like oxidoreductases, transferases, ligases, hydrolases, lyases and isomerases. An oxidoreductase catalyses the oxidation or reduction of a substrate; transferases transfer phosphate groups to substrates and vice versa; ligases, hydrolases and lyases are able to form, hydrolyse or cleave a covalent bond between two substrates, respectively, and isomerases catalyse the conversion of isomers. With the help of enzymes, a cell can fully control metabolic reactions. Enzymes have typically a binding site for the substrate and occasionally another allosteric binding site for their cofactors which induces a conformational change and hence the catalytic conversion of

the substrate. In general, mostly the three glucose converting enzymes glucose oxidase, glucose dehydrogenase and hexokinase are used in biosensor developments with different readout configurations. Glucose oxidase naturally occurs in the fungi aspergillus niger which catalyses the oxidation of glucose with oxygen to gluconolactone. Consequently, the free electrons will be transferred to the cofactor flavine-adenine-nucleotide (FAD) which will be reduced to $FADH_2$. In a second reaction, hydrogen peroxide will be released from $FADH_2$ (see figure 4). Glucose dehydrogenase can cleave a hydrogen from glucose in a similar redox reaction using another coenzyme called nicotinamide adenine dinucleotide phosphate (NADP+) and consequently form the oxidized product gluconolactone. The enzyme hexokinase (HK) plays a crucial role in the early carbohydrate metabolism of mammalians which is called glycolysis. This enzyme transfers a phosphate group to glucose and forms the reaction product glucose-6-phosphate. The conversion of the oxidized form NADP+ to the reduced form can be spectroscopically analysed due to a colour change of the cofactor. The different reactions mentioned can be detected in multiple ways (see figure 5).

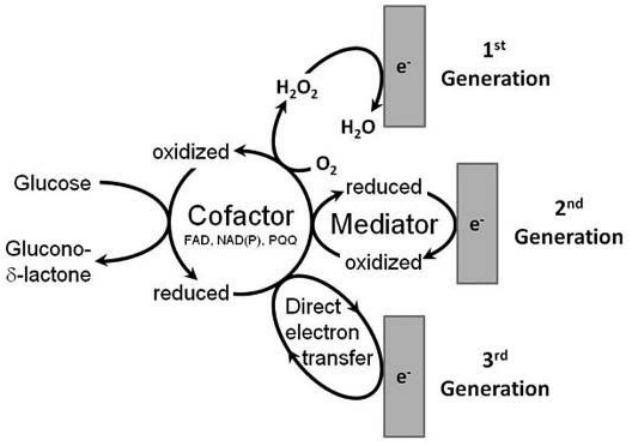

Figure 5: Schematic representation of different glucose sensor generations based on the enzymes such as glucose oxidase or glucose dehydrogenase.
The schematic was copied from the review of Ferri et al.(19)

Glucose sensor developments based on intrinsic fluorescence of enzymes

Glucose oxidase is by far the most intensively studied recognition element for glucose and is predominantly used in commercial sensors for glucose to date.(17, 20, 21)
Initially, the intrinsic fluorescence of the tryptophan residues of glucose enzymes was used for glucose sensor developments. Sierra et al. developed a glucose sensor that was able to detect concentrations in a linear range of 0.5-20 mM in the UV range (em. 335 nm). Glucose oxidase was entrapped into a sol-gel matrix for immobilisation (22). Due to interference of other proteins in the UV, the intrinsic green fluorescence (em. 500

nm) of the coenzyme FAD was rather preferred and therefor glucose oxidase and the respective cofactor were entrapped in a semipermeable membrane. The dynamic range of glucose, however, was rather low of 1.5-2 mM.(23) Other sensor schemes used the intrinsic decrease of the fluorescence of hexokinase upon binding of glucose. A broad dynamic linear range of 1-120 mM for glucose could be obtained.(24) An optical-fiber glucose sensor based on glucose dehydrogenase used the intrinsic fluorescence of its cofactor NADH (em. 460 nm) that increased upon addition of glucose. A fast reaction time of 5 min was obtained.(25) A thermostable glucokinase was used in a competitive biosensor assay where the intrinsic tryptophan fluorescence was decreased upon binding of a labelled sugar(26). The fluorescence was quenched in a resonance energy transfer (FRET) from the acceptor-labelled sugar when glucose concentration was low. This mechanism is reversible when glucose is increasing again. The underlying principle of FRET will be discussed in detail in chapter 1.8.6. Another sensor scheme that made use of the intrinsic fluorescence was a development from Singh et al.(27) GOx was entrapped in a gel matrix on top of an optical fiber that was initially coated with film layers of silver nanoparticles and silicon. Surface plasmon resonance was obtained after excitation and GOx showed a blue shift in the resonance wavelength with increasing concentrations of glucose. The sensor can measure low physiological concentrations of glucose (0-260 mg/dl) and shows best results at a neutral pH. However, the sensitivity of the recognition element is decreasing when higher concentrations of glucose are present.

Glucose sensor developments based on oxygen consumption / hydrogen formation of GOx

A different approach detecting glucose by glucose oxidase is the fluorescent quenching of oxygen-sensitive probes upon oxygen consumption of the sensor which is directly proportional to the concentration of glucose in solution (see figure 4). Endo et al.(28) immobilized an oxygen-sensitive ruthenium-complex and GOx in a sol-gel matrix and covered it with a dialysis membrane on the top of an optical fiber. The fiber was placed in a needle-type hollow container for measuring glucose levels in fish caudal veins. The sensor was able to measure physiological glucose concentrations (50-150mg/dl). A GOx-fiber optic oxygen sensor was developed by Klimant et al.(29). Oxygen consumption and respective quenching was measured by the phase-shift of the lifetime of the fluorescent chromophore. A dual senor was used to obtain a reference oxygen signal that enables internal calibration. The sensor was implanted afterwards.(30) A very similar sensor system was further optimized from our group.(8)

Besides oxygen consumption, also other products of the oxidation of glucose can be used for the development of a glucose biosensor. An intensity & lifetime-based sensor incorporated into a hydrogel was developed by Wolfbeis group (31, 32). The probe europium tetracycline forms a strong fluorescent complex with hydrogen peroxide that can be exited at around 400 nm. This method was unfortunately not sensitive though reversible. In a different approach, glucose was determined by GOx and a pH-sensitive dye 8-Hydroxypyrene-1,3,6-trisulfonic acid (HPTS*)* immobilized in a hydrogel at the tip of an optical fiber.(33) An analytical range of 0.1-2 mM and a response time of 10 min was obtained. A similar approach with immobilized fluorescein isothiocyanate (FITC) as pH-sensitive dye was patented.(34)

Glucose sensor developments based on labeled GOx

Furthermore, glucose oxidase was labeled with fluorescent dyes to shift the optical emission towards higher wavelengths and hence to diminish interference with other proteins and molecules that typically have high absorbance in the ultra-violet (UV) spectrum. GOx was for example labeled with a coumarin-derivative that shows a fluorescent emission at 450 nm, thus in the visible spectrum. Upon binding of glucose, the respective fluorescence increases linearly between 0.5 and 6 mM.(35) In order to further shift the fluorescence emission towards higher wavelengths (em. 515 nm), GOx was labeled with a fluorescein-derivative and immobilized in sol-gel. A similar analytical range was obtained. To enhance the analytical range, fluorescein was coupled to GOx and immobilized in a polyacrylamide matrix. Thus, glucose concentrations could be obtained in a linear range from 2-11 mM.(36) A quantum dot (Qdot) labeled approach was used in a different sensing approach for measuring glucose. CdSe/ZnS core-shell quantum dots were conjugated with the enzymes GOx and horseradish peroxidase (HRP). The non-radiative energy transfer from the QDs to the enzymes resulted in fluorescence quenching of the QDs, corresponding to the increase in glucose concentration.(37)

1.4.2 Boronic acids

Boronic acids are lewis acids and bind 1,2- or 1,3-diols reversibly but covalently in aqueous solution to form cyclic boronate esters.(12) The fluorescence changes that occur due to this formation are leveraged for biosensor developments. Initial studies to investigate this mechanism were done already in the 1960s and later.(38) Boronic acid itself shows a higher selectivity for fructose over glucose which led researchers to improvements of the binding properties and adaptions of the recognition element.(39) In

addition, boronic acids do not have the best fluorescent properties such as a low fluorescence intensity. Therefore, boronic acids were attached to fluorophores that displayed a high fluorescence intensity, emission and lifetime which change by geometric changes of the boronic acid molecules attached to the fluorophore.(40) Biosensor developments based on anthracene boronic acid have been reported. The selectivity for glucose was enhanced by attaching a diboronic acid to anthracene (Shinkai *et al.)*. Although a variety of research has been done and is still done in the field of boronic acids, a systematic research approach is missing and only little progress has been made.(40) New materials such as a quantum dots and gold nanoparticles attract the researchers attention recently and boronic acids are still a hot topic in today's research of glucose biosensor.

1.4.3 Glucose Binding Proteins

Besides biological and chemical receptors for glucose such as enzymes or boranic acids, there exists a large group of biomolecules, namely glucose binding proteins (GBPs) that can also be used as recognition elements in a glucose biosensor. The beauty of binding proteins is a reagentless sensing since no further cofactors or substrates are needed. Hence, potential toxic compounds will not be formed that could influence the sensor stability. Depending on the specific binding protein, glucose itself will bind reversibly and will not be consumed. These characteristics enable measurements in extremely low reaction volumes without influencing the actual concentration.

Glucose sensor developments based on Concanavalin A

The most prominent protein of this source is Concanavalin A (Con A), a plant lectin from the jack bean that can bind carbohydrates such as glucose in a reversible manner. The monomer of the protein consists of 237 amino acids which is stabilized by Calcium and Mangan. At neutral pH, Con A presents itself as a tetramer which can bind 4 molecules of glucose. Con A was one of the first proteins that were crystallized in the early 20th century. For this work, James Batcheller Sumner was awarded with the Nobel prize in 1946. The crystal structure itself was finally determined a couple of years later. Most glucose sensor developments based on binding proteins either use fluorescence intensity, FRET or SPR as readout. A competitive assay scheme uses Sephadex beads that were covalently liked with glucose molecules which in turn were labeled with Safranin O and Pararosanilin to block the emission of Alexa-488 labeled Con A that binds to the glucose groups inside the beads.(41) Upon increased glucose concentration in the

analyte solution, Con A will diffuse out of the beads to bind to free glucose in order to maintain an equilibrium. Consequently, Alexa-488 that is bound to Con A will now be fully excited by light and emits a strong fluorescence at 522 nm. This signal is directly proportional to the respective free glucose that is present in the analyte solution. The beads are embedded in a hollow dialysis fiber in a fiber-optic setup which can detect glucose concentrations between 0.2 and 30 mM. A similar scheme was developed by the same group that used a near infrared dye Alexa-647 which emits a strong fluorescence at 670 nm.(42) The response time, however, was increased to 15-30 min, but the sensor system showed an overall high operational stability. Schultz et al.(43) developed earlier a competitive Con A-sensing scheme with FITC-labeled dextran immobilized in a hollow dialysis fiber. Only glucose can pass the sensor membrane which enables competitive binding inside the hollow fiber, and consequently free labeled dextran will emit a stronger fluorescence. Further improvements were made to enhance the response time to an average of 6 min(44) and to shift the analytical range towards physiological concentrations. The general sensor scheme was patented early in 1980.(45) The same group presented some years later a FRET based sensing scheme between TRITC-labeled Con A and FITC-labeled dextran immobilized on an optical hollow fiber.(46) TRITC acts as acceptor molecule and is excited at 480 nm. When in proximity, FITC will be excited and a strong fluorescence emission can be detected at 550 nm. When glucose is present in solution, TRITC-labeled Con A dissociates from FITC-dextran and binds to glucose. Consequently, FRET is decreased in a linear manner between 0 and 83 mM with a response time of 10 min. Another group incorporated the sensor scheme into a hydrogel.(47) A response time of 10 min and an analytical range of glucose between 0-44 mM were obtained. The aggregation of Con A was reported quite frequently, so improvements were needed that prolonged sensor lifetime. A FRET sensor was developed (48) that uses Cy5-labeled Con A as donor and insulin labeled with Malachite green and maltose as acceptor. The fluorescence intensity and lifetime of Cy5 were restored upon addition of glucose. The proteins showed improved aggregation and a better reversibility compared to the usage of dextran in former sensor developments. The same group(48) reported a very similar concept but labelling of Con A with a short wavelength excitation ruthenium-complex $Ru(bpy)_3$. The sensor had similar good properties with a longer lifetime. Several FRET sensor schemes using the explained combination of FITC and TRITC together with dextran as competitive molecule to glucose were patented.(49, 50) The latter was patented from Novartis and displays a FRET sensor incorporated into a contact lens.(50) Unfortunately, Con A tends to irreversibly aggregate quite rapidly over time and also toxicity on cells has been investigated which forced researchers considering new binding proteins for glucose with

less aggregation and no cell toxicity. Even newer approaches that were more recently established using surface plasmon resonance and silver nanoparticles(51) or gold nanoparticles(52, 53) for detection could not significantly improve the stability of the sensors in general.

Glucose sensor developments based on apo-enzymes

Another elegant strategy is using apo-enzymes. Apo-enzymes are enzymes that lack their respective co-factors and therefore lose their catalytic activity. In the most prominent example apo-GOx, glucose can reversibly bind to the enzyme. Consequently, a conformational change in the enzyme occurs which can be used for the detection of glucose, either through the intrinsic tryptophan fluorescence or through labeling of the enzyme with fluorescence labels near the binding site. The intrinsic fluorescence change of apo-GOx with increased glucose concentrations was measured. The intrinsic fluorescence decreased by 18 % upon binding of glucose which was not useful for medical purposes. Therefore, apo-Gox was non-covalently labeled with the dye 8-Anilino-1-naphthalenesulfonic acid (ANS)(54) which resulted in a 40 % decrease in the lifetime of ANS (em. 480 nm) and an analytical range of 10-20 mM which is comparable to the hole-GOx. A similar approach was patented from D'Auria and Lakowicz.(55) A competitive FRET sensor approach with apo-Gox was developed using FITC-labeled dextran and TRITC-labeled apo-Gox. FRET was decreased upon binding of glucose. A large linear range for glucose was observed between 0-90 mM(56) The labeled molecules were embedded into microcapsules (57) using a layer-by-layer principle. This work showed that using microcapsules for embedding a competitive assay is highly recommended as they provide free movement while the constant total sensing assay concentration can be maintained. The sensor principle showed a five times greater specificity for glucose over other sugars. The dynamic range suffered a bit but was still linear in the broad range between 0 and 30 mM. A very similar approach was developed by embedding Cy5-labeled apo-Gox and TRITC-labeled dextran multilayer films into microcapsules.(58) The affinity constant (k_D) was slightly increased, the specificity for glucose was retained. Other near-infrared dyes and respective quenchers were tested.(59)

1.4.4 Glucose-Galactose binding protein in E. coli

Since the focus of this work is based on the glucose galactose binding protein in e. coli, this section will be discussed in more detail. Besides Concanavalin A and apo-enzymes, another large family of binding proteins is represented by bacterial periplasmic binding

proteins. The natural functions of these soluble proteins are various; they mediate the active transport of small molecules (chemotaxis) or serve as intermediary receptors to facilitate ABC transporters. All periplasmic binding proteins share some common structural similarities. They consist of two globular domains that are connected by a hinge(60), a Venus flytrap-like architecture which is also seen in other intracellular bacterial proteins(61). One member of the periplasmic sugar-binding proteins that has been object of intense structural and functional studies is the Glucose-Galactose binding protein (GGBP) in Eserichia coli (E. coli). This protein has a size of 34 kDa and consists of 309 amino acids and a signal peptide of 23 amino acids which regulates chemotaxis within the cell. Naturally, GGBP mediates D-glucose and D-galactose transportation via the MglABC transporter(62-64). The structure of GGBP was structurally solved in 1983, a Calcium-binding site was discovered and the binding towards D-glucose and D-galactose were characterized within the following years.(65-68) A large conformational change was observed when glucose binds to GGBP and a similar systematic approach was observed for other binding proteins and their endogenous ligands.(69)

Borrok et al. were able to obtain an ultra-high-resolution structure of the glucose-bound form of GGBP which was refined against 0.92Å resolution data where nitrogen (N), oxygen (O) and carbon (C) atoms could be distinguished and even C-H and N-H hydrogen placement could be resolved.(70) This ultra-high-resolution quality of a protein structure can be only rarely obtained for non-enzymatic proteins which was a first sign that glucose highly stabilizes GGBP in the bound state.(71) These findings support the exo-anomeric effect which explains a ring-opened resonance form of glucose that contributes to a ß-conformation in the latter which is the preferred bound form in GGBP.(72) GGBP exists either in its open (unliganded) or closed (glucose-bound) conformation which is facilitated by the connecting hinge. The hinge region consists of three molecular strands that separate the N-terminal and the C-terminal binding domain.(70, 73) The amino acid residues 109-111, 253-256 and 293-296 that form the hinge have been identified by sequence alignments.(74) Upon ligand binding, this cleft closes and opens back up to an angle of 31° (high torsion angles changes).

The glucose-galactose binding protein is suitable as a biosensor because of the fact that its binding the ligand and also refolding of the protein upon denaturing with Gdn-HCl is fully reversible.(75) Besides glucose as the ligand itself, a crucial role of further stabilizing GGBP plays the calcium-binding site within the protein. Furthermore, the natural protein variant is characterized by having a sub micromolar affinity for its target (0.1µM) and is therefore only suitable as biosensor for sub-micromolar glucose concentrations.(76) However, extensive research was undertaken to characterize important amino acid

residues for binding the ligand which were used in mutation studies.(77-79) The details of this research can be found in the following chapter.

1.4.4.1 Glucose sensor developments based on Glucose-Galactose binding protein in E. coli

GBP mutant research:

To be able to detect the binding of a ligand to a binding protein in an reagentless setting, specific amino acid sites in the protein have to be identified that undergo local changes in the enviroment when the endogenous ligand binds. Several examples have been successfully demonstrated for different binding proteins from the E. coli family.(80-85) In consequence, a ligand-mediated bending of the hinge region of periplasmic binding proteins is activated.(86) To observe this movement, fluorophore molecules can be bound to these sites by introduction of cystein mutations in the protein sequence. For the specific case of the glucose-galactose binding protein in E. coli this is strategically favorable as there are naturally no cysteine residues encoded in the gene sequence. This enables highly selective introduction of fluorophores at specific sites. In general, two possibilities of fluorophore attachment are possible according to de Lorimier and co-workers, an endosteric and a peristeric attachment. An endosteric attachment is a linkage of the fluorophore to an amino acid residue that is directly involved in ligand binding. A peristeric attachment involves identification of residues that are located in the vicinity of the binding site which are not directly involved in the binding of the ligand but which are highly likely to be involved in a conformational change. Introduction of allosteric sites(87), amino acid sites that are not located in close proximity to the binding site, represent another option which will be further dicussed in chapter 4.2 and 4.3 regarding the concept of FRET. Hellinga et al. did an extensive mutational screening study on 11 different sugar binding proteins and identified 9 different endosteric, peristeric and allosteric mutations for the selective labeling of an environmental fluorophore to GGBP.(86) The respective mutations are listed in table 2.

Table 2:Endosteric, peristeric and allosteric binding sites of GGBP for the attachment of environmentally sensitive fluorophores were identified.
The results were obtained from Hellinga et al., 2002.(86)

mutation	attachment
Y10C	endosteric
N15C	peristeric
E93C	peristeric

E149C	peristeric
H152C	endosteric
W183C	endosteric
L255C	allosteric
D257C	allosteric
V296C	allosteric

Based on this initial screening, several combinations of biosensor recognition elements with environmental sensitive dyes attached to the single cysteine residues were developed. Acrylodan and pyrene showed the best results for position 152. Pyrene showed the largest stokes shift. However, the affinity for glucose of single mutations is still very low and unsuitable for measuring physiological concentrations. Even before this study, Hellinga et al. mutated position 14 and 16 and obtained a binding constant (Kd) of 3.9 mM, however, with a very low analytical range.(83) The same group also used a therophilic variant of GBP and attached the fluorophores acrylodan, Cy3, Cy5 and IANBD to single cysteine mutations even with millimolar affinities for glucose.(88) Similar approaches have been reported, some were also patented by Becton Dickinson.(81, 82) Daunert et al. improved the single mutations 148, 152 and 182 with the fluorophores Acrylodan, IANBD, IAEDANS, and MDCC. Pitner et al. were the first to develop a triple mutant E149C, A213S, L238S with an equilibrium dissociation constant of 0.5 mM.(89) The same group modified this mutant later on to E149C/ A213R/L238S which yielded a Kd of 10mM. The single mutation A213R was responsible for a 5000-fold lower affinity for the ligand to bind (90). However, the triple mutation H152C/A213R/L238S showed an even better Kd of 11mM when attached to BADAN (Acrylodan-derivative).(91) Intensity- as well as lifetime measurements were performed whereas lifetime was concluded to be more suitable in biosensor approaches due to the possibility of ratiometric measurement. Consequently, a fiber-optic glucose sensor was developed by Birch et al. and was patented.(92, 93) These three papers were used as a starting point of this work. Parts of this work were also inspired by another previous work from the same group that used the NIR dye Blue Oxazine. In general, excitation of a biosensor within a cell culture environment at higher wavelengths is more favourable than excitation at lower wavelengths (optical interference, high energy). However, the higher the wavelength for excitation is, usually the larger is the size of the fluorophore. This can cause problems within the binding pocket. The triple mutant H152C/A213R/L238S showed a 21% increase on addition of saturating glucose with a binding affinity of 25mM. The fluorophore was attached by click chemistry.(94)

Moreover, the ratiometric measurements attracted researchers to test several FRET labeled variants for GGBP. GGBP was labelled either with two fluourescence proteins (genetic incorporation) or with two fluorophores enzymatically catalyzed and attached on the N- or C-terminus of GGBP. (76, 95). However, selective attachment of more than one fluorophore is very limited so Pitner et al. developed the so called ligand protection strategy. This smart strategy involves the attachment of the first fluorophore outside of the binding pocket when glucose is present and GGBP consequently in its closed state. After the attachment glucose is depleted, GGGBP opens up and an attachment site in the binding cleft such as position 152 can be labelled.(96).

1.5 Half a Century of intense glucose monitoring research – A critical comparison of current continuous glucose monitoring developments and learnings

Although glucose biosensors have been under extensive research for over 40 years, only very few have reached the market during that time.(97) Most of the developed sensor systems can only work properly for a few days and every sensor can only work in a specific range of glucose concentrations. That means that for every different application a specific sensor must be developed. Only one implanted sensor for continuous diabetes monitoring has entered the market just recently which can measure glucose online up to three months when implanted under subcutaneous tissue.(98) Many factors such as for example the detection element of the sensor, the therapeutic range of the system or the stability of the biomolecules extend the development time of a continuous glucose monitoring system.

Table 3: Comparison of optical glucose recognition elements based on enzymes, boronic acids and glucose-binding proteins for their features such as stability, sensitivity, reagentless sensing ability, formation of cell-toxic by-products, ratiometric and small volume measurement capability.

			glucose binding proteins		
	enzymes	boronic acids	Con A	apo-enzymes	GGBPs
stability	+	+	-	+	+
sensitivity	+	-	+	+	+
selectivity for glucose	++	-	+	++	+
reagentless	-	+	+	+	+
no toxic by-products	-	+	-	+	+
ratiometric	+	-	+	+	+
small volume measurements	-	+	+	+	+

But still the need of such a sensor for measuring glucose continuously is of high relevance for the biopharmaceutical industry as well as for the food/beverage industry and in pharmaceutical research. And there still is a lack of continuous glucose monitoring systems that work properly for a longer period. Since glucose metabolism plays a crucial role in the development of cancer, a glucose sensor would help to monitor the influence of glucose depletion on different types of cancer cells.

1.6 Fluorescence spectroscopy

1.6.1 Underlying Basics of Fluorescence Spectroscopy

What is Fluorescence?

During the past 30 years fluorescence became extremely popular as research tool in biological sciences due to high sensitivity of fluorophores. Fluorescence mainly replaced radioactive tracers that were commonly used in research, but which were difficult in handling and raised more and more environmental concerns. In 1845, Sir John Fredrich William Herschel, reported the phenomenon for the first time in tonic water, whose solution is made from quinine powder that is famous for its bitter taste.(99)

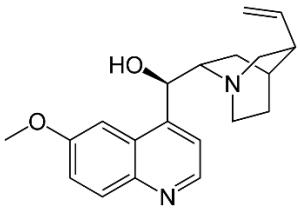

Figure 6: Chemical structure of quinine.
Quinine emits fluorescent light at 450nm upon excitation.

When continuously excited with ultraviolet light, this compound emits an intense blue light at around 450 nm. This emission of light is called fluorescence, has typically lower energy and in the case of quinine is emitted in the visible spectrum of light that can be seen by eye starting at around 400nm.
The processes that occur between the absorption and emission of light are illustrated in the Jablonski diagram, which is named after Prof. Alexander Jablonski from Poland, who was one of the early pioneers in photoluminescence research.

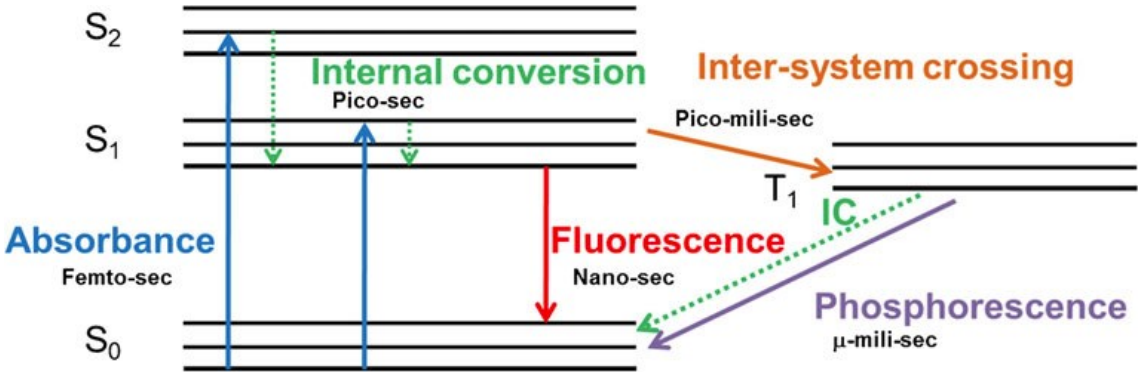

Figure 7: Jablonski diagram.
Fluorescence (green) and phosphorescence (red) occur after excitation of electrons by light to an electronically excited state and subsequent return to the electronic ground state in form of photons, hence light. Fluorescence has typically a lower lifetime (ns) and a lower wavelength than the respective phosphorescence. The loss in energy of phosphorescence is due to an intersystem crossing of electrons while changing its spin which is a forbidden state (Pauli-principle). A spin reversal takes more time and energy which results in a stokes-shift in the wavelength. The schematic was copied from Toseland, 2013.(100)

Fluorescence has a short lifetime of only a few nanoseconds and even less. That can be explained by the transition of electrons from electronically excited states (S_1, S_2, …) to ground states (S_0) (see figure 3). By absorption of light, electrons can be excited at certain wavelengths and the respective energy to an excited state. When the electrons go back to the ground state, they will lose their energy either through relaxation (radiation-free) or through light emission. If the spin of the electron does not change during excitation and emission, the electron will be exited into a single state (S_1) and fall immediately back to the ground state and can emit light. If the electron changes its spin (intersystem-crossing) into a triplet state(T_1) it will take longer for the electron to fall back to the ground state as it has to undergo an additional intersystem crossing (parallel spin is forbidden according to Pauli-principle); this phenomenon is call phosphorescence. During that process, the electrons lose energy and therefore, the resulting emission spectrum of the photons has typically its maximum at higher wavelengths compared to the respective fluorescence. The natural shift in the wavelength of the emission spectrum is called Stokes-shift; the shift to higher wavelengths is calls red shift, named respectively to the red light which has the lowest energy (highest wavelengths) in the visible spectrum of light. Consequently, a shift of the emission wavelength towards lower wavelengths is called blue shift, as blue light has the lowest wavelengths and the highest energy in the visible spectrum of light.

Both, fluorescence, and phosphorescence are displayed under the name of luminescence that generally describes the emission of light from a substance. Fluorescence and phosphorescence are distinguished by the time the electron remains

in the excited states to return to the ground state to be emitted as a photon, hence as light.
Only specific substances can emit fluorescent light due to their electronic structure. Aromatic compounds like quinine have aromatic functional groups whose electrons are delocalized in pi-orbitals that can be easily excited in the UV-VIS range. That is because the energetic difference between ground state and excited state is much smaller for aromatic electrons and excitation of an electron in the next higher energy level is can be achieved with less energy (lower wavelengths).

1.6.2 Fluorescence Detection Principles

Fluorescence can be measured in different ways. Device usually detect fluorescence in a 90° angle to the excitation source separated through lots of mirrors inside a fluorescence spectrometer to avoid interference with the higher energy and intensity of the excitation light source. The different methods to detect fluorescence are described in the following:

Intensity

Fluorescence intensity displays the most common measurement principle. Intensity is the radiative relaxation of photons upon excitation from the excited state (S1) to the ground state (S0). The energy of the photons and more accurately, the emitted light, is measured from the detector and shown in a fluorescence emission spectrum with broad bands. The band structure results from the different energetically transitions between different vibrational and rotational states (Franck-Condon-principle). A drawback of intensity measurements is the dependency on the fluorophore concentration ad hence, the sensitivity to photobleaching.

Anisotropy

Anisotropy measurements are commonly used to study the interactions of macromolecules, e.g. protein-protein interactions and their molecular environment. These measurements can provide information of the size and shape of proteins. Anisotropy, also called fluorescence polarization, can be measured by photo selective excitation of fluorophores with polarized light. Photo selection is a result of the polarized light that only excites fluorophores whose absorption transition dipole is parallel oriented to the electric vector of the excitation. The fluorescence anisotropy changes upon binding to proteins and is defined by the Perrin equation,

$$r = \frac{r_0}{1+(\frac{\tau}{\theta})}$$

where r_0 gives the theoretical anisotropy value of the fluorophore in the absence of any rotational diffusion, θ is the rotational correlation time for the diffusion process and teta the fluorescence lifetime of the fluorophore. The rotational correlation time of proteins are comparable to typical fluorescence lifetimes. Therefore, fluorescence anisotropy is sensitive to any event that influences the rate of rotational diffusion and thus makes molecular studies on membranes attractive.

Lifetime

The lifetime of a fluorophore is measured by the decay of fluorescence intensity over time. Fluorescence lifetimes can be determined by using a pulsed source. When a population of fluorophores is excited by pulses of light, time-resolved fluorescence will decay exponentially. Time-correlated single-photon counting and frequency-based phase modulation by pulsed or modulated light at high frequency, are two additional methods how to measure fluorescence lifetime.

1.6.3 Environmental factors that can influence fluorescence spectroscopy

Fluorescence is a highly sensitive analytical method that can be influenced by different environmental factors such as solvent polarity, solvent relaxation, high energy light sources or inorganic or organic materials that would absorb (quench) the energy of the fluorophore non-radiatively. Hence the quantum yield will be influenced. Photobleaching of the dye occurs when the dye is exposed to high energy light and can lose its ability to fluoresce irreversibly. Quenching of fluorescence is mostly induced by solvents and (in-)organic materials but also solute or self-quenching is a present phenomenon.

1.7 Environmental-Sensitive Sensing

Fluorescence measurements have been used widely in the life science research field to study binding processes at biological membranes, drug delivery, protein-protein interactions as well as conformational changes of molecules. Due to its high sensitivity, fluorescence allows the observation of events on a single-molecular level. Besides intrinsic fluorescence of proteins from tryptophan residues, the incorporation of extrinsic fluorophores (also called labels) offers greater advantages on a single molecular level. Extrinsic labels can be incorporated at desired positions of interest in a protein or molecule and a label can be chosen by its enhanced fluorescence properties. A variety

of different labels exists such as genetically encoded fluorescent proteins, organic fluorophores as well as quantum dots. The latter are inorganic molecules with an extremely bright fluorescence emission. These molecules are widely used for quenching experiments due to their relatively large size. Regarding their size, large fluorescent proteins and quantum dots can perturb the structure of proteins. Organic fluorophores, however, are relatively small and are less likely to have the same effect. They mostly consist of planar aromatic ring structures and can be exited from UV light to near infrared light, but it has to be considered that the larger the molecule becomes, the more the absorbance of the same shifts to higher wavelengths. In biological applications such as cell culture or biotechnology, excitation with short, high energy light (e.g. UV) is often not desired as cells or molecules could be easily destroyed. On the other hand, smaller molecules can be more accurately positioned within a binding pocket compared to bigger molecules.

The read-out of environmental sensitive dyes can be either done by intensity, anisotropy, or lifetime measurements. Intensity measurements of organic fluorophores depend strongly on the concentration of the labeled fluorophore and are therefore sensitive to photobleaching reactions. Hence, a calibration of a potential biosensor is needed. Intensity measurements, however, are still preferably used for the biosensor read-outs as they are universally applicable, easy to read-out with a relatively low device-related expenditure. A read-out device for a biosensor could be easily miniaturized enabling a portable sensor system, which is favourable for in-patient applications as well as in the biotechnological industry.

1.7.1 Site-selective labeling of proteins with environmental-sensitive dyes

Proteins are build of 22 different amino acids which consist of characteristic side chains with different functional groups. The naturally occuring reactive groups in the residues lysine and cysteine, that can be easily labeled, are amines and thiol groups, respectively. Amine-reactive labels are mainly used in immunochemistry applications due to the stability of the formed bond to amines. The reactivity of the amines is determined by its class (aliphatic or aromatic) and it’s basicity. The free base of a lysine residue (aliphatic amine) is mainly present above an pH of 8.5. Thiol-reactive labels are predominantly used for the detection of conformational changes in proteins, protein complex formation or ligand-bindind events. Thiol-reactive labels react as alkylation of free thiol groups to a stable thioether bond at an optimal pH between 7.0-7.5. Therefore the labeling of proteins with thiol reactive probes is a milder procedure than that with amine reactive

probes. Given the fact, that mammalian proteins have a very low occurence frequency (3.3%) and some peptides and proteins have only very few cysteines in their protein sequence, this method enables the selective labeling of single cysteine residues. Hence, site-directed mutagenisis can be used to exchange single cysteine residues without significantly disrupting the structure of the protein. In bacterial proteins, cysteine residues, which mainly stabilies the tertiary structure, are extremely rare. Interestingly, the glucose-galactose binding protein in E.coli does not comprise any cysteine residues, which simplifies the labeling strategy. A single cysteine mutation was therefore incorporated in the bacterial gene encoding for the GGBP protein.

Thiol-reactive labels can contain functional groups like iodocetamides or maleimides which readily react with free thiol groups to thioethers. Since iodocetamides have a lower selectivity, can more easily react with amines and are less photostable as maleimides, therefore the latter were used in this work. Under physiological conditions, cysteines form disulfide bonds, called cystines, amongst themselves to stabilize the protein structure. Hence, cystines have to be reduced with regents such as dithiothreitol (DTT) or ß-mercaptoethanol prior to labeling. The work mechanism of these agents is based on a thiol-disulfide exchange reaction as they contain free thiol groups themselves.(101) DTT and ß-mercaptoethanol, however, have to be removed before the reaction with the thiol-reactive probe for this reason.

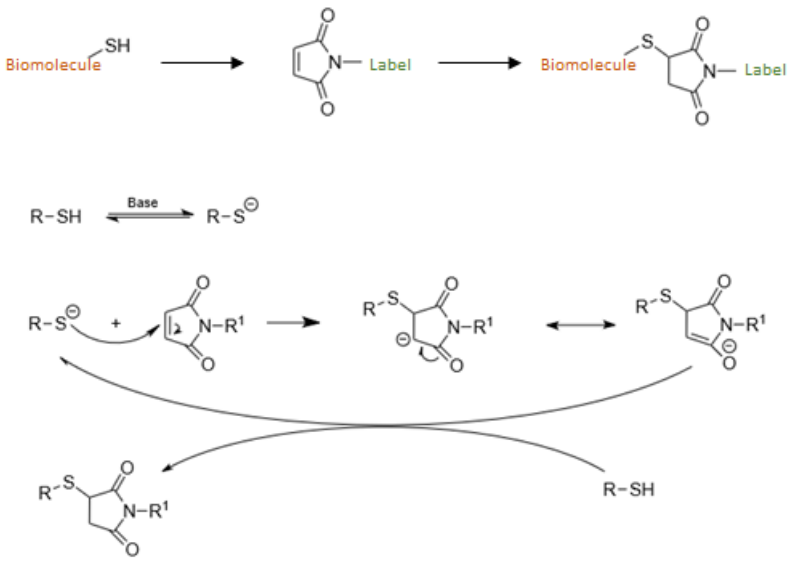

Figure 8: Maleimids as reactive functional groups for the selective labeling of proteins.
Addition reaction mechanism of maleimides with thiol groups. At a pH of 7.4 the free thiol group is predominantly present in its thiolate form and can form a thioether bond by attacking one of the electrophilic carbon atoms of the maleimide. In consequence, a succinimide product is formed.

1.8 Förster-Resonance-Energy-Transfer used as a strategy in biosensors

The Förster-(Fluorescence-) Resonance-Energy-Transfer (shortly called FRET) is a mechanism that describes the energy transfer between a donor and an acceptor molecules and provides the opportunity of an ratiometric measurement system that is independent from fluorophore concentration and therefore used in biosensor developments. FRET enables the detection of molecular events such as dynamic protein folding, structural dynamic processes and molecular reactions on a single-molecule level. FRET is, when combined with fluorescence microscopy techniques, not only able to resolve these events on an angstrom level, it can nowadays also be applied to detect these events in nearly real-time (nanosecond decay of fluorophores) using time-resolved fluorescence.(102)

In this work, an alternative approach with a FRET labelling of GGBP is achieved to evade difficulties that are often reported in the literature. Most developed sensors have not reached the market because of drawbacks when used in applications. Either the sensors use fluorescence intensity measurements that reveal to be unsuitable for measurements in blood or medium since it requires several calibration steps per day or the background fluorescence which is typical below 400nm is disturbing the actual fluorescence of the sensor-related process.

Unlike molecular probes that are highly dependent on their environment such as pH, temperature or ionic strength, fluorescent labels can be relatively inert against these conditions. Fluorescent labels are more and more under extensive research and more stable reagents are developed for different purposes. In contrast to environmental-sensitive dyes, the fluorescence of insensitive dyes is typically more stable, the fluorescence emission is brighter and the quantum yield of the dye is highly increased which makes the label itself a useful tool to develop more stable sensors. The combination with the highly selective principle of analyte recognition with a binding protein allows the development of a highly selective sensor for glucose with a stable label as detection element. Since these labels are less environmentally sensitive and therefore the fluorescence quantum yield is less influenced, a change in fluorescence intensity can be measured with FRET.

Simultaneously, FRET enables a ratiometric measurement that is independent of analyte concentration, photobleaching of the fluorophore and background fluorescence due to a second label that is excited with the energy of the blue-shifted fluorescence emission of a first label (see Figure 2)

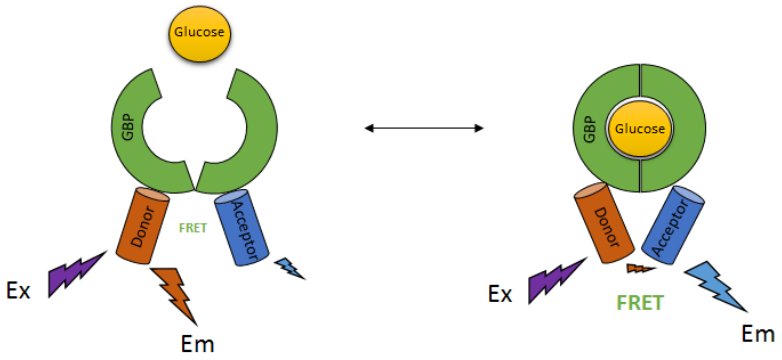

Figure 9: Schematic principle of a FRET-labeled Glucose binding protein.
A) GGBP consists of two binding domains which are connected by a hinge region. When glucose is present, the binding domains change their local environments and entrap the glucose molecule which is stabilizing the transition state. A donor and an acceptor fluorescent label (FRET pair) can be attached to each one of the binding domains and interact. B) When dipoles of the attached FRET pair come into proximity (<10Å) the energy of the donor emission overlaps with the excitation energy of the acceptor (energy transfer). This figure was jointly done with Tatjana Roth.

Ratiometric measurements therefore provide a good signal-to-noise ratio as the background is eliminated. However, the most challenging part of a dual labelling of a protein is the selective labelling of one amino acid in the protein sequence. In peptides with a few amino acids, the number of individual amino acids can be quite low, but larger peptides and proteins require a distinct labeling strategy. An overview of these labeling strategies can be found in the next chapter.

1.8.1 Site-selective labeling of proteins: introduction of a recently discovered peptide tag ‘π-Clamp’

As mentioned in chapter 1.9.6, selective labeling of single sites within a protein is challenging due to similar reactivities amongst amino acids. There have been different approaches published that enable site-selective modifications.(100, 103, 104) Frequently used methods for site-selective labeling and examples thereof are the introduction of natural and/or unnatural amino acids into the protein sequence by gene synthesis, site-selective mutagenesis or solid-phase peptide synthesis. The label itself can then be introduced by:

1. Bioorthogonal chemistry (e.g. azide-alkyne chemistry (click chemistry), Diels-Alder reaction (105, 106), Staudinger ligation (107)
2. Enzymatic modification of protein tags e.g. SNAP-tag, Halo-tag, CLIP-tag (108-111)
3. Chemical modification of small peptide tags e.g. tetracysteine tags like FlAsH-tag and ReAsH-taq (112)
4. Enzymatic or chemical biotinylating of proteins (e.g. avidin-, streptavidin-conjugation) (113)
5. Ligand protection/deprotection (96)

The bioorthogonal labeling of biological molecules makes use of chemical reactions which are not interfering with biological processes. It is a helpful tool to label molecules such as nucleic acids, glycans and lipids which is not possible by genetically encoding reporter genes. In addition, bioorthogonal chemistry enables synthetic post-translational modifications for various purposes. Protein and peptide tags are sequences encoded within the gene that encodes for the protein of interest and were developed to have an easy and appropriate labeling of molecules under non-harsh conditions. These tags can either be labeled chemically or be recognized accordingly by an enzyme. The same accounts for the biotinylation of proteins and its consecutive labeling with avidin- and streptavidin-conjugated labels. The non-covalent interactions between these species are one of the strongest that have been reported for biological molecules. A very elegant yet not universally applicable protein labeling method is the ligand protection/deprotection strategy. This strategy makes use of the varying reactivity of individual cysteine residues due to their local environment or the hydrophobicity of the label.(114)

Selective labeling of proteins is manifold, and, in most applications, labeling is a bottleneck. It is cost-and labour-intensive and not appropriate for the use in large scale applications. Zhang et al. described for the first time the site-specific modification of a

single cysteine among many within a protein without the need of a reaction catalyst or multiple chemical steps. In 2016, they presented the “π-clamp mediated cysteine conjugation”, a simple conjugation technique which is easily scalable.(115) The concept has been confirmed by other researchers as promising tool in the whole field of selective chemistry(116). Earlier, in 2013, Zhang et al. developed an regioselective enzymatic perfluoro arene-cysteine-“click ligation” that enables modifying cysteine residues in peptides catalysed by the Glutathione S-Transferase(117). They discovered that perfluoro aromatic compounds are less reactive in aqueous solutions and enzyme catalysis is essential. Inspired by their findings, they screened small peptides to facilitate the reaction in an analogous manner to enzymes. They called their most promising peptide motif ‘pi-clamp’.

Pi-Clamp is a method that tunes the local environment of a single amino acid cysteine and makes this single amino acid more reactive for perfluoro arylated probes and labels. **Figure 10** describes the structure and reaction of the pi-clamp.

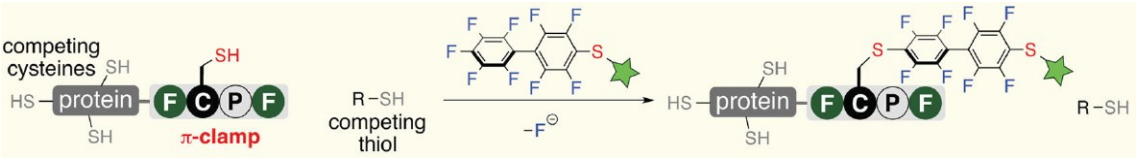

Figure 10: Pi-clamp as depicted from and described by Zhang et al., 2016.(115)

The pi-clamp consists of a short four amino acid sequence Phenylalanine (Phe), Cysteine (Cys), Proline (Pro), Phenylalanine (Phe) (short: F-C-P-F). The cysteine in this motif is enhanced in its reactivity for a perfluoro-arylated reagent by a pi-stacking between the phenyl rings in phenylalanine. The pi-clamp can be genetically incorporated into a protein sequence of interest at various sites (C-terminal, N-terminal and in the middle of the sequence, depending on the tertiary structure). It has been shown, that regardless of the position, the reactions occur within 60min to maximum 120 min for a perfluoro-arylated fluorescein. Furthermore, molecular dynamics simulations showed that Phe 1 and Phe 4 in the pi-clamp are essential for the stabilization of the transition state of the reaction with perfluoro arylated probes and the stabilization of the product. **Figure 11** shows the free energy of the overall reaction of a pi-clamp compared to a glycine motif indicating this importance. Phe 1 and Phe 4 show a parallel orientation of the phenyl groups, hence they stabilize the cysteine residue and tune its reactivity for an electrophilic reaction partner.

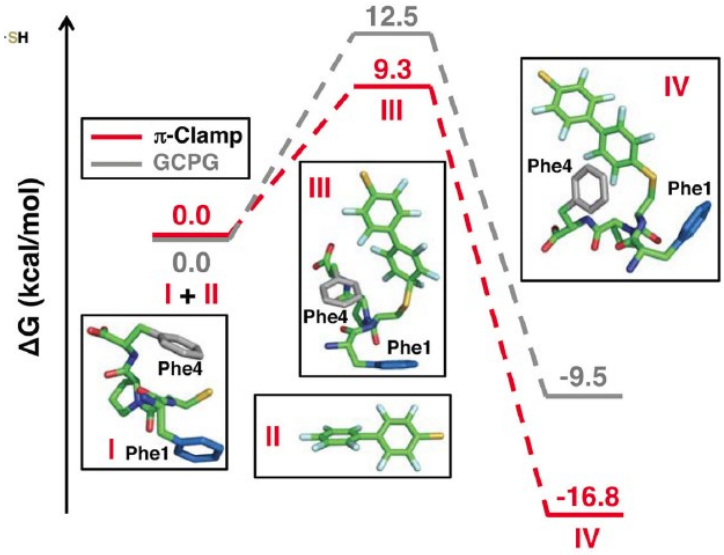

Figure 11: Reaction mechanism of the nucleophilic aromatic substitution (S_NAr) reaction of a perfluoro arylated thiol with the pi-clamp motif FCPF compared to GCPG.
ΔG describes the free energy of a molecule or complex in its different states. The transition state as well as the overall complex of the perfluoro arylated FCPF motif shows a significant stabilization with a free energy difference of 7kcal mol^{-1}. This figure was copied from Zhang et al. (2016).(115)

By LC-MS studies, Zhang et al. showed that amongst many cysteines in an engineered 55 kDa fusion protein of anthrax toxin lethal factor and diphtheria toxin domain A, only the pi-clamp was site-specifically conjugated by a perfluoro arylated probe. Furthermore, they showed that the method can be used in the antibody-drug-conjugate (ADC) space. They site-selectively labeled trastuzumab that binds HER2 positive breast cancer cells. Monomethyl auristatin F (MMAF) as conjugated drug, selectively killed these cells.(115)

In this work, the pi-clamp motif was synthetically incorporated into specific sites in the MglB gene for selective modification of several single-cysteine residues in the GGBP that were introduced to design a FRET labeled GGBP biosensor. The experiments are explained in detail in results part 2.

1.8.2 Choice of FRET pairs

FRET requires a careful choice not only of the position and the distance of the attached fluorophore pairs within a protein, but also the spectral properties. The energy of the donor molecule can only be transferred to the acceptor molecule if the energy of the donor emission equals the excitation energy of the acceptor molecule. In other words, the emission of the donor molecule must overlap with the excitation spectrum of the acceptor molecule. The general rule applies, the larger the overlap the more efficient the energy transfer and the higher the emission of the acceptor molecule that is measured.

However, care must be taken that the excitation of the donor molecule does not overlap with the excitation of the acceptor. Otherwise, the acceptor molecule would already be excited by the excitation of the donor fluorophore. The context of this phenomenon is visualized in figure 12.

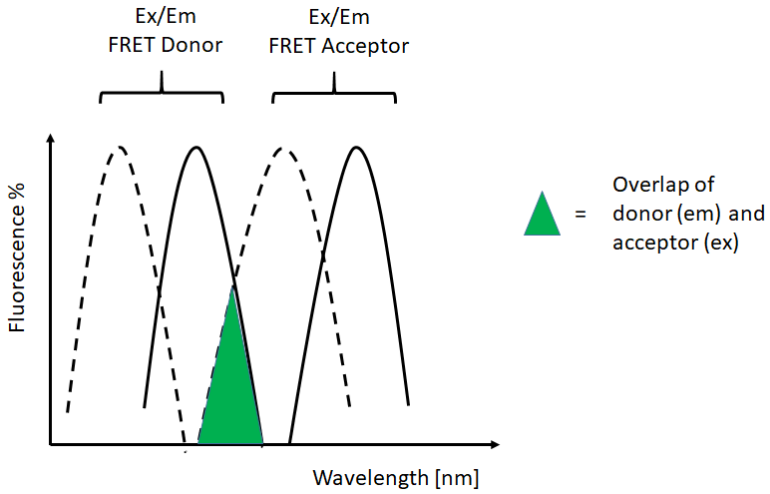

Figure 12: Fluorescence overlap of FRET donor and FRET acceptor molecule.

2 Objectives

The overall objective of this work was to develop optical glucose sensor recognition elements based on the glucose-galactose binding protein (GGBP) in E. coli, which display enhanced optical properties for the use in cell culture and biomanufacturing environments as integrated monitoring solution of nutrients.

This work is structured into two parts.

The first part inspired me by previous work that has been done by researchers in the field. The objective here was to find newly developed & commercially available environmental sensitive fluorophores that are attached to GGBP which show enhanced fluorescence properties in the read-out of a glucose biosensor. The challenge was to find suitable fluorophores that show both, a sensitive large change in fluorescence intensity upon binding of glucose as well as molecules that can be excited above wavelengths of 400nm (UV). The reason is to minimize optical interference at lower wavelengths which highly limits the read-out and can disturb cells in growing. Previous research could not present a combined solution due to limitations in conventionally used fluorophores. Therefore, six highly efficient environmentally sensitive fluorophores from Dyomics GmbH and Atto-Tec GmbH were chosen and tested for the glucose sensitivity of GGBP.

The second part of this work was inspired by the deep need of ratiometric read-out measurements in biosensing. FRET experiments show attractive opportunities in this field being independent from fluorophore concentration and background fluorescence when designed correctly. However, labeling FRET molecules selectively to proteins is extremely labour intense, not universally applicable and in some cases even impossible by design. This work presents for the first time, FRET-based biosensor recognition elements based on the recently discovered π-clamp strategy (Nature Chem., 2016) using the glucose-galactose binding protein in E. coli.

3 Results & Discussion Part 1

3.1 Terminology of gene and protein variants

In the following chapters the terminologies and abbreviations of different genes and proteins and their respective genetic and proteomic variants are discussed. The basic terminology is in accordance with the terminology of the UniProt knowledgebase (118) and the protein databank (RCSB PDB) (119). The following two crystal structures from the RCSB PDB were used for the investigation of mutant forms of the Glucose-Galactose binding protein (GGBP) in E. Coli:

- ***2HPH* (120):**

  High resolution structure of E. coli glucose/galactose binding protein bound with glucose (please see appendix for full structure)

- ***2fw0 (121):***

  Apo Open Form of Glucose/Galactose Binding Protein (please see appendix for full structure)

The following two genes were used as basis for the genetic modification and are described in the UniProt knowledgebase (118):

- ***mglB:***

  gene that encodes the Glucose-Galactose protein in E. coli (UniProt – Database Code)

- ***GGBP:***

  glucose-galactose binding protein in E. coli (UniProt database)

The terminology of the following protein variants was used for newly developed variants that were developed in this work:

- ***GGBP_wt:***

  natural variant of the glucose-galactose binding protein in E. coli.

- ***GGBP_mut_H152C/A213R/L238S:***

  mutated variant of the glucose-galactose binding protein in E. coli with three single point mutations at position 152, 213, 238. The letters reflect the amino acids at the respective position within the protein according to the ‘one letter code’. The variant *GGBP_mut_H152C/A213R/L238S* was used as basis for five further variants of GGBP

where, in addition, the four amino acid sequence FCPF or FPCF was incorporated at five different positions within the protein.

The variants of GGBP_mut_H152C/A213R/L238S are described as followed (Results Part 2):

- ***GGBP_mut_H152C/A213R/L238S_QNDQ42-45FPCF:***

(mutated position in this work: QNDQ42-45FPCF in 2HPH)

- ***GGBP_mut_H152C/A213R/L238S_VDPA68-71FCPF:***

(mutated position in this work VDPA68-71FCPF in 2HPH)

- ***GGBP_mut_H152C/A213R/L238S_EPSR93-96FPCF:***

(mutated position in this work EPSR93-96FPCF in 2HPH)

- ***GGBP_mut_H152C/A213R/L238S_DGTN280-283FCPF:***

(mutated position in this work DGTN280-283FCPF in 2HPH)

- ***GGBP_mut_H152C/A213R/L238S_KIDN285-288FCPF*:**

(mutated position in this work KIDN285-288FCPF in 2HPH)

3.2 Design and cloning of GGBP analogues

For cloning of the mglB gene we kindly obtained the PtZ18U-mglB vector plasmid from Prof. S. D'Auria from Napoli university, Italy as a gift. After amplifying the gene, the DNA turned out to have a single cysteine mutation at position 49 (Q49C), so it could unfortunately not be used for further experiments. Hence, the wildtype coding gene sequence of GGBP_wt (mglB_wt: 0,93 kb) in E. coli was amplified by Polymer Chain Reaction (PCR) from the genomic DNA of a K-12 MG1655 strain. The DNA was a kind gift from Prof. Dr. Matthias Mack and his group. The GGBP_wt variant was used as a reference to validate cloning efficiencies since a mutated form of a protein might face difficulties in the cloning and transforming processes. The gene encoding for the triple mutation **GGBP_mut_H152C/A213R/L238S** was individually designed according to our inhouse cloning systems and finally ordered from GeneArt® to save time and costs. This triple mutant was previously reported (91) and showed an enhanced affinity constant (K_D) of 11 mM towards glucose compared to the single mutation GGBP_mut_H152C-Badan (K_D = 0.005 mM). From the literature, this triple mutant showed excellent properties for cell culture and bioreactor environments since the glucose biosensor recognition element should have an affinity towards glucose that represents the range of physiological conditions (10-30 mM).

The coding genes were amplified using designed forward and reverse primers that contained appropriate restriction sites for two restriction enzymes NdeI and XhoI. The primers were designed according to AddGene's protocol for primer design. The following characteristics were considered to ensure optimal aligning:

- Length of approximately 20 ± 2 amino acids
- GC-content: 40-60% (starting & ending with G/C)
- Annealing temperature between 50-60 °C (Tm) for both primer (max. 5 °C)
- Avoiding complementary regions within the protein itself
- Restriction sites plus 3-6 base pairs to ensure correct cleavage

The expression vector pET24a was used to ensure optimal protein yield which carried a C-terminal sequence that encodes for an affinity tag of six histidine amino acids (His-Taq). In figure 8, a transformation control digestion with NdeI and XhoI was carried out. The insert band of 0,93kb and the vector band (5,3kb) clearly indicate a successful transformation of the cloning strain.

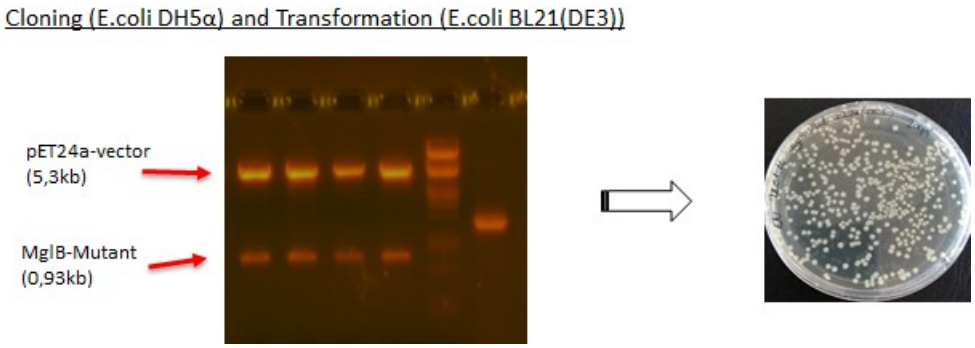

Figure 13: Control digestion of the wildtype and mutant gene encoding for GGBP_wt and GGBP_mutant.
A) The vector plasmid pET24a was cut with NdeI and XhoI and the insert (0,93 kb) could be detected indicating a successful transformation of the E. coli cloning strain. B) The plasmid was successfully transformed into the expression strain E. coli BL21(DE3).

The extracted DNA was sequenced and transformed into the expression strain BL21(DE3) for optimal production of the proteins. **Figure 8B** shows a high number of individual bigger colonies which indicates an efficient transformation rate of the triple mutant. The expression of GGBP_wt led to similar results.

3.3 Expression of GGBP-variants

After the successful transformation of the genes encoding the wildtype and the variant GGBP_mut_H152C/A213R/L238S with the help of the pET24a vector, several aliquots of

bacterial cultures enriched with 10% glycerol were shock frozen in liquid nitrogen and stored at –80 °C for inoculation of bigger cultures.

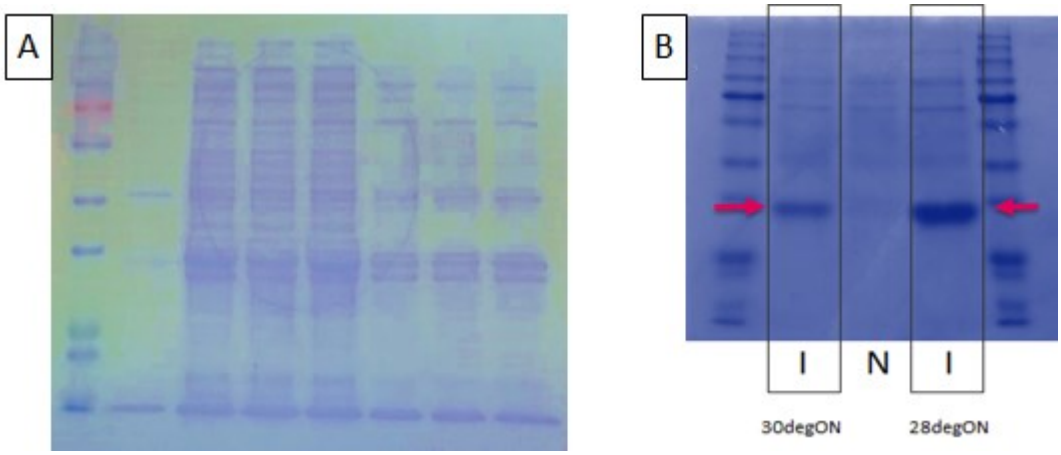

Figure 14: Test expression of 50ml inoculation media with triple mutant to screen for optimal expression conditions. A) Lines 1-7 indicate several independent experiments from the same colony of the checked sequence. Line 1: Pre-Induction (control) Line 2-4: overnight expression at 25 degrees with 1mM, 1,5 mM and 2 mM IPTG, respectively. Line 5-7: 3h expression at 37 degrees B) An expression at reduced temperature (28°C) leads to higher overexpression of the protein of interest.

An expression screening was carried out using 50 ml of medium in a 250 ml- Erlenmeyer vessel to test for optimal conditions of the expression. The cultures were inoculated from a 10 ml pre-culture. Prior to the induction, the cultures were stirred for initial growth until they reached an optical density at 600 nm (OD_{600}) of 0,1µM. The results in figure 14A showed that the optimal expression conditions for this pET24a vector system was an overnight expression at lower temperature (25 °C) and an induction with 1 mM of IPTG. A higher temperature (37 °C) and 3 hours led overall to a significantly lower yield of total protein as well as a significantly lower yield of the target proteins. Even a higher concentration of IPTG (1,5 mM and 2 mM) as inducer could not compensate for that. The non-induced pET24a system was used as a control which indicated a low expression of certain protein bands prior to induction.
A second experiment (figure 14B) showed that an overnight expression yields a significantly higher protein amount below 30 °C after induction. The highest protein yield of 40 mg per liter LB medium after induction with 1 mM was obtained at 28 °C overnight and was therefore used for all further expressions.

Pellet formation after centrifugation and washing

3.4 Purification of GGBP_wt and GGBP_mut_H152C/A213R/L238S

The purification of all mglB variants was performed on the Äkta purifier system (GE Healthcare) in Prof. Mack's laboratory. The mglB_wt variant was used in a first purification procedure to characterize the protein and to establish a protocol for further purifications of the respective

variants. The overall purification strategy to remove impurities consists of mainly three purification types.

1. His-Tag affinity chromatography
2. Gel filtration chromatography
3. Ion exchange chromatography (optional purification step is dependent on desired purity)

Please note, in this work only step 1 and 2 were used. A higher purity, as it has been obtained with the two respective purifications, was not intended to be needed for the characterization of the following experiments.

As part of the cloning strategy the his-tag (6x His) was introduced into all protein variants for an affinity-based chromatography by the cloning vector pET24a. The chromatogram of a His-Trap purification of GGBP_wt is depicted in figure 15. The left chromatogram reflects the His-Trap purification step. In the sample loading phase, the UV signal at 280 nm increases up to a plateau of 1800 mAU (upper limit of detection) due to the overall protein concentration. On average, 20-25 ml of disrupted cell extraction is loaded onto the column in each his-tag purification. The protein of interest which is attached to the his-tag binds reversibly to the Ni Sepharose resin in the His Trap column on a constant flow of 5 ml/min. Once the unspecific proteins leave the column (decrease of UV signal to almost 0 mAU), the bound protein of interest is washed by 5 times the column volume (at least 25ml) and is eluted by an imidazole-enriched buffer (buffer B: 400mM) in a competitive manner. Imidazole binds to the Ni Sepharose resin with a higher affinity and competes with the his-tag of the proteins. In a second step, the imidazole is removed from the eluted protein solution by gel filtration for optimal storage conditions. The gel filtration for GGBP_wt is shown in the right chromatogram in figure 15. A single protein band (blue) is obtained and indicates a protein fraction of high purity. The imidazole is removed effectively from the protein band as indicated by the followed band (brown). Overall, the gel filtration step also supports the separation from excess proteins by their size which could have interfered in step 1 (Histidine rich proteins) and results therefore in a higher purity. The purity of the proteins was observed with denaturing gel electrophoresis (SDS-PAGE, upper middle figure 15). For this purpose, sample fractions were taken at protein loading (FT), in the washing phase (2) and after starting of the elution with a 20% gradient (4, 5, 6, 7, 8). A non-induced (NI) and an induced protein sample were taken prior to the purification as controls. The fractions 6, 7 and 8 were combined as one fraction (3 x 8 ml) for the gel filtration step. Overall, high purity of the desired proteins was obtained for GGBP_wt and GGBP_mut_H152C/A213R/L238S (> 95%) already after step 2 and could therefore be

used for the following experiments of characterization without the need for further purification steps.

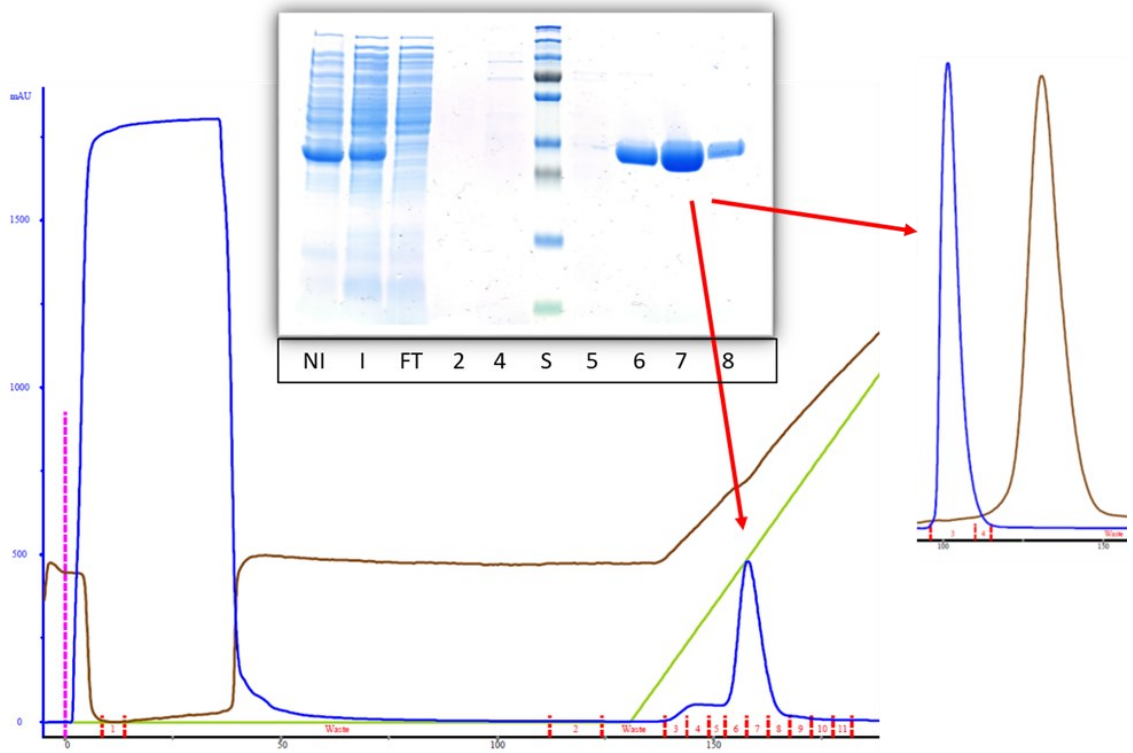

Figure 15: Purification of GGBP_wt using a 5ml His-Trap column from GE Healthcare on the Äkta purifier system. Left: A 20% gradient (100ml) was applied with a dual buffer system (buffer A & B: 10mM imidazole & 400mM imidazole). SDS-PAGE profiling of the respective fractions was carried out (upper middle). Fraction 6, 7 and 8 were combined and further purified on a 50ml desalting column from GE Healthcare (right) to remove imidazole for optimal storage conditions. Colour coding: blue: UV-signal in mAU, brown: conductivity in mS, red: fractions in ml volume, green: gradient, pink: sample injection

3.5 Environmentally sensitive glucose sensors based on the Glucose-Galactose Binding Protein

In this work, new, commercially available extrinsic fluorophores with excitation maxima above 400 nm (visible range) were chosen for the development of a glucose sensor element which can be later on used in bioreaction vessels or cell culture approaches. The option for commercial up-scaling of the final sensor element was considered. It is noteworthy that the continuous excitation of an optical online sensor below 400 nm can harm surrounding cells and organisms irreversibly due to the high energy of the light. Especially, in bioreactor environments this should be overall avoided. In recent papers, the small planar molecule BADAN showed the most promising results as an extrinsic label. It seems obvious that this might be in correlation with its size and structure to be able to perfectly fit into the binding pocket of GGBP. Upon binding of glucose small planar molecules might be more impacted by the environmental changes in polarity than larger molecules with more degrees of freedom. Therefore, optimized extrinsic labels were chosen which either displayed a similar planar

structure with functional groups that increased the excitation wavelength or labels with optimized environmental sensitive structures. The extrinsic labels were introduced at position 152 within the glucose-galactose protein by a cysteine mutation and respective selective labeling.

3.5.1 Cysteine labeling of GGBP_mut_H152C/A213R/L238S

The labeling of the single cystein residue 152 within GGBP_mut_H152C/A213R/L238S was achieved by a standard maleimide coupling procedure. The labeling reaction was stopped after 3 hours by a gel filtration process which was either done by a desalting purification on the Äkta purifier system (**see figure 16**) with the HiPrep 26/10 column or by PD-10 flow-through column for smaller samples below 5 mg of protein.

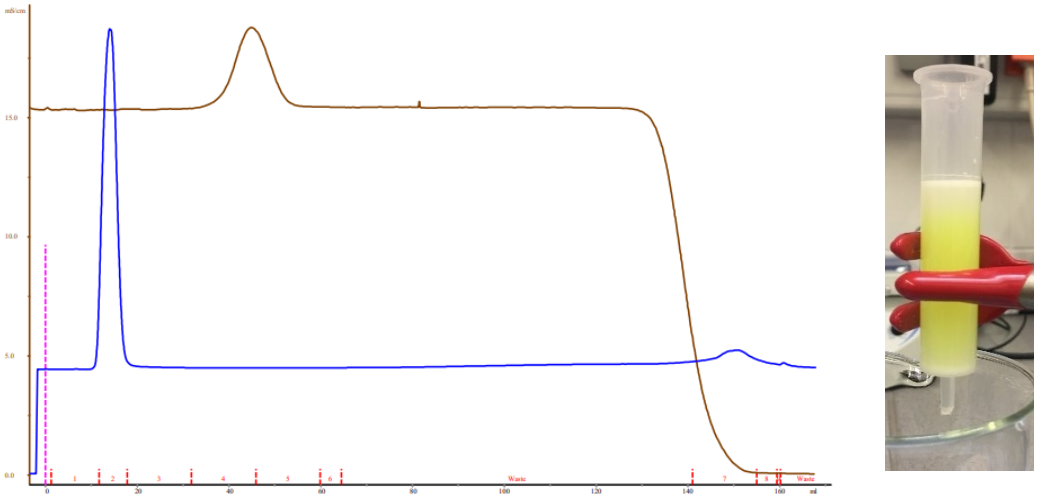

Figure 16: Gel filtration of GGBP_mut_H152C/A213R/L238S-BADAN after labeling.
Left: Purification chromatogram of GGBP_mut_H152C/A213R/L238S-BADAN with the column HiPrep26/10 50 ml Desalting from GE. The protein is eluted 2,7 column volumes before the free dye BADAN. TCEP is removed from the protein fraction in the same purification step as indicated by the brown conductivity curve. Right: gel filtration of GGBP_mut_H152C/A213R/L238S-BADAN with a PD-10 flow-through column from GE Healthcare. Colour coding: blue: UV-signal in mAU, brown: conductivity in mS, red: fractions in ml volume, green: gradient, pink: sample injection

The UV-signal of the chromatogram in figure 16 clearly indicates the separation of the large protein and the small molecule BADAN. Due to its size the protein readily elutes after 15 ml DPBS pH 7.4. The small molecule elutes after three column volumes (3 x 50 ml) finally. The brown curve represents the conductivity and indicated a buffer exchange from buffer A to storage buffer (DPBS pH 7.4). Considering the laborious work, PD-10 flow-through columns were tested for their separation quality. In order to control the labeling procedure, the labeling efficiency was determined.

3.5.2 Labeling efficiency

The labeling efficiency of the reaction of protein and dye was determined according to the procedure described in chapter 5.3.4. Therefore, the molar extinction coefficient of GGBP (ε = 32.673 M^{-1} x cm^{-1}) was measured at a fixed concentration of GGBP in solution. The concentration of the unlabeled protein was determined by a Bradford assay. For the single cysteine mutation, an overall labeling efficiency of 1.1 to 1.3 (dye: protein) was achieved. For BADAN, a higher labeling efficiency was obtained (on average 1.7), which means almost two molecules of BADAN were bound to the protein with a single cysteine mutation. The high labeling rate was counteracted by reducing the molar excess of the dye to 1.3-fold. It is noteworthy that in this work dialysis was not carried out after the purification step. However, the molar excess reduction could obtain labeling efficiencies of 1,1: 1 (dye: protein).

3.6 BADAN used for optimization of glucose sensing & validation system

BADAN derives of the basic structure of Prodan (reactive form: Acrylodan) and is usually used as a protein staining dye that is extremely sensitive to the polarity of the local environment. In this work, BADAN (figure 17) was used as a reference for the generated triple mutation of GGBP to verify the ability of the glucose sensing system to work accurately.

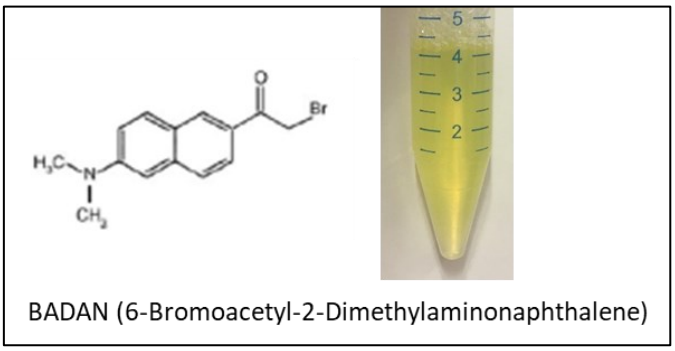

Figure 17: Molecular structure of BADAN (6-Bromoacetyl-2-Dimethylaminonaphthalene).

Therefore, the following experiments (except figure 25) with the dye BADAN were repeated according to the literature.(91) BADAN was dissolved in DMSO and shows an excitation and emission peak at 365 nm and 492 nm, respectively, with an extremely large stokes shifts of 128 nm. Once dissolved in phosphate buffer, the excitation maximum is slightly increasing to 381 nm (red-shift of 17 nm), the emission maximum is shifted to 530 nm and shows an even larger stokes-shift of 150 nm. Indeed, BADAN shows an untypical large stokes-shift for its small size and displays an exception over typical fluorescent dyes and their reactive groups. The excitation and emission spectra of BADAN in solvent and buffer are depicted in **figure 18**.

The red shift of the absorption maximum of GGBP-H152C/A213R/L238S from solvent to phosphate-buffered saline (DPBS pH 7.4) must be considered in all further experiments as well as glucose-dependent measurements (excitation at 381 nm).

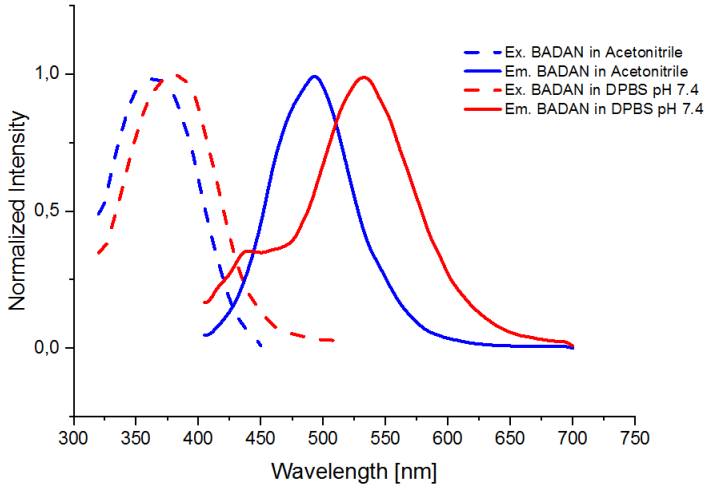

Figure 18: Excitation and emission spectra of 6-Bromoacetyl-2-Dimethylaminonaphthalene (BADAN) in acetonitrile and DPBS pH 7.4.

When BADAN is bound to the cysteine mutation at position 152 of GGBP_mut_H152C/A213R/L238S, the absorption maximum increases by 35 nm to 400 nm and shows a fluorescence emission maximum at 533 nm, slightly increased by 3 nm. The excitation and emission maxima in the phosphate-buffered system have been considered in glucose-dependent measurements. The covalent linkage to the glucose-galactose binding protein has no influence on the emission maximum of BADAN which is shown in **figure 19**. For glucose-dependent intensity measurements with GGBP_mut_H152C/A213R/L238S-BADAN, the excitation wavelength was adjusted to 400nm.

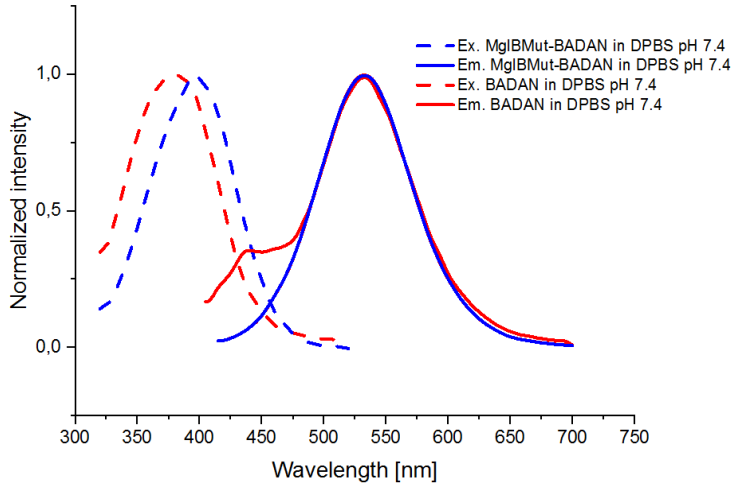

Figure 19: Excitation and emission spectra of 6-Bromoacetyl-2-Dimethylaminonaphthalene (BADAN) covalently bound to the triple mutation GGBP-H152C/A213R/L238S are compared to the excitation and emission profile of unlabelled BADAN.

3.6.1.1 Polar-sensitivity BADAN

When looking at environmentally sensitive dyes, they are typically sensitive to polarity changes such as solvent polarity and microenvironmental changes within proteins upon ligand binding. Changes in solvent polarity might give hints if a dye is sensitive enough to indicate such polarity changes within the protein of interest. For this purpose, BADAN was dissolved in equal concentrations in acetonitrile, in DPBS pH 7.4 and gradient mixtures of both solvents and the fluorescence emission was measured. The results are shown in **figure 20**.

Compared to acetonitrile, the fluorescence intensity of BADAN is reduced up to 90% when exposed to phosphate-buffered saline (100% acetonitrile vs. 100% DPBS pH 7.4). Moreover, the emission maximum undergoes a red shift of 40 nm from 100% acetonitrile to 100% DPBS. By exchanging 25% of solvent to buffer, the fluorescence intensity is already decreased by 54%. At an equal mixture, the intensity is reduced by 70%. A saturation seems to be reached at around 25% acetonitrile and 75% DPBS pH 7.4. The excitation of all spectra was adjusted to 372 nm, which displayed the spectral intersection of solvent and buffer for BADAN. The results have been repeated and are in accordance with the literature.

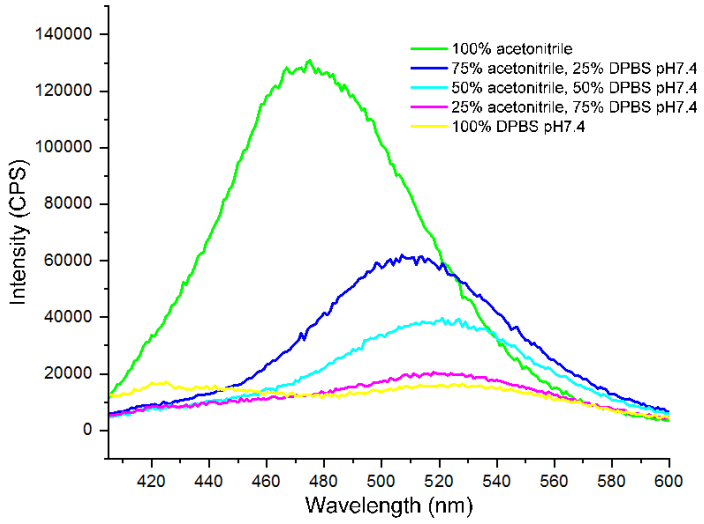

Figure 20: Polar-sensitivity BADAN: Fluorescence emission spectra of BADAN in different concentration ratios of acetonitrile and DPBS pH 7.4 (in accordance with literature).

3.6.1.2 Glucose sensitivity of GGBP-BADAN

According to the literature, both the fluorescence intensity as well as lifetime of BADAN show a linear dependency towards glucose concentrations between 0 and 100mM when linked to the mutated glucose galactose binding protein GGBP-H152C/A213R/L238S at position 152. Furthermore, the fluorescence is increased by 200% on the addition of glucose from 0 mM to 150 mM with a binding constant (Kd) of 11 mM.(91)

To validate the results according to the literature, emission spectra of GGBP-H152C/A213R/L238S-BADAN were recorded at different glucose concentrations ranging from 0 mM to 200 mM, one representative spectrum for each concentration. The emission profiles are depicted in **figure 21**.

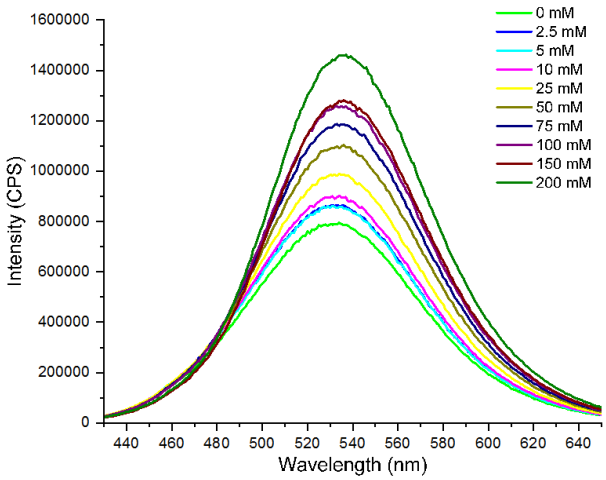

Figure 21: Fluorescence emission spectra of GGBP-H152C/A213R/L238S-BADAN in response to different glucose concentrations between 0mM and 200 mM Glucose at pH 7.4. Excitation of all spectra was at 397 nm. The fluorescence increases by 190% on addition of 200 mM glucose. The emission maximum is slightly red shifted by 4 nm.

BADAN, when attached to the GGBP mutant, shows an 184 % total fluorescence increase upon binding of 100 mM glucose. The emission maxima show a small red shift of 4nm upon binding of 200 mM glucose compared to 0 mM glucose. To obtain the binding constant of the mutant, single data points of the emission maxima at different glucose concentrations (0-200 mM) at 533 nm were fitted. The graphs are shown in **figure 22**.

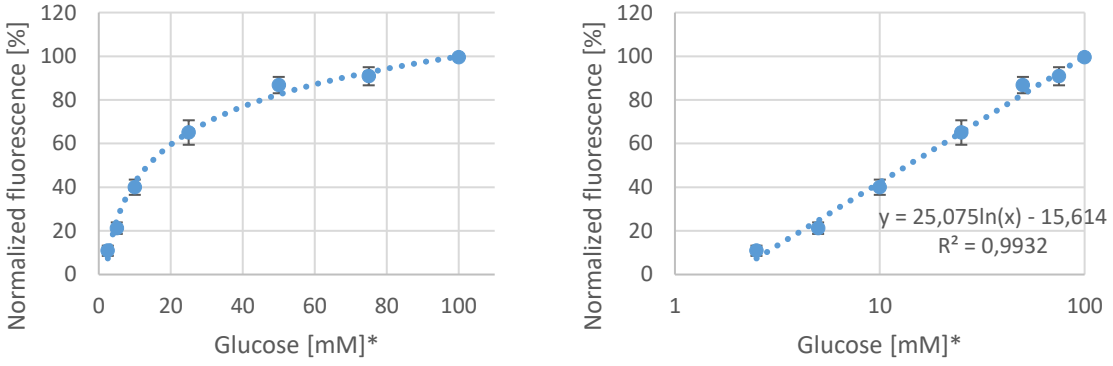

Figure 22: The fluorescence of GGBP-H152C/A213R/L238S-BADAN shows a linear correlation between 2.5 mM and 100 mM.
*Three technically independent replicates are shown. The statistical variance is represented by the standard error of the mean (SEM).

A binding constant of 20 mM was obtained A linear fit of three technically independent replicates resulted in an exceptionally good linear correlation coefficient of 0.99 with an

operating window from 2.5-100 mM of glucose. Furthermore, GGBP-H152C/A213R/L238S-BADAN was tested for different decimal concentrations of glucose ranging from 1 µM to 1 M.

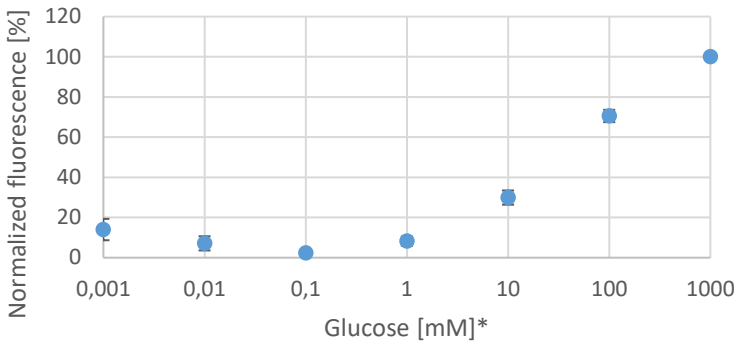

Figure 23: Glucose dependency of GGBP-H152C/A213R/L238S-BADAN between 1 µM and 1 M.
*Three technically independent replicates are shown. The statistical variance is represented by the standard error of the mean (SEM).

Interestingly, the labeled mutant seems to have not only a correlation between 1 mM and 100 mM but as well a correlation between 1 mM and 1000 mM (1 M). It should be noted, that GGBP-H152C/A213R/L238S-BADAN even shows a reversed correlation for glucose concentrations below 1 µM where the fluorescence increases with decreased concentrations. However, the difference in the total fluorescence amounts 10% on average from one power of ten to another without a statistical significance. The graph is shown in **figure 23**.

3.7 Dyomics Dyes have optimized environmental sensitive fluorescence properties when bound to proteins

The Dyomics dyes DY V11, DY 610 and DY 490 were chosen because of their known enhanced properties when bound to proteins. The structures of these dyes can be found here.

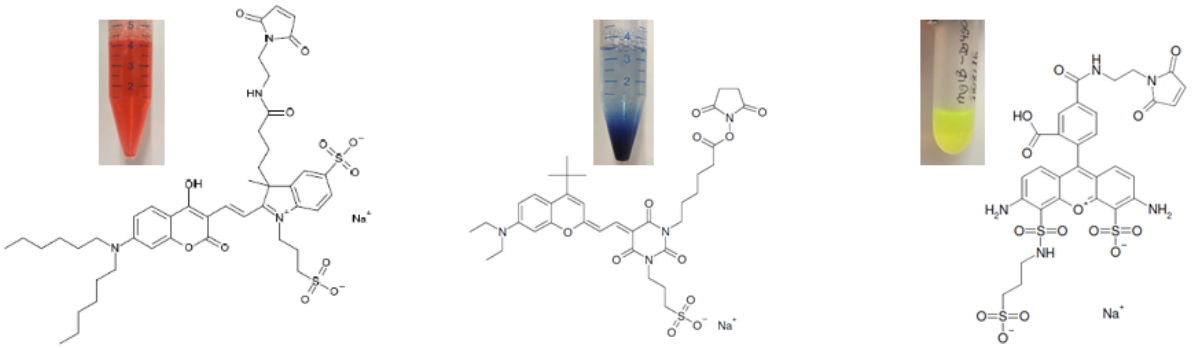

DY V11 DY 610 DY 490

3.7.1 Spectral Characteristics of DYV11 and GGBP-DYV11

DY V11 was kindly provided from Dyomics GmbH, Jena, Germany. DY11 was dissolved in DMSO and DPBS pH 7.4 for the characterization of excitation and emission profile (see **figure 26**). When DY V11 is dissolved in DMSO an excitation band from about 425 nm to 525 nm with a local maximum at 509 nm was observed. Compared to the excitation spectrum, the emission band is relatively broad and spans from 525 nm to 700 nm with a local maximum at 560nm. Hence, DY V11 shows a large stokes shift of 51 nm. When the dye is dissolved in DPBS pH 7.4, the excitation maximum undergoes a blue-shift of 14 nm to 495 nm and the emission maximum undergoes a large red shift of 40 nm, to 600 nm, respectively. This results in an extremely large stokes shift of 105 nm for DY V11 when dissolved in phosphate buffer at pH 7.4. The bandth withs do not undergo a remarkable change. It must be noted that the total fluorescence emission of DY V11 in DPBS pH 7.4 is extremely reduced (by 98%, see chapter 3.7.1.1) which resulted in a less optimal normalization of the spectra overall in **figure 24** and **25** as the statistical variance in fluroescence was highly increased.

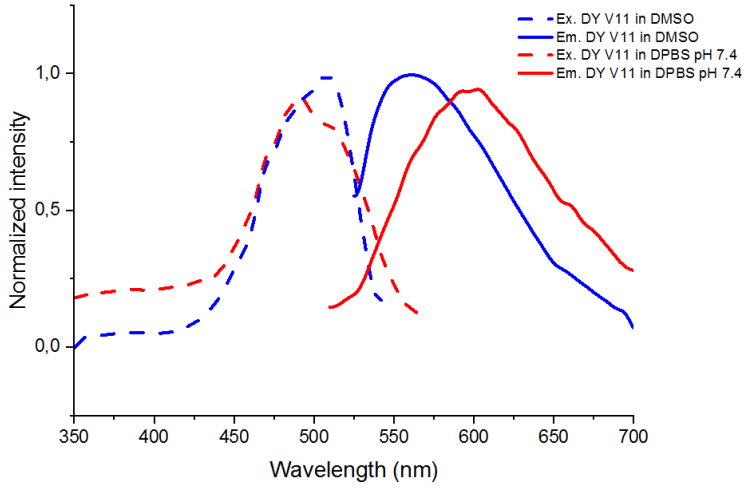

Figure 24: Excitation and emission spectra from DYV11 in DMSO and DPBS pH 7.4 at concentrations of 1 ng/ml.

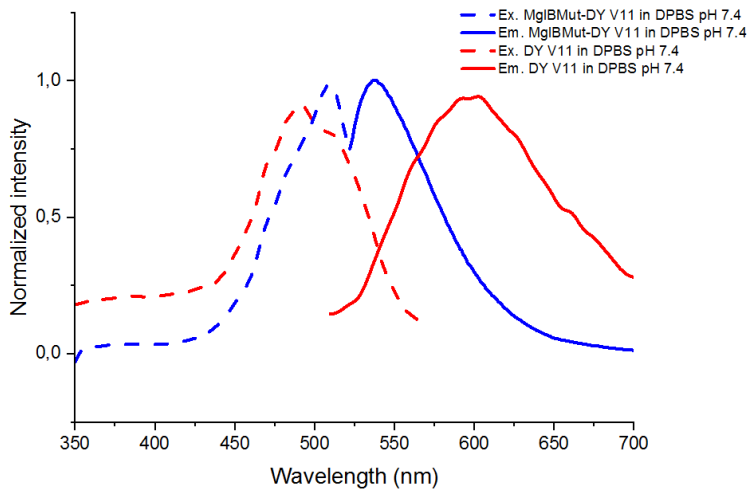

Figure 25: Excitation and emission spectra from DYV11 covalently bound to the triple mutation GGBP-H152C/A213R/L238S are compared to the excitation and emission profile of unlabelled DYV11.

When DY V11 is bound to position 152 in GGBP (in aquaeous, buffered solution), the excitation spectrum is further shifted to longer wavelengths (+17nm) with an excitation maximum of 512 nm. Interestingly, the emission spectrum shows a more distinct band from 525 nm to 600nm with an emission maximum at 538 nm. As a result, the stokes shift of 105 nm that DY V11 shows when dissolved in DPBS pH 7.4 is highly reduced to 26 nm when the dye is bound to the GGBP mutant. The results can be found in **figure 25**.

3.7.1.1 Polar-Sensitivity DY V11

DY V11 was dissolved in concentrations of 1 ng/ml in DMSO and phosphate-buffer (pH 7.4) and emission spectra were recorded. Gradient solvent mixtures of the dye at equal concentrations in 75% DMSO, 50% DMSO and 25% DMSO were filled up with buffer (DPBS pH 7.4) and measured. The fluorescence emission spectra of the gradient solvent mixtures were excited at 495 nm (local maximum of DY V11 in DPBS pH 7.4). The spectra are shown in **figure 26**.

DY V11 shows a strong fluorescence emission when dissolved in pure DMSO (700.000 CPS) with a broad emission band. By adding 25% of DPBS at physiological pH (75%DMSO), the fluorescence of DY V11 is already reduced by 63% with an emission maximum at 582 nm. For the samples of 50% and 25% of DMSO, the fluorescence emission is further reduced by 87% and 94%, respectively. The emission maxima are further shifted to longer wavelengths with 595 nm and 597 nm for the above-mentioned samples, respectively. When DY V11 is dissolved in 100% DPBS, the fluorescence intensity is extremely reduced by 98% when compared to 100% DMSO. However, DY V11 is still highly soluble in DPBS. The emission maxima of the 100% DPBS sample stays at 600 nm, as described in chapter 3.7.1. For all experiments, the

excitation wavelength was at the excitation maximum of DY V11 dissolved in 100% DMSO (419 nm) and 100% DPBS pH 7.4, namely at 502 nm.

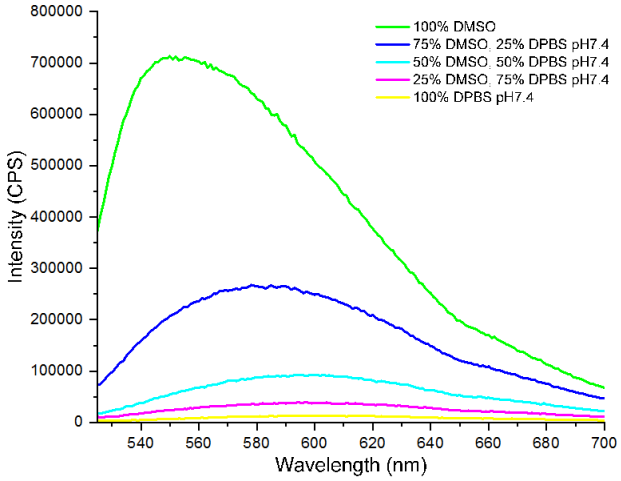

Figure 26: Polar-sensitivity DY V11: Fluorescence emission spectra of DY V11 in different concentration ratios of DMSO and DPBS pH 7.4.
* Excitation of all spectra was at 502 nm (Mean value of excitation wavelengths of DY V11 in DMSO and DPBS pH 7.4. DY V11 was kindly provided from Dyomics GmbH, Jena, Germany.

3.7.1.2 Glucose sensitivity of GGBP-H152C/A213R/L238S-DY V11

GGBP-H152C/A213R/L238S-DY V11 was tested for a linear dependency of different glucose concentrations in the mM range. Two biological and each four technically independent replicates show a statistically significant linear dependency of the protein-dye complex from 2.5 to 100 mM with a 26% total fluorescence increase. A good correlation of the linear dependency was obtained (R square of 0.96). The results are shown in **figure 27**.

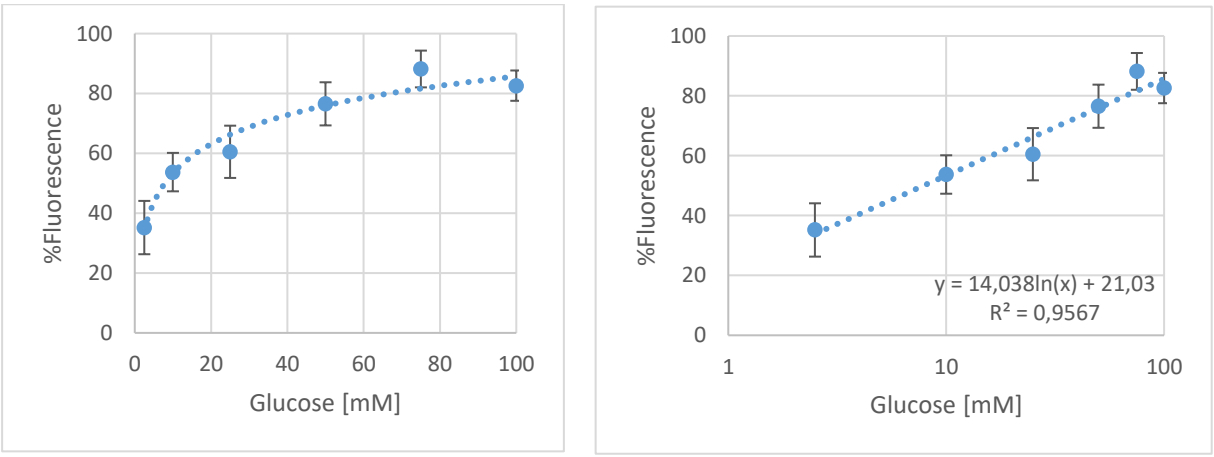

Figure 27: Glucose dependency of the fluorescence intensity of GGBP-H152C/A213R/L238S-DY V11 between 2.5 mM and 100 mM.
*Eight technically independent replicates and two biological independent replicates are shown. Variance is represented by the standard error of the mean (SEM). The replicate experiments were done by our bachelor student Tatjana Roth under my supervision.

3.7.2 Spectral Characteristics of DY 610 and GGBP-DY610

DY 610 was kindly provided from Dyomics GmbH, Jena, Germany. DY 610 was dissolved in DMSO as well as DPBS pH 7.4 for the characterization of excitation and emission properties (see **figure 28**). The excitation spectrum of DY 610 spans from 450-625 nm for both solvents, DMSO and DPBS in which three local maxima could be found: one shoulder at 520 nm, one local maximum at 565 nm and the global maximum at 613 nm. The excitation maximum in DPBS is slightly blue shifted to 602 nm. The dye shows an emission band of 630 nm to about 700 nm with a local maximum at 642 nm and 640 nm in DMSO and DPBS, respectively. DY 610 displays a stoke shift of 29 nm and an increased stokes shift of 38 nm when dissolved in DMSO and DPBS, repsectively. Hence, the solvent effect of the buffered solution increases the stokes shift by almost 10 nm.

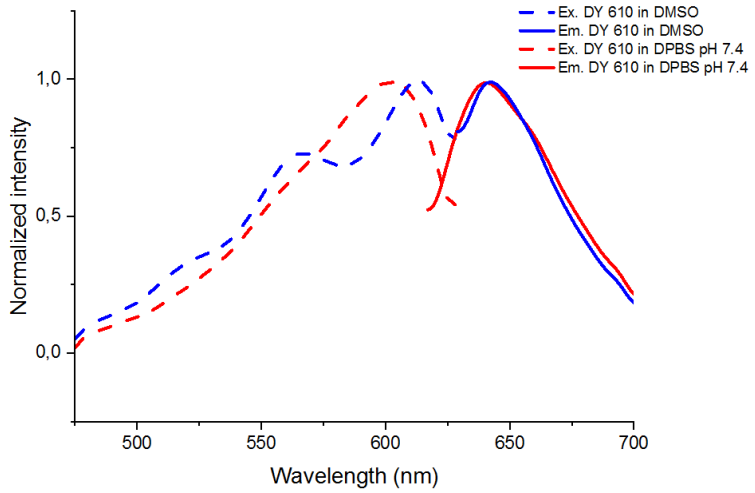

Figure 28: Excitation and emission spectra from DY 610 in DMSO and DPBS pH 7.4 at concentrations of 1 ng/ml. DY 610 was kindly provided from Dyomics GmbH, Jena, Germany.

When DY 610 is bound to the cysteine residue in mutant GGBP-H152C/A213R/L238S (=GGBP-DY 610), the excitation maximum is red shifted with a fluorescence maximum at 612 nm, similar to the maximum shown in DMSO (613 nm). The emission profile, however, is very similar to the emission of the unbound state with a maximum at 639 nm. The band widths of the excitation and emission profiles from GGBP stay constant from 450-620nm and 625-700 nm, respectively. The stokes shift is decreased to 27 nm when DY 610 is bound to the GGBP mutant form. The results can be found in **figure 29**.

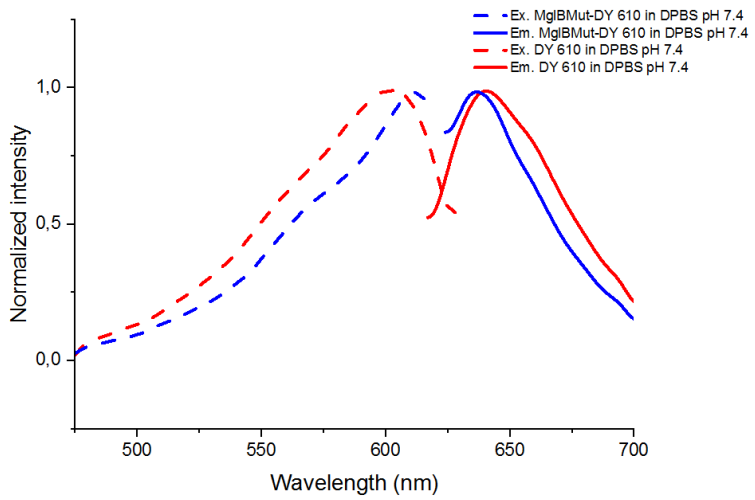

Figure 29: Excitation and emission spectra from DY 610 covalently bound to the triple mutation GGBP-H152C/A213R/L238S are compared to the excitation and emission profile of unlabelled DY 610. DY 610 was kindly provided from Dyomics GmbH, Jena, Germany.

3.7.2.1 Polar-Sensitivity

DY610 was dissolved in equal concentrations (1 ng/ml) in DMSO and phosphate-buffered saline and emission spectra were recorded. Gradient solvent mixtures of the dye in 75% DMSO, 50% DMSO and 25% DMSO were produced and filled up with buffer. Similarly, the emission spectra of the gradient solvent mixtures were measured. The spectra are shown in **figure 30**.

The fluorescence emission spectra of the 100% DMSO and 75% DMSO samples show a strong total fluorescence of about 780.000 CPS with emission maxima at 642 nm and 644 nm, respectively. The total fluorescence emission of the 50% DMSO/50% DPBS sample is reduced by 32% to 530.000 CPS. Furthermore, the total fluorescence of the 25% DMSO sample is reduced by 67% when compared to 100% DMSO. The emission maxima for DY 610 dissolved in 75%, 50% and 25% DMSO stay at 644nm. However, when DY 610 is dissolved in 100% DPBS at pH 7.4, and the emission maximum is shifted to 640nm. It must be noted that the overall fluorescence emission is highly reduced by 93% when dissolved in phosphate-buffered saline.

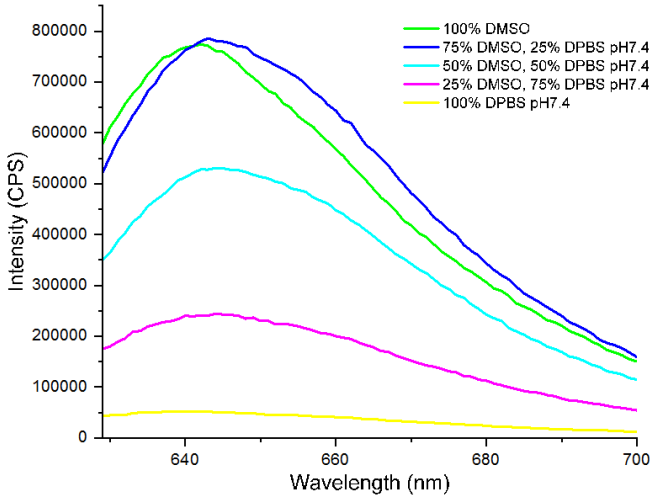

Figure 30: Polar sensitivity DY 610: Fluorescence emission spectra of DY610 in different concentration ratios of DMSO and DPBS pH 7.4.
* Excitation of all spectra was at 607 nm (Mean value of excitation wavelengths of DY 610 in DMSO and DPBS pH 7.4. DY 610 was kindly provided from Dyomics GmbH, Jena, Germany.

3.7.2.2 Glucose sensitivity of GGBP-H152C/A213R/L238S-DY 610

Solutions of the labeled mutant GGBP-H152C/A213R/L238S-DY 610 were tested towards different glucose concentrations between 0 and 100mM. Eight technical as well as two biological independent replicates show a statistically significant increase of 19% total fluorescence upon binding of 100 mM glucose with an acceptable linear correlation (R square of 0.96). The values for the standard error of the mean were increased due to the low relative total fluorescence of the dye. The results are shown in **figure 31**.

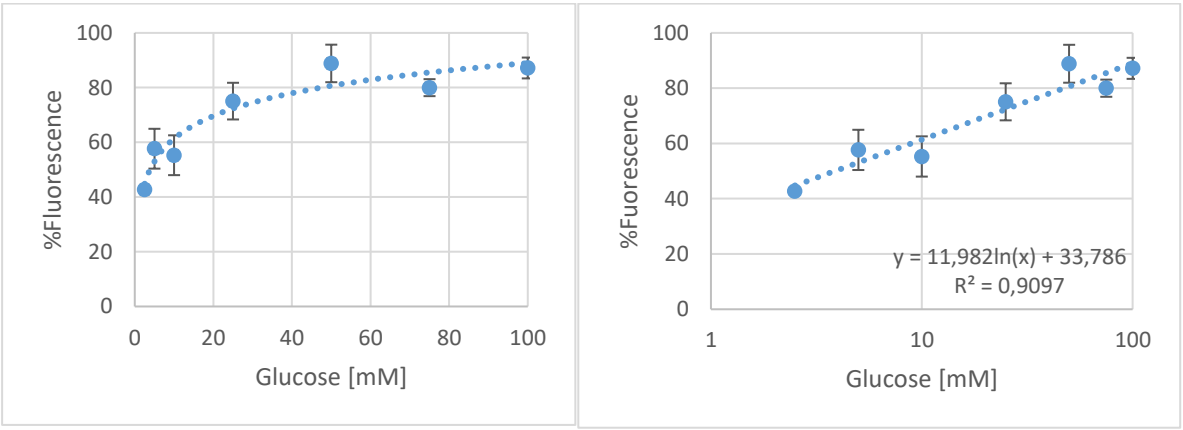

Figure 31: Glucose dependency of the fluorescence intensity of GGBP-H152C/A213R/L238S-DY 610 between 2.5 mM and 100 mM.
*Eight technically independent replicates and two biological independent replicates are shown. Variance is represented by the standard error of the mean (SEM). DY 610 was kindly provided from Dyomics GmbH, Jena, Germany.

Showing a 40% fluorescence already at 2.5 mM glucose indicated that this compound shows a larger analytical range when attached to GGBP. Therefore, DY 610 was tested for a broader

range of glucose concentrations from 1µM to 100 mM. A total fluorescence increase of 21% was obtained upon binding of 100 mM glucose. High linear correlation was observed (0.99). It must be noted that only three technically replicates are considered in the following graph. The results are shown in **figure 32**.

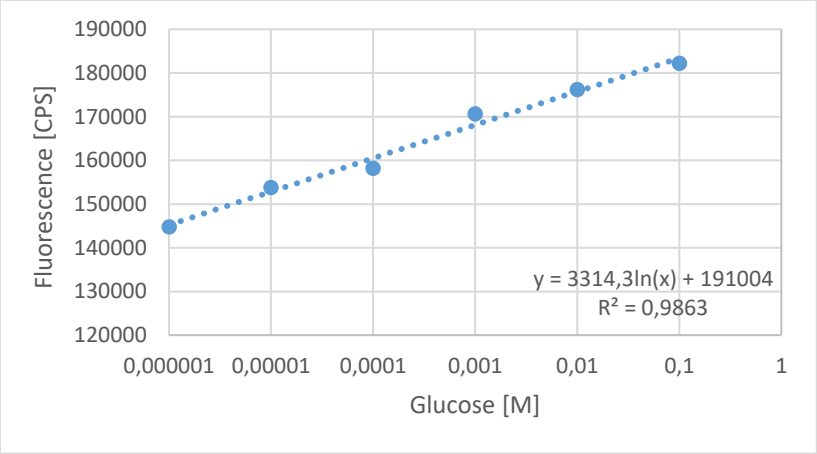

Figure 32: Glucose dependency of GGBP-H152C/A213R/L238S-DY 610 between 1 µM and 100 mM.
*Three technical independent replicates are shown. Variance is represented by the standard error of the mean (SEM). DY 610 was kindly provided from Dyomics GmbH, Jena, Germany.

3.7.3 Spectral Characteristics of DY490 and GGBP-DY490

DY 490 was kindly provided from Dyomics GmbH, Jena, Germany. DY 490 is an optimized derivative of Alexa 488 with a fluoresceine backbone, which was traditionally used in fluorescence microscopy applications due to its strong fluorescence in phosphate buffered solutions. It displays therefore a unique role compared to the other fluorescent dyes that have been tested in this work. However, fluorescein is very photosensitive for which reason optimized dyes such as Alexa Fluor 488 (ThermoFisher) and DY 490 (Dyomics GmbH), an alternative to Alexa Fluor 488, have been designed.

DY 490 was dissolved in DMSO, as well as in DPBS pH 7.4 for the determination of excitation and emission characteristics. The spectra are shown in **figure 33**. DY 490 shows steep excitation as well as emission bands from 400-500 nm and 515-650nm, respectively, with an excitation maximum at 497 nm as well as an emission maximum at 527 nm when dissolved in DMSO. When DY 490 is dissolved in DPBS pH 7.4,the excitation and emission maxima are blue shifted by 7 nm and 10 nm and show an excitation maximum at 490 nm as well as an emission maximum at 517 nm. The stokes shifts is represented by 30 nm and 27 nm, for DMSO and DPBS, respectively.

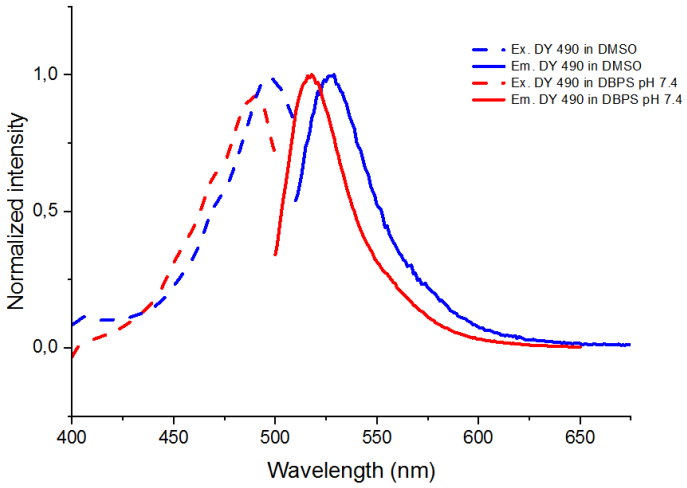

Figure 33: Excitation and emission spectra from DY 490 in DMSO and DPBS pH 7.4 at concentrations of 1 ng/ml. DY V11 was kindly provided from Dyomics GmbH, Jena, Germany.

When DY 490 is bound to cysteine at position 152 in GGBP-H152C/A213R/L238S (in aquaeous, buffered solution), the excitation as well as the emission profile is identical compared to the excitation and emission of the unbound state in DMSO and DPBS. Moreover, the excitation and emission maxima as well as the stokes shifts are identical to the unbound state. It seems that the fluorescence of DY490 stays unaffected when bound to GGBP. The results can be found in **figure 34.**

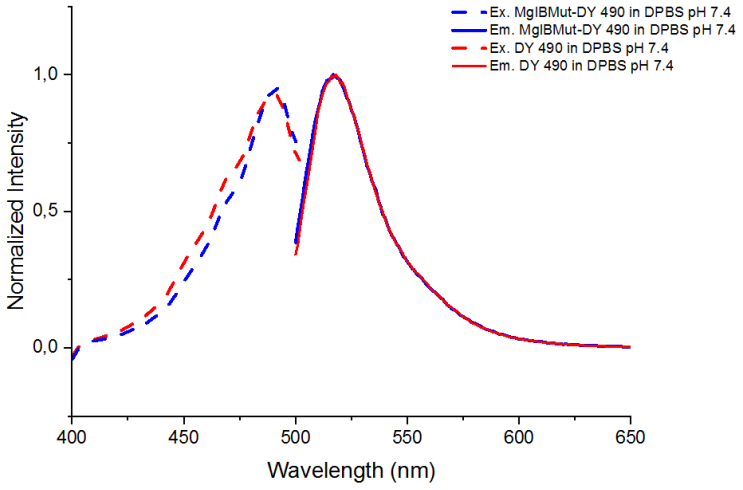

Figure 34: Excitation and emission spectra from DY 490 covalently bound to the triple mutation GGBP-H152C/A213R/L238S are compared to the excitation and emission profile of unlabelled DY 490.
This dye was kindly provided from Dyomics GmbH, Jena, Germany.

3.7.3.1 Polar-Sensitivity

DY 490 was dissolved in equal concentrations (1 ng/ml) in DMSO and phosphate-buffered saline and emission spectra were recorded. Gradient solvent mixtures of the dye in 75%

DMSO, 50% DMSO and 25% DMSO were produced and filled up with buffer. Similarly, the emission spectra of the gradient solvent mixtures were measured. The spectra are shown in **figure 35**.

Since DY 490 shows strong absorbance as well as a strong emission (high quantum yield) in phosphate buffered solution, the maximum total fluorescence emission is obtained at 100% DPBS pH 7.4 with almost one million counts (CPS). Fluorescence emission spectra of DY 490 dissolved in 25% and 50% DMSO show decreased total fluorescence emission by 6% as well as 38% with emission maxima at 520 nm and 522 nm, respectively. When DY 490 is dissolved in 75% of DMSO, the fluorescence emission is highly reduced by 94% to 53.000 CPS. The emission maximum in 75% DMSO is further increased to 523 nm. The lowest fluorescence is obtained at 100% DMSO with only 3000 CPS and a loss in total fluorescence of 99,7%. This indicates the dye having almost no quantum yield when dissolved in organic solvent. The overall emission maxima undergo a blue shift of 9 nm from 527 nm to 518 nm, for 100% DMSO to 100% DPBS, respectively. Excitation of all spectra was at the excitation maximum of DY 490 dissolved in 100% DPBS pH 7.4 (490 nm).

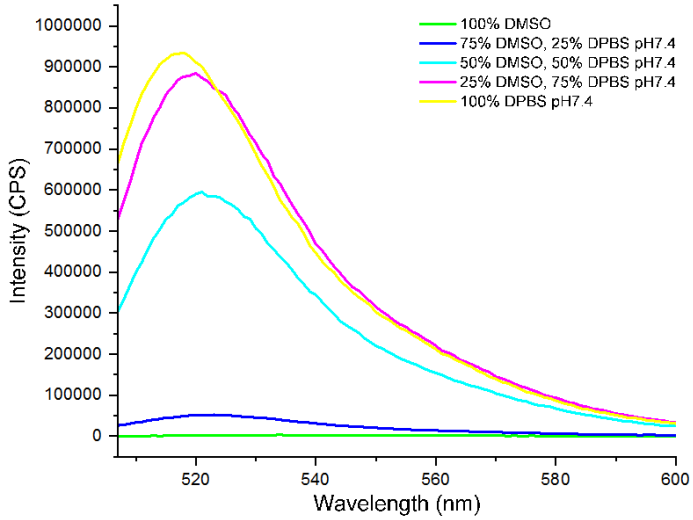

Figure 35: Polar sensitivity of DY 490: Fluorescence emission spectra of DY490 in different concentration ratios of DMSO and DPBS pH 7.4.
* Excitation of all spectra was at 490 nm (excitation maximum of DY 610 in DPBS). This dye was kindly provided from Dyomics GmbH, Jena, Germany.

3.7.3.2 Glucose Sensitivity of GGBP-H152C/A213R/L238S-DY 490

The labeled mutant of GGBP-H152C/A213R/L238S-DY 490 was tested at different glucose concentration between 0 and 100mM. Six technical as well as two biological independent

replicates show a statistically significant increase of 25% maximal fluorescence intensity upon binding of 100 mM glucose with an acceptable correlation (R square of 0.90). However, compared to other correlation coefficients, DY490 attached to GGBP shows only intermediate results. The results are shown in **figure 36**.

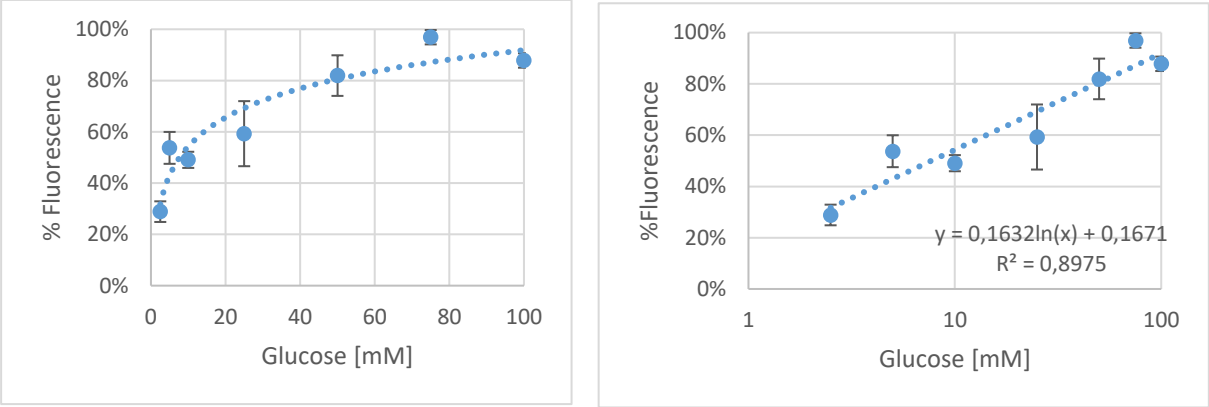

Figure 36: Glucose dependency of the fluorescence intensity of GGBP-H152C/A213R/L238S-DY 490 between 2.5 mM and 100 mM.
*Six technically independent replicates and two biological independent replicates are shown. Variance is represented by the standard error of the mean (SEM).

3.8 Atto Dyes are highly effective environmental sensitive dyes in aqueous solutions

Atto-Dyes from the company Atto Tec GmbH in western Germany show improved fluorescence properties over conventional dyes. They show strong absorptions and high quantum yields. Especially in aqueous solution where most dyes strongly lose the ability for strong absorption with increasing excitation wavelengths, Atto dyes show improved results. In this work, three dyes with excitation wavelengths above 400 nm were commercially purchased and tested. Atto 425 was chosen because its strong structural similarities to BADAN. The fluorophore of Atto 425 (structure in the backup of this work) represents a coumarin backbone with functional side chains. Like the coumarin structure in BADAN, yet less distinct, Atto 425 displays a characteristic high stokes shift. Atto 465 and Atto 495, two dyes excited at longer wavelengths show a characteristic small structure with a rigid acridine orange backbone. Both dyes differentiate themselves by an Acriflavine structure (2 amino groups in meta position) in Atto 465 (structure attached in backup) and methylated amino groups of Acriflavine in Atto 495. All three dyes were chosen due to their small, rigid structure, and their strong absorption capabilities. The characteristics of the dyes in aqueous solution and the results of glucose sensitivity of the conjugated dyes to GGBP attached to the cysteine residue in position 152 are shown in the following.

3.8.1 Spectral characteristics of Atto 425 and GGBP-Atto 425

Atto 425 was dissolved in DMSO, as well as in DPBS pH 7.4 for the determination of excitation and emission maxima wavelengths (**see figure 37**).

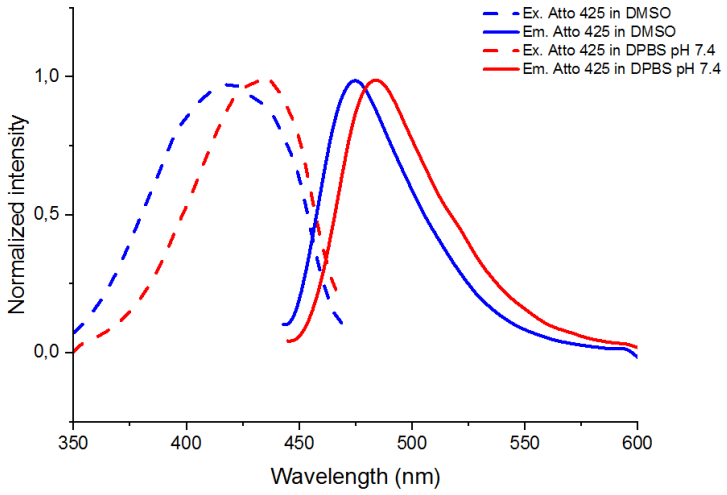

Figure 37: Excitation and emission spectra from the coumarin derivative compound Atto 425 dissolved in DMSO and DPBS pH 7.4 at concentrations of 1 ng/ml.

The excitaton maximum in solvent is at 419nm and shows a large red shift emission maximum of 56 nm at 475 nm. When dissolved in DPBS pH 7.4, the excitation maximum is shifted to 434 nm whereas the emission is shifted to 484 nm. When Atto 425 is bound to position 152 in GGBP (in aquaous, buffered solution), the excitation and emission spectra are comparable to the unbound state. The excitation and the emission maxima are at 436 nm and 482 nm respectively. The results can be found in **figure 38**.

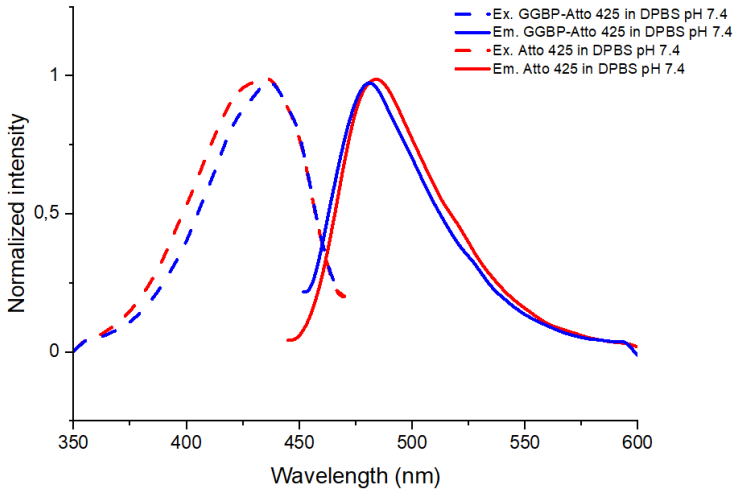

Figure 38: Comparison of excitation and emission spectra from Atto 425 and GGBP-H152C/A213R/L238S-Atto425. Excitation and emission spectra from Atto 425 are shown in its free state and upon covalent attachment to the triple mutation GGBP-H152C/A213R/L238S in Dubelco's phosphate buffered saline (DPBS pH 7.4).

3.8.1.1 Polar-Sensitivity

Atto 425 was dissolved in equal concentrations (1 ng/ml) in DMSO and phosphate-buffered saline and emission spectra were recorded. Gradient solvent mixtures of the dye in 75% DMSO, 50% DMSO and 25% DMSO were produced and filled up with buffer. Similarly, the emission spectra of the gradient solvent mixtures were measured. The spectra are shown in **figure 39**.The fluorescence emission spectra of Atto 425 dissolved in 100%, 75% and 25% DMSO show a similar strong total fluorescence of around 500.000 CPS at a concentration of 1 ng/ml. Interestingly, the emission spectrum of the 50% DMSO, 50% DPBS mixture sample shows an 55% increase in total fluorescence with a maximum at 483 nm. The emission maxima undergo a red shift of 5 nm from 475 nm to 482 nm, for 100% DMSO to 100% DPBS, respectively. It must be noted that the emission maxima from 100% to 25% DMSO are continuously increasing up to 484 nm and then undergo a blue shift of 2 nm to 482 nm. The overall fluorescence emission of Atto 425 decreases by 60% when exposed to phosphate-buffered saline. Excitation of all spectra was at the excitation maximum of Atto 425 dissolved in 100% DMSO (419 nm) which represents the maximum band in DPBS pH 7.4 (419-435 nm).

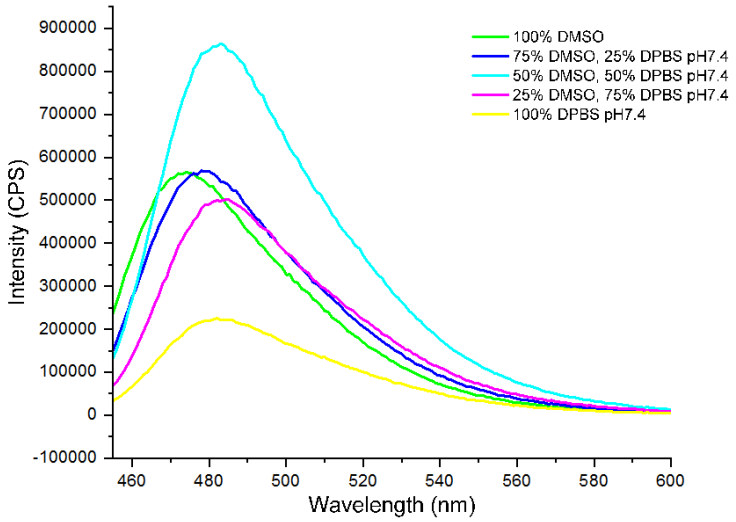

Figure 39: Polar sensitivity of Atto 425: Fluorescence emission spectra of Atto 425 in different concentration ratios of DMSO and DPBS pH 7.4. All spectra were excited at 419 nm (exc. max. of Atto 425 in DMSO).

3.8.1.2 Glucose Sensitivity of GGBP-H152C/A213R/L238S-Atto 425

The labeled mutant of GGBP-Atto 425 was tested at different glucose concentration between 0 and 100mM. Technical as well as biological independent replicates show a statistically significant increase of 27% maximal fluorescence upon binding of 75 mM glucose with a good fit (R square of 0.96). When Atto 425 is bound to GGBP, the Kd value of the mutant is slightly decreased compared to GGBP-BADAN. The results are shown in **figure 40**.

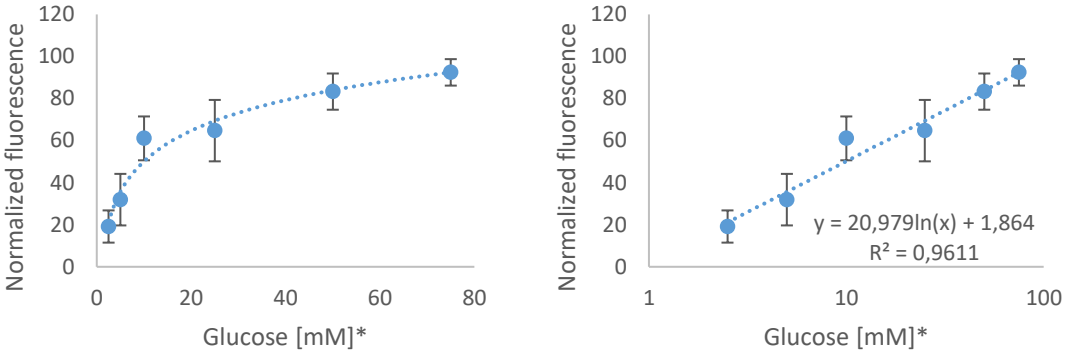

Figure 40: Glucose dependency of the fluorescence intensity of GGBP-H152C/A213R/L238S-Atto 425 between 2.5 mM and 75 mM.
*Six technically independent replicates and two biological independent replicates are shown. Variance is represented by the standard error of the mean (SEM). The replicate experiments were done by our bachelor student Tatjana Roth under my supervision.

3.8.2 Spectral characteristics of Atto 465 and GGBP-Atto 465

For characterization, Atto 465 was dissolved in DMSO, as well as in DPBS pH 7.4 for the determination of excitation and emission maxima wavelengths (see **figure 41**). Atto 465 shows a broad excitation band from 360-500 nm with an excitation maximum at 468 nm when dissolved in DMSO. With an emission maximum at 498 nm, it displays a relatively large stokes shift of 30 nm. However when dissolved in DPBS pH 7.4, the excitation maximum undergoes a blue-shift of 18 nm and the emission maximum a red shift of 7 nm, to 450 nm and 505 nm, respectively. It has to be noted, that the solvent effect of phosphate-buffere saline increases the stokes shift of Atto 465 to 55 nm as well as the excitation band width remarkably.

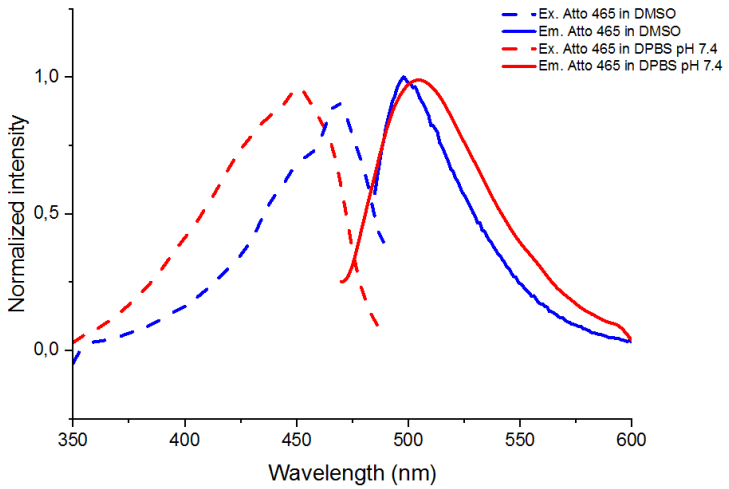

Figure 41: Excitation and emission spectra from the Acridine-orange derivative compound Atto 465 dissolved in DMSO and DPBS pH 7.4 at concentrations of 1 ng/ml.

When Atto 465 is bound to position 152 in GGBP (in aquaeous, buffered solution), the emission profile is highly similar compared to the emission in DMSO. The excitation band remains distinct narrow compared to the excitation profile of the unbound state in DMSO. However, the the stokes shift is shortened to 40 nm with an excitation maximum of 460 nm and an emission maximum of 499 nm, respectively. The results can be found in **figure 42**.

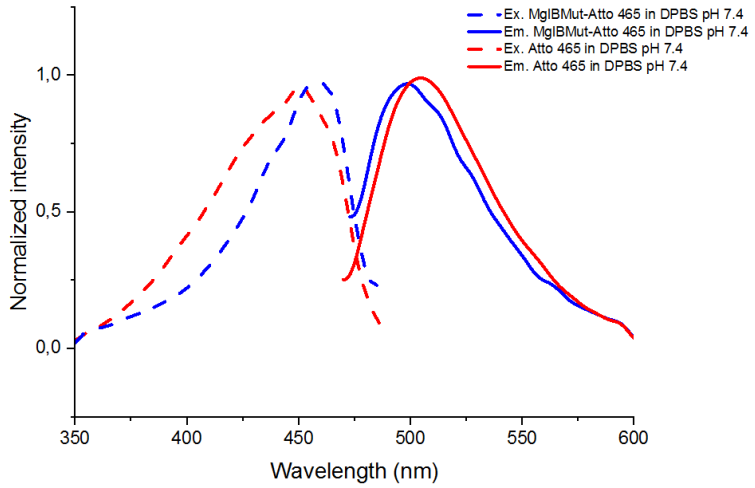

Figure 42: Comparison of excitation and emission spectra from Atto 465 and GGBP-H152C/A213R/L238S-Atto465. Excitation and emission spectra from Atto 465 are shown in its free state and upon covalent attachment to the triple mutation GGBP-H152C/A213R/L238S in Dubelco's phosphate buffered saline (DPBS pH 7.4).

3.8.2.1 Polar-Sensitivity of Atto 465

Atto 465 was dissolved in equal concentrations (1 ng/ml) in DMSO and phosphate-buffered saline and emission spectra were recorded. To identify the ability of the dye to have environmental sensitive properties, gradient solvent mixtures of the dye in 75% DMSO, 50% DMSO and 25% DMSO were produced and filled up with phosphate-buffer saline. Similarly, the emission spectra of the gradient solvent mixtures were measured. The spectra are shown in **figure 43**.

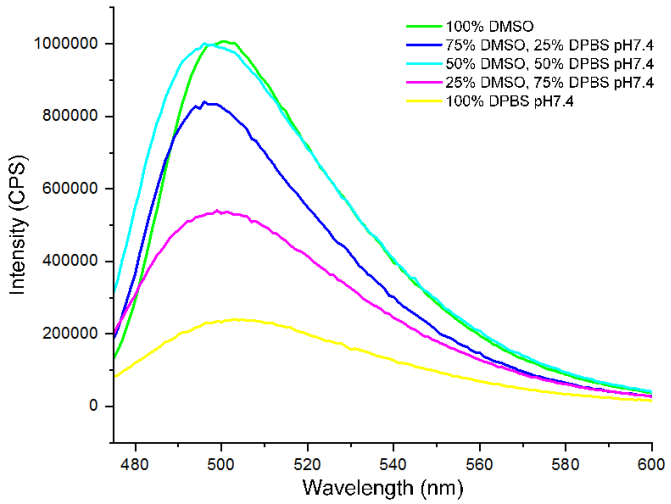

Figure 43: Polar sensitivity of Atto 465: Fluorescence emission spectra of Atto 465 in different concentration ratios of DMSO and DPBS pH 7.4. All spectra were excited at 450 nm (exc. max. of Atto 425 in DMSO. This graph was accomplished by our intern Laura Freitag under my supervision.

The sample dissolved in 100% DMSO shows a high total count of 1.000.000 CPS at a concentration of 1ng/ml. The fluorescence of Atto 465 in organic solvent (DMSO) is decreased by 76 % when exposed to 100% phosphate-buffered saline. Interestingly, the samples of Atto 465 dissolved in 50% DMSO, shows a similar high total fluorescence compared to the 100% sample. The fluorescence of the dye dissolved in 75% DMSO is decreased by 17% and further decreased by 46% when exposed to 25% of DMSO. Overall, the total maximum fluorescence emission of Atto 465 remains relatively high when exposed to phosphate buffer at physiological conditions, with 240.000 CPS (1ng/ml). The emission maxima vary across the different samples only slightly between 497 nm (75% and 50% DMSO) and 503 nm (100% DPBS). Excitation of all spectra was at the excitation maximum with the lowest wavelength at 450 nm (Atto 465 in DPBS).

3.8.2.2 Glucose Sensitivity of GGBP-Atto465

Atto 465 was covalently attached to GGBP-H152C/A213R/L238S and exposed to glucose concentrations ranging from 0-100 mM. The maximal fluorescence intensity is shown to be linearly dependent by increasing glucose concentrations with a 36% total fluorescence intensity increase upon binding of 75 mM glucose. The 100 mM sample was excluded from the correlation as it resulted in a less good correlation coefficient. A correlation coefficient (R square = R^2) of 0.98 was obtained. The results are depicted in **figure 44**.

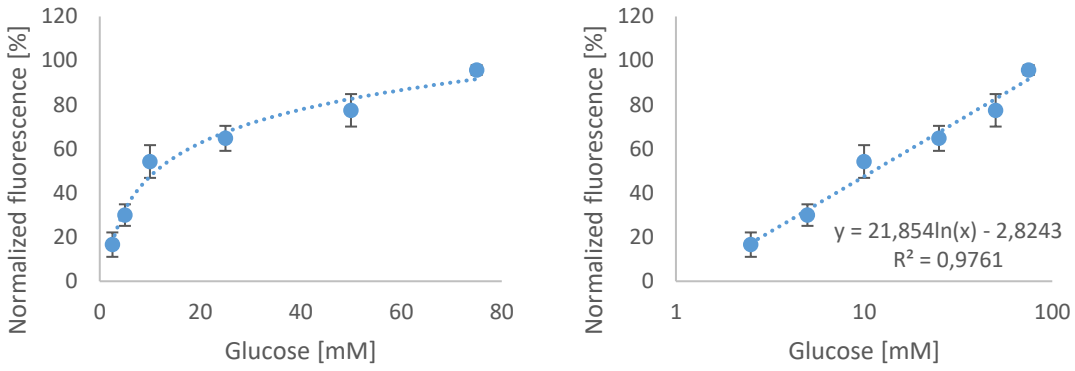

Figure 44: Glucose dependency of the fluorescence intensity of GGBP-H152C/A213R/L238S-Atto 465 between 2.5 mM and 75 mM.
*Nine technically independent replicates and two biological independent replicates are shown. Variance is represented by the standard error of the mean (SEM). The replicate experiments were done by our bachelor student Tatjana Roth under my supervision.

3.8.3 Spectral characteristics of Atto 495 and GGBP-Atto 495

Atto 495 was dissolved in DMSO, as well as in DPBS pH 7.4 for the determination of excitation and emission spectra (see **figure 45**).

Atto 495 shows a distinct excitation band from 450-550 nm with an excitation maximum at 500 nm when dissolved in DMSO. The emission maximum shows a stokes shift of 34 nm to 534 nm, hence it displays a comparably large stokes shift similarly to Atto 425. When dissolved in DPBS pH 7.4, the excitation maximum is decreased by 5 nm and the emission maximum displays a blue shift of 9 nm, to 495 nm and 525 nm, respectively. Under the influence of phosphate-buffered saline, the stokes shift of Atto 495 is only slightly reduced from 34 nm to 30 nm. It should be noted that the band widths of both, the excitation and emission spectra of Atto 495, do not undergo significant changes.

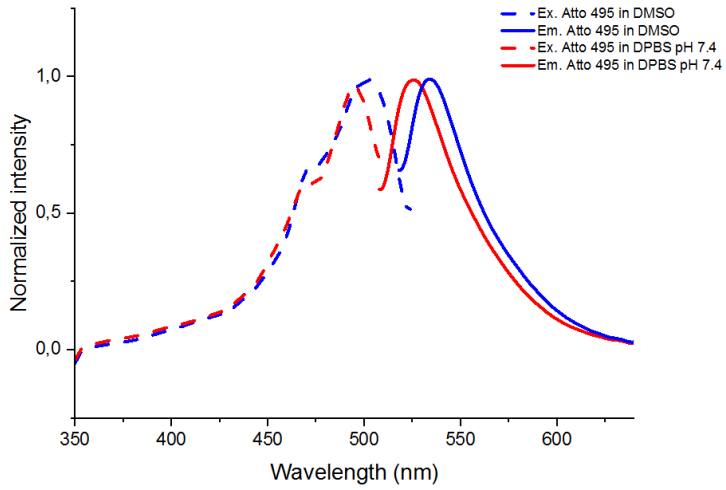

Figure 45: Excitation and emission spectra from the Acriflavine-orange derivative compound Atto 495 dissolved in DMSO and DPBS pH 7.4 at concentrations of 1 ng/ml. This graph was accomplished by our intern Laura Freitag under my supervision.

Upon attaching Atto 495 to position 152 in GGBP-H152C/A213R/L238S (in aquaeous, buffered solution), the excitation as well as the emission profile can be considered similar. However, the stokes shift becomes reduced to 25 nm with an excitation maximum at 500 nm and an emission maximum at 525 nm, respectively. This fact is shown in the less resolved overlap of the excitation and emission spectra of the protein-dye complex compared to the free dye. The results can be found in **figure 46**.

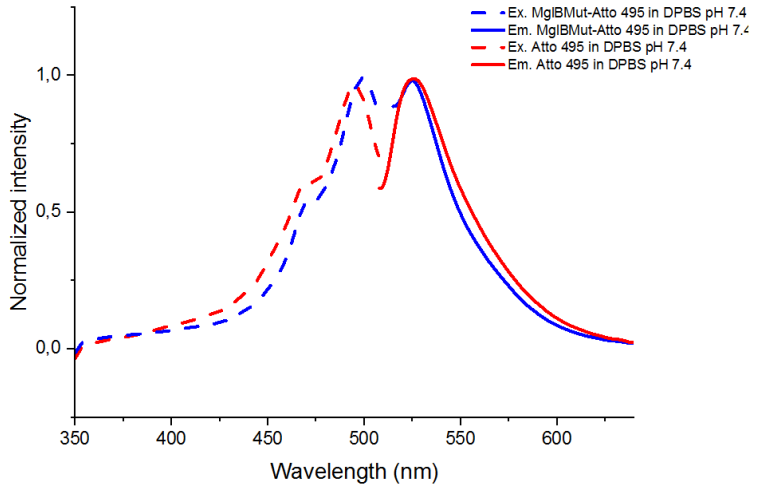

Figure 46: Comparison of excitation and emission spectra from Atto 495 and GGBP-H152C/A213R/L238S-Atto495. Excitation and emission spectra from Atto 495 are shown in its free state and upon covalent attachment to the triple mutation GGBP-H152C/A213R/L238S in Dubelco's phosphate buffered saline (DPBS pH 7.4). This graph was accomplished by our intern Laura Freitag under my supervision.

3.8.3.1 Polar-Sensitivity of Atto 495

Atto 495 was dissolved in equal concentrations (1 ng/ml) in DMSO and phosphate-buffered saline and emission spectra were recorded. Gradient solvent mixtures of the dye were measured at 75% DMSO, 50% DMSO and 25% DMSO which were filled up with phosphate-buffer saline. The emission spectra of the gradient solvent mixtures were measured. The spectra are shown in **figure 47**.

The highest total fluorescence is displayed by the Atto495 when dissolved in equal concentrations of DMSO and DPBS (50%/50%) with more than one million counts (1.270.000 CPS) with an emission maximum at 529 nm. Interestingly, the dye‘s fluorescence, when dissolved in 100% DMSO, is decreased by 13% compared to the 50% solvent concentration and shows the longest wavelength at 534 nm. The fluorescence of the dye dissolved in 75% DMSO is decreased by 9% and is decreased by 37% when exposed to 25% of DMSO (both values compared to 100% DMSO). The fluorescence of Atto 495 in DMSO is decreased by 81 % when exposed to 100% phosphate-buffered saline. It implies also for this Acriflavine

derivative that the total maximum fluorescence emission of Atto 495 remains similarly high when exposed to phosphate buffer at physiological conditions, with 245.000 CPS (1ng/ml). The emission maxima constantly increase from 526 nm to 534 nm for 0% and 100% DMSO, respectively. This reflects a blue shift in the emission maxima when DMSO is exchanged by DPBS. Excitation of all spectra was at the excitation maximum with the lowest wavelength at 495 nm (Atto 495 in DPBS).

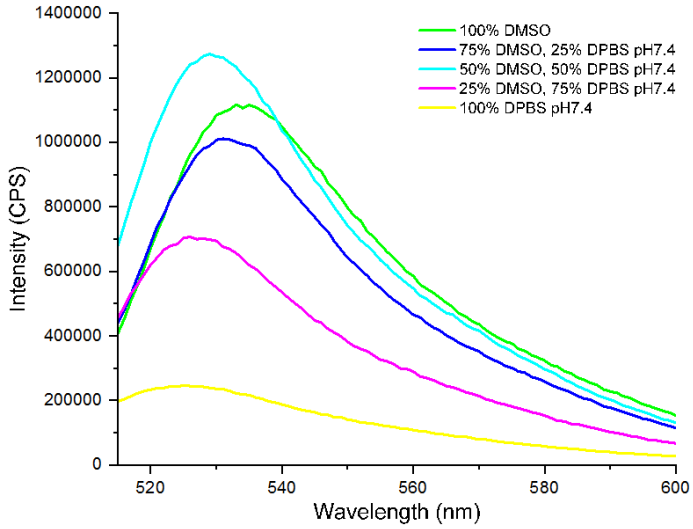

Figure 47: Polar-sensitivity Atto 495: Fluorescence emission spectra of Atto 495 in different concentration ratios of DMSO and DPBS pH 7.4. All spectra were excited at 495 nm (exc. max. of Atto 495 in DPBS pH 7.4.

3.8.3.2 Glucose Sensitivity

Atto 495 was covalently attached to GGBP-H152C/A213R/L238S and exposed to glucose concentrations ranging from 0-100 mM. The maximal fluorescence intensity is shown to be linearly dependent by increasing glucose concentrations with a 44% total fluorescence intensity increase upon binding of 100 mM glucose. A good linear correlation coefficient (R square = R^2) of 0.96 was obtained. The results are depicted in **figure 48**.

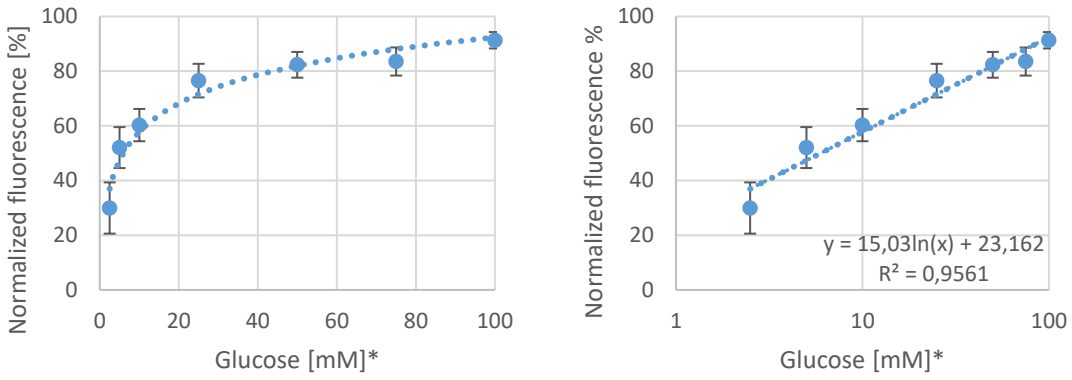

Figure 48: Glucose dependency of the fluorescence intensity of GGBP-H152C/A213R/L238S-Atto495between 2.5 mM and 100 mM.
*Nine technically independent replicates and two biological independent replicates are shown. Variance is represented by the standard error of the mean (SEM).

3.9 Discussion environmentally sensitive fluorescent labels for GGBP

To summarize the results of part 1: Newly developed environmentally sensitive dyes with enhanced properties were tested for the triple mutation H152C/A213R/L238S of the glucose binding protein in Eserichia coli. The protein and its mutant form were well characterized within the last years in the literature resulting in a sensitive sensor element of GGBP_H152C/A213R/L238S attached to BADAN at position 152 with a 200% total fluorescence increase upon the binding of 150mM of glucose. However, drawbacks for the use of this sensor within a cell culture or bioreactor environment were obvious (e.g. excitation in the UV range). Hence, new commercially available fluorophores with excitation maxima above 400nm were screened and tested for their environmental sensitivity.

BADAN, attached to the variant protein, was used as a validation system for the expressed proteins. The DNA insert sequence of 0.93kb has been commercially synthesized and was ligated into the expression vector pET24a containing a 6xHis tag for protein purification. Protein yields of 40mg/l could be achieved with large scale overnight bacterial expressions at 28°C and 1mM IPTG. The proteins could be successfully purified on the Äkta purifier in Prof. Mack's laboratory at the University of Applied Science Mannheim. A 2-step purification combining affinity and gel chromatography was sufficient to obtain a high protein purity.

GGBP_H152C/A213R/L238S-BADAN showed an 84% increase of total fluorescence intensity upon binding of 100 mM glucose with a linear correlation of 0.99, the increase is comparable to the increase reported in the literature.(91) A Kd-value of 20 mM was also comparable to 11mM that has been demonstrated. BADAN was labeled at a quotient of 1.7:1 (dye: protein) which was further improved by reducing the molar excess of the dye to 1.3-fold in the labeling procedure. Reasons for the high labeling rate could be unspecific binding of the highly unpolar molecule.

Fluorescent dyes from Dyomics GmbH were chosen because of their enhanced environmentally sensitive fluorescence properties upon the attachment to proteins. DY V11 shows an extremely large stokes shift of 105 nm in DPBS pH 7.4, however when bound to GGBP_H152C/A213R/L238S it is decreased to 26 nm. DY V11 is a highly polar sensitive dye, however, when dissolved in DPBS at pH 7.4 is loses 93% of its total fluorescence intensity. A good linear dependency of GGBP_H152C/A213R/L238S-DY V11 to glucose was observed (R^2=0.96) with a total fluorescence intensity increase of 26%. DY 610 showed a fluorescence emission from 630-700 nm with good environmentally sensitive properties with a 93% decreased total fluorescence intensity when dissolved in DPBS at pH 7.4. A linear dependency to glucose between 1-100 mM was observed for the protein-dye complex with a good correlation (R^2=0.96) and a total fluorescence intensity increase of 21%. Interestingly,

GGBP_H152C/A213R/L238S-DY 610 even showed an increased linear window from 1µM to 100mM (5x the power of 10) with a correlation coefficient of 0.99. This combination makes the protein-dye complex suitable for environments with a large concentration range. However, it must be noted that the experiment was done with three technically and one biological independent measurement and should also be repeated for a second biologically experiment. The third Dyomics dye used was DY 490, an enhanced fluorescein derivative. This dye shows, compared to other environmental sensitive dyes, an extremely high increase of total fluorescence intensity when dissolved in aqueous solutions. When attached to GGBP, DY490 does not show a difference in the excitation or emission spectra and demonstrated a linear glucose dependency from 0-100 mM with an acceptable correlation coefficient of 0.9.

Furthermore, fluorescent dyes from Atto-Tec GmbH were tested for their environmental sensitivity. Atto 425 consists of a coumarin backbone with a large stokes shift of 50nm in DPBS pH 7.4 and displays the most similar structure to BADAN out of the chosen dyes. A linear glucose dependency was observed from 2.5-75 mM with a 27% increase in total fluorescence intensity. Atto 465, an acriflavine derivative showed a strong absorbance with an increased stokes shift of 55 nm when dissolved in DPBS pH 7.4. Interestingly, Atto 465 loses only 76% of its total fluorescence intensity when dissolved in DPBS. GGBP_H152C/A213R/L238S-Atto 465 showed a linear glucose dependency between 2.5 mM and 75 mM with a particularly good correlation coefficient of 0.98 and a total fluorescence intensity increase of 36%. When Atto 465 is extrapolated to 100 mM it would show a 48% increase compared to 84% increase of BADAN. Atto 495 when attached to GGBP_H152C/A213R/L238S, behaves similarly to Atto 465 with an 44% increase in total fluorescence intensity upon binding of 100 mM glucose. This is probably because Atto 495 consists of unpolar methylated amine groups attached to the acriflavine body in the molecular structure. Furthermore, Atto 495 shows a smaller stokes shift of 30nm in DPBS and loses only 81% of total fluorescence intensity.

Overall, Atto 465 and Atto 495, when bound to the triple mutant H152C/A213R/L238S of GGBP, show extremely good environmentally sensitive fluorescence properties and could be used in glucose biosensor systems as glucose recognition elements with a particularly high molecular absorbance.

4 Results & Discussion Part 2

4.1 Using the Pi-Clamp strategy for FRET-based glucose biosensors based on GGBP

(Förster-) Fluorescence energy transfer (FRET experiments on a single molecular level enable identification of conformation changes and folding processes of proteins by introducing fluorophores at specific sites. Testing several different labeling combinations allows to map complex conformational changes as well as interactions.(122) A new approach of site-selective attachment of fluorophores to cysteine residues in proteins was used in this work, the pi-clamp.

The relatively large conformational change in GGBP upon binding of glucose (31°) is suitable for a Förster-Resonance Energy transfer (FRET) between two attached fluorophores when they are in proximity (<10Å).(123) This can be achieved by introducing the two fluorophores at specific sites with nearest distance between each other when GGBP is in its closed state and compared to that, a large distance when the protein is in its open state. The difference in the positions of bound and unbound state are determining. The strategy in this work was to attach the fluorophores at the N-terminal and the C-terminal binding domains of GGBP. This strategy is obvious to have the highest impact possible and a likely chance for a successful energy transfer between the two fluorophores.

For the correct determination of suitable positions of these fluorophores, computational mutation studies were performed with the crystal structures of GGBP in its open and closed form. PyMol, a standard molecular structure displaying software was used to visualize the protein structure as well as for the determination of atom distances. It must be noted that computational studies such as ligand binding studies, when performed correctly, should be done by energy refinement of the whole protein together with the attached molecules/ligands. However, this would have resulted in the requirement of a supercomputer with a computing time of several weeks due to the high number of degrees-of-freedom for the modeling of protein, ligand as well as the two covalently attached molecules. Therefore, the crystal structure of GGBP in its open and closed form were modeled by the and single cysteine mutations were mapped (see chapter 4.3)

…

Alternative modeling strategy (easier, still accurate) –> 4 amino acid mutation modeling with swiss model based on the crystal structure

Pi-clamp 4 AA sequence

Summary of chapter 4.2 to 4.10

4.2 Sequence Alignments

For the identification of suitable labeling combinations, a multiple sequence alignment of several different bacterial organisms was performed. The mglB gene encodes the glucose-galactose binding protein (also known as D-galactose-binding periplasmic protein or Methyl-galactoside ABC transporter) in organisms such as Shagella flexnen, Citrobacter freundi, Salmonella bongon as well as Eserichia coli and many more (see pdb database: mglB). The six different sequences mapped are shown in **table 2**.

Table 4: BLAST entries of sequence alignment (figure 49) of different bacterial glucose ABC transporter proteins

UniProt ID	*Entry name*	*Protein name*	*Organism (Gene name)*	*Similarity*
P0AEE5	DGAL_ECOLI	D-galactose-binding periplasmic protein	Eserichia coli K12 (mglB)	-
P0AEE7	DGAL_SHIFL	D-galactose-binding periplasmic protein	Shagella flexnen (mglB)	100%
P23925	DGAL_CITFR	D-galactose-binding periplasmic protein	Citrobacter freundi (mglB)	96,1%
A0A447M233	_SALBN	Galactose/glucose ABC transporter	Salmonella bongon (mglB)	93,1%
A0A0H3FYT0	_KLEAK	Methyl-galactoside ABC transporter	Klebsiella aerog. (EAE_23940)	92,8%
A0A1XOWDR1	_9GAMM	Methyl-galactoside ABC transporter	Rouxiella badens. (BS640-13365)	84,9%

The 1.3 Å crystal structure of sequence DGAL_ECOLI from GGBP in Eserichia coli (strain K-12) was used as a structural reference. The heuristic algorithm BLAST (basic local alignment search tool) heuristic algorithm was used for alignment of sequences and for similarity determination. The overall sequence identity of all six structures was 76,9%. The protein DGAL_SHIFL from Shagella flexnen shares a 100% structure similarity. DGAL_CITFR, A0A447M233_SALBN and A0A0H3FYT0_KLEAK from Citrobacter freundi, Salmonella bongon and Klebsiella aerogenesis, share a 96,1%, 93,1% and 92,8% sequence identity with DGAL_ECOLI, respectively. When comparing the structural motifs, the following results were obtained. The sequence alignment is depicted in **figure 49**.

The GGBP protein in E. coli shares a common signal peptide chain of 23 amino acids (position 1-23) which is split off upon the relocation of the transporter protein into the cell membrane. Hence the actual protein sequence starts with the three amino acid sequence alanine, aspartate, and threonine (ADT). According to the crystal structure of E. coli, the protein consists of 10 bigger α-helices (pink) as well as 10 β-helices (yellow) (120) which are located in both binding domains. The protein itself is highly symmetric shares a configuration of 5 helices and 5 strands in each binding domain (see structure of GGBP in chapter 4.3). The residues highlighted in grey indicate absolute similarity between the different sequences. The overall similarity is relatively high across the entire sequence with multiple highly conserved sections. The GGBP crystal structure (pdb ID: 2HPH) also consists of loop regions which connect the two domains in the so called ‘hinge’ region. The loops are located at position 108-112 (amino acid sequence: VGTDS), 255-258 (amino acid sequence: LNDA) and a larger loop 275-296

which forms the hinge region from position 293-296 (amino acid sequence: VPYV). In this work, it was avoided to mutate regions that are actively involved in the binding event such as direct and indirect stabilization of the ligand as well as loop regions involved in the hinge. The mutation of single amino acids that form either stabilizing α-helices or β-sheets should be generally avoided as this might conflict with the overall stabilization of the protein.(124)

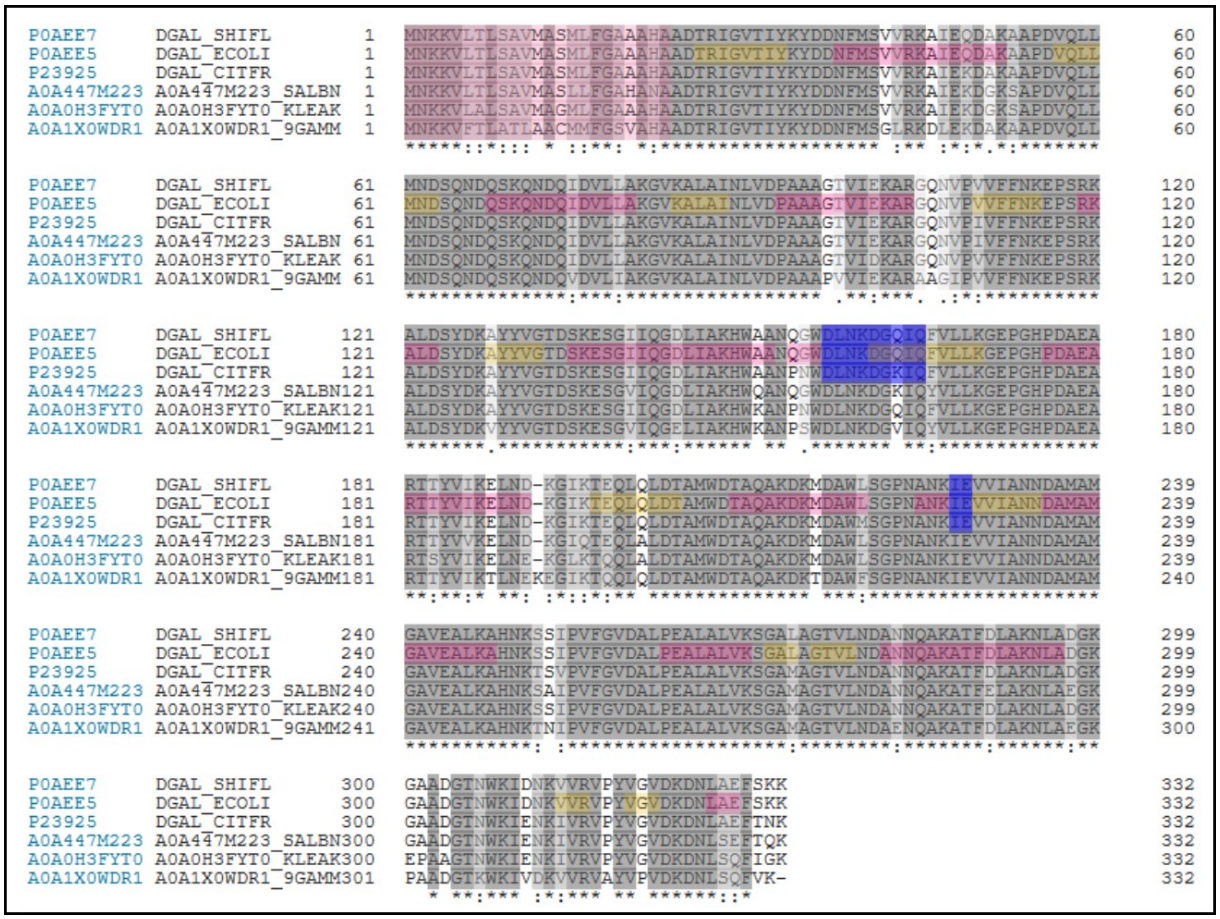

Figure 49: Multiple sequence alignment of glucose ABC transporters in different bacterial organisms. The structural motifs are obtained from the crystal structure (UniProt ID: P0AEE5) of E.coli (light pink: signal peptide, pink: α-helix, yellow: β-sheet, blue: calcium binding site, dark grey: similarity between amino acids)

According to the alignment, the following residues were considered as being tolerant to mutations: amino acid regions from N-terminal to C-terminal: 11-14, 30-33, 41-44, 69-72, 93-96, 193-197, 147-150, 169-172, 181-184, 197-200, 225-238 and 274-308. These regions were further investigated for their role in direct and indirect ligand stabilization in the crystal structure of GGBP in Eserichia coli in its closed state (2HPH).

4.3 Identification of suitable FRET positions in GGBP using Swiss Model

The mutation modeling based on the crystal structure of GGBP (2HPH) has been done with the swiss model software. Swiss model is a protein structure homology-modelling server, which is accessible via the ExPASy web server. This tool calculates homology model

structures based on stored structure data from similar sequences. However, it can also make use of templates, such as existing crystal structures with a certain quality. Existing crystal structure provide the opportunity to model single mutations or a group of mutations in alternative to an energy refinement of the protein based on the best obtained stability. The quality of the models with the added pi-clamp sequences (FCPF or FPCF) were assessed showing one example of the model quality in **figure 50**.

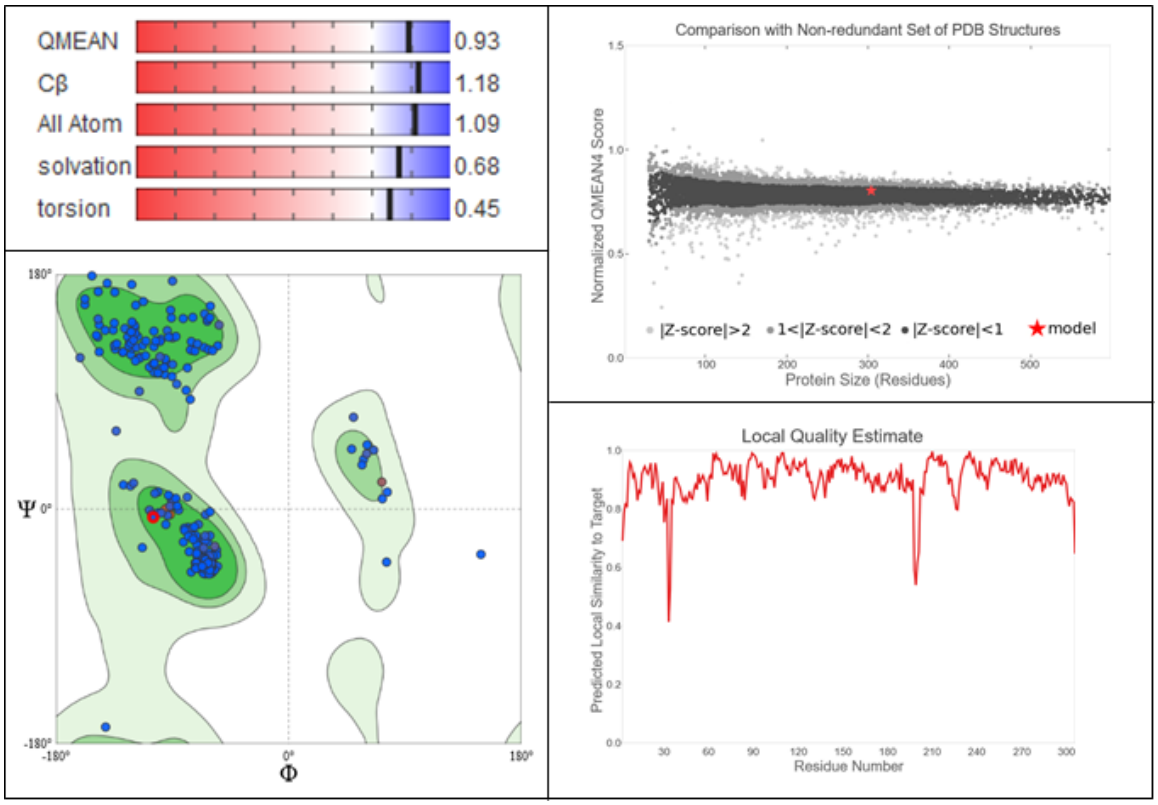

Figure 50: Quality assessment of generated mutants (GGBP_mut_H152C/A213R/L238S_QNDQ42-45FPCF as example). The calculations are based on QMEAN scoring function, Ramachandran Plot, upper right: Z-score (model prediction compared to other models in databank), quality of the model, as normalised QMEAN score (y-axis), in comparison to the scores obtained for high-resolution crystal structures

The QMEAN scoring function predicts quality parameters for a secondary structure.(125) It reflects and evaluates criteria such as the torsion angles (allowed/unallowed angles) of the polypeptide bonds within the protein, the solvation potential, the interaction potential (Cß , all-atom, local potential between a chain of amino acids), solvent accessibility and z-score. GGBP, in the mutated example in figure 51, shows a particularly good quality of the model compared to other non-redundant protein structures within the pdb database with an overall z-score below 1 (upper right). The individual contributions to the QMEAN scoring function results in individual z-scores mainly below 1 (upper left). The Ramachandran plot (126) (lower left) indicates allowed dihedral angels of the overall protein except for two outliers which can be also identified in the local quality estimate (lower right) in the beginning and towards the end of the protein which repeat in the unmutated protein.

In addition, the glucose binding pocket was visually investigated and the mutation tolerating regions that have been identified in chapter 4.2 (from N-terminal to C-terminal: 11-14, 30-33, 41-44, 69-72, 93-96, 147-150, 169-172, 181-184, 197-200, 225-238 and 274-308) were further validated for their ligand interaction. The overall structure of GGBP in its bound state and the interactions in the binding pocket are shown in **figure 51**.

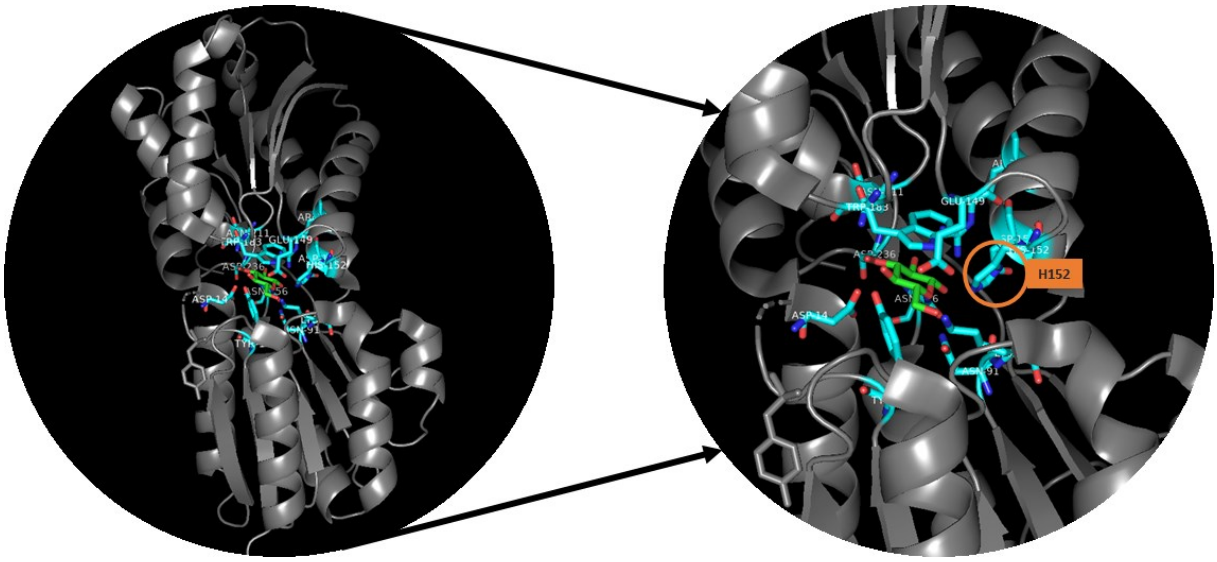

Figure 51: Ligand binding site of the wild-type glucose-galactose binding protein (GGBPwt) with its natural ligand glucose.
The position H152 were all fluorophore attachments are done via a cysteine mutation, is highlighted. The crystal structure modelling was done with the PyMol displaying software.

In the ligand binding event of the GGBP protein, several amino acids are involved in direct as well as indirect binding of the ligand. The indirect binding involvement of these amino acid is considered being a stabilization of the amino acids that directly interact with the ligand either by hydrogen, van-der-waals or pi-stacking bonds (non-covalently).

Eight amino acids are directly involved in ligand binding. The C1-atom of glucose is stabilized by hydrogen bonds by Asn91, Asp154, Arg158 and Asn256. Arg158 simultaneously stabilizes the neighbour atom C2 of glucose which is further stabilized by Asn211 and Asp236. Asn211 and Asp236 also stabilize the C3 atom. The C4 in glucose forms hydrogen bonds to Asp14 as well as Asn211. C5 is not involved in binding. The oxygen bond within glucose is further stabilized by Asn91 which also binds to the C6 atom. Indirect binding of the glucose molecule involves the amino acids Tyr10, Lys92, Thr110, Glu149, His152, Thr159, Trp183, Asn210 and Tyr295. The most prominent roles play here Tyr295 which further stabilizes Thr110, Asp154 and Arg158, and Asn210 which further stabilizes Thr159 and Arg158. His152 and Trp183 stabilize each other by a pi-stacking within the binding pocket. Some of the above mentioned indirect stabilizing amino acids have been mutated earlier by other groups to adapt the Kd value of GGBP from µM affinity to mM affinity and to insert a cysteine mutation for the attachment of environmentally sensitive dyes (see chapter 1.5.4) (86, 91) The prominent

example was His152 which forms the basis of the triple mutant used in the environmental sensitive part of this work. His152 also plays a significant role in the FRET experiments being an already validated position within GGBP which is most influenced upon ligand binding. In addition to H152 which serves as the acceptor fluorophore attachment site and the two mutations A213R and L238S, four amino acid sequences forming the pi-clamp, have been introduced at various sites. After evaluating the amino acids being involved in the binding site, some of the mutation tolerating regions identified earlier were revalidated. The regions **11-14** and **181-184** were distracted from the list of potential mutation tolerating amino acid regions. The other regions were inspected in the crystal structure and several mutation combinations were evaluated according to the positioning of the cysteine residue to be easily accessible by the NHS-functionalized fluorophore. The swiss model experiments used the open and closed crystal-structures 2FW0 and 2HPH, respectively.

The results were five mutants based on the triple mutation (GGBP_H152C/A213R/L238S) that are shown in the following. It must be noted that that pi-clamp was introduced in different combinations at each site. According to the literature, the important function of the pi-clamp in the two phenylalanine residues at each end of the motif. It does not exclude the usage of FPCF (reverse motif) compared to the traditional motif FCPF. Hence, both motifs were used in structure modelling to obtain the optimal conformation of the residues for a successful labeling. The first GGBP mutant generated was GGBP_mut_H152C/A213R/L238S_QNDQ42-45FPCF. The reverse pi-clamp motif FPCF was introduced at positions 42-45 into the second helix of the N-terminal domain near the ligand binding pocket. The fluorophore acceptor site at position 152, is located at the C-terminal domain. The model is shown in **figure 52**.

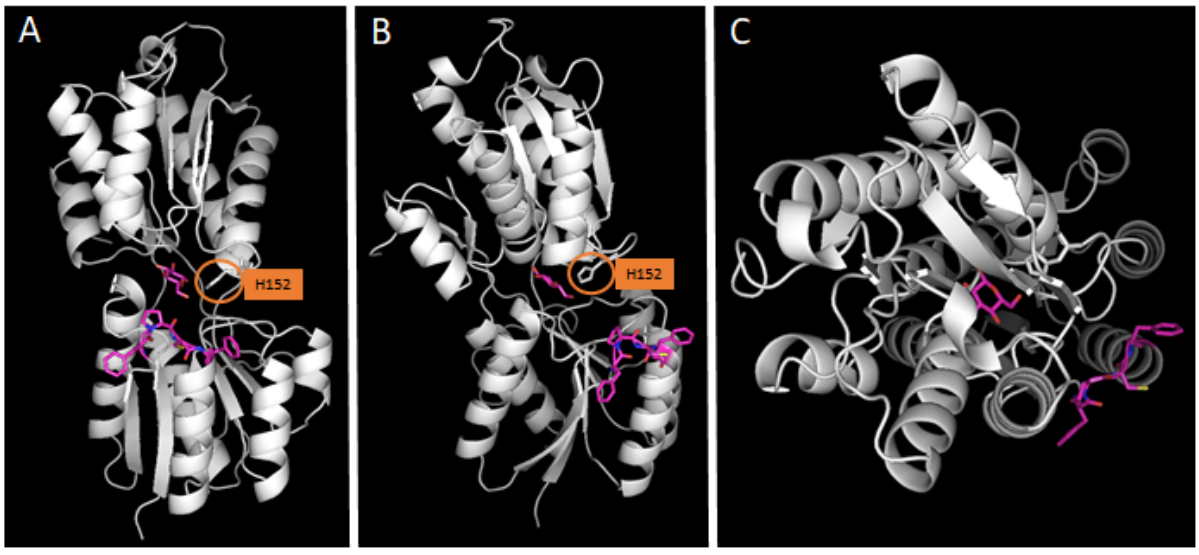

Figure 52: Crystallographic structure of GGBP_mut_H152C/A213R/L238S_QNDQ42-45FPCF.
The reverse pi-clamp motif FPCF was introduced in the N-terminal domain of helix 2 for the attachment of the FRET donor. The attachment site of the acceptor is located at position 152 within the binding pocket in the C-terminal domain. A) Front view into binding pocket of GGBP towards the hinge-region with lower N-terminal domain and upper C-terminal domain B) Anticlockwise rotation of structure by about 45° and C) View from above to C-terminal domain of GGBP with 45° rotation compared to A (hinge on the left).

According to the predetermined allowed regions of the pi-clamp motif within the protein, region 41-44 was not involved in ligand binding. However, the formation of the pi-clamp was unfavorable as the phenylalanine rings were not able to form a pi-stacking between each other for both combinations 41-44FCPF and 41-44FPCF. Therefore, the amino acids 42-45 (QNDQ) were chosen because of their location on top of the N-terminal helix 2. When glucose is bound, this site is in proximity to position 152 and will be further apart once GGBP is within its unbound state. The angle of GGBP between bound an unbound state equals 31° at the hinge region and results in a movement of all helices of the N-terminal domain by a few Angstroms. However, also the C-terminal helix including position 152 shows a small movement of a few angstroms, which could result in smaller FRET distance differences. For the region 42-45 the reverse mutation was not chosen as the free thiol group of the cysteine mutation was directed into the inside of the binding pocket which could have influenced the binding event.

The second GGBP mutant generated was GGBP_mut_H152C/A213R/L238S_VDPA68-71FCPF. The pi-clamp motif was introduced on top of the third α-helix of the N-terminal domain similarly to the first mutation. The region 69-72 was neither involved in ligand binding nor stabilizing the binding process and connects the second with the third helix by ß-sheet 3 and a short loop. However, modeling of positions 69-72 with either FCPF or FPCF resulted in an unfavorable conformation of the pi-clamp where the rather big phenyl residues in were unable to form a pi-pi-interaction. Nevertheless, position 68-71 resulted in a more favorable conformation which is also shown in **figure 53**.

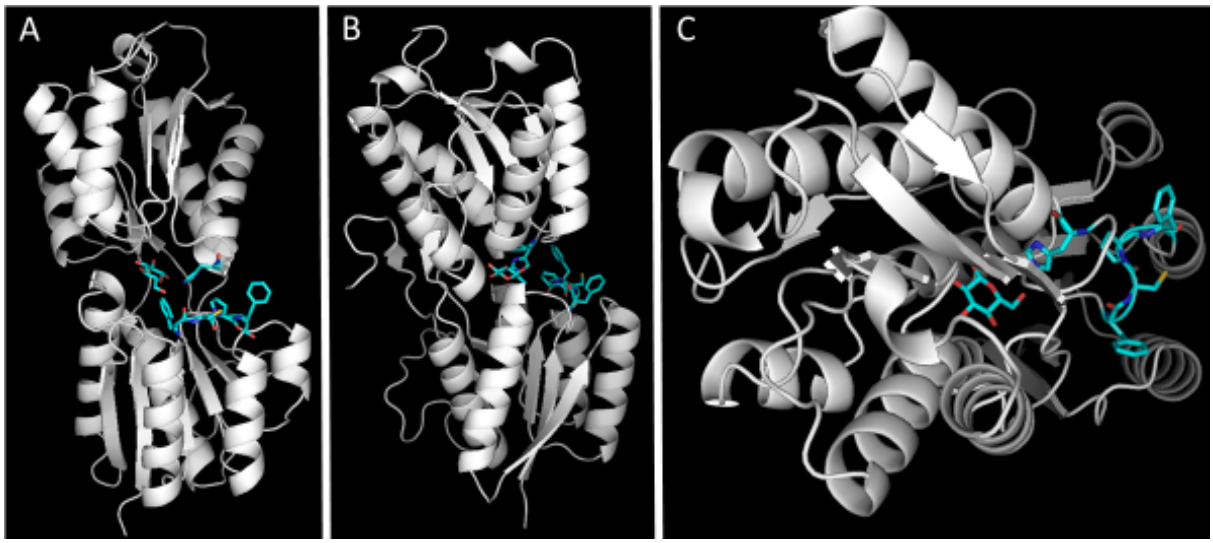

Figure 53: Crystallographic structure of GGBP_mut_H152C/A213R/L238S_VDPA68-71FCPF.
The pi-clamp motif FCPF was introduced in the N-terminal domain of helix 3 for the attachment of the FRET donor. The attachment site of the acceptor is located at position 152 within the binding pocket in the C-terminal domain. A) Front view into binding pocket of GGBP towards the hinge-region with lower N-terminal domain and upper C-terminal domain B) Anticlockwise rotation of structure by about 45° and C) View from above to C-terminal domain of GGBP with 45° rotation compared to A (hinge on the left).

The pi-clamp was inserted as FCPF motif because of the conformation of the cysteine residue with its free thiol group presented to the outside of the domain. Consequently, the reverse motif FPCF resulted in a presentation of the thiol group towards the binding pocket which could hinder the ligand to enter the binding pocket. In both motifs, the phenyl rings have the freedom to rotate towards a parallel orientation for the activation of the thiol group.

The second GGBP mutant generated was GGBP_mut_H152C/A213R/L238S_EPSR93-96FPCF. Like the mutants described above, the reverse pi-clamp motif was introduced on top of the fourth α-helix in the N-terminal domain close to the binding site. This helix is rather short and flexible. It is connected by a loop structure of 7 amino acids from parallel beta sheet 4 to helix 4 and continues into a longer loop and beta sheet 5 towards the C-terminal domain, forming the hinge region. The mutant structure is depicted in **figure 54**.

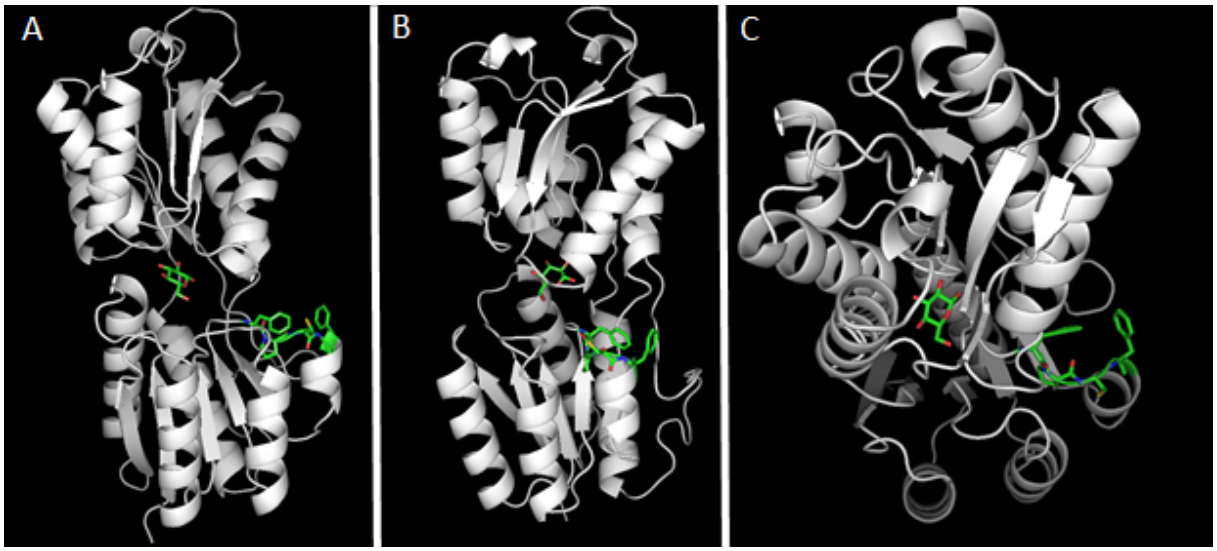

Figure 54: Crystallographic structure of GGBP_mut_H152C/A213R/L238S_EPSR93-96FPCF.
The reverse pi-clamp motif FPCF was introduced in the N-terminal domain of helix 2 for the attachment of the FRET donor. The attachment site of the acceptor is located at position 152 within the binding pocket in the C-terminal domain. A) Front view into binding pocket of GGBP towards the hinge-region with lower N-terminal domain and upper C-terminal domain B) Anticlockwise rotation of structure by about 45° and C) View from above to C-terminal domain of GGBP with 45° rotation compared to A (hinge on the left).

GGBP_mut_H152C/A213R/L238S_EPSR93-96FPCF contains the reverse pi-clamp motif at positions 93-96 by exchanging the amino acid sequence EPSR. Both pi-clamp combinations were modelled, however, FPCF showed a suitable conformation displaying the free thiol group towards the outside. In contrary, FCPF displayed the free thiol towards the inside of the stabilizing structure of the N-terminal binding domain for the positions 93-96. According to the pre-evaluation, region 93-96 was not involved in ligand binding or stabilization of the binding event and could be exchanged accordingly.

The predefined regions comprising of the positions 147-150, 169-172, 197-200, 225-238 were not further mutated as they are part of the C-terminal domain. It was considered that as long

as the acceptor molecule is attached to position 152 of the C-terminal domain, the FRET donor should not be attached at the same binding domain as this would probably not result in a change of the energy transfer. Consequently, the remaining region that would tolerate a 4-amino acid mutation started from positions 274-308. All together this amino acid sequence forms an extremely long loop from the N-terminal binding domain all the way to the C-terminal binding domain. It is mainly stabilized by one short ß strand at the C-terminal site. The C-terminal part starts around amino acid residue 293 and continues to residue 308. The remaining region of position 274-292 was carefully modelled and several combinations have been tried out. The section from 280-288 was most promising with a loop structure that shows high flexibility and could easily tolerate a 4-amino acid mutation.

The fourth GGBP mutant, GGBP_mut_H152C/A213R/L238S_DGTN280-283FCPF, has been built by inserting the pi-clamp motif into the loop of the lower end of the N-terminal binding domain with the pi-clamp motif inserted at positions 280-283. The structure is shown in **figure 55**.

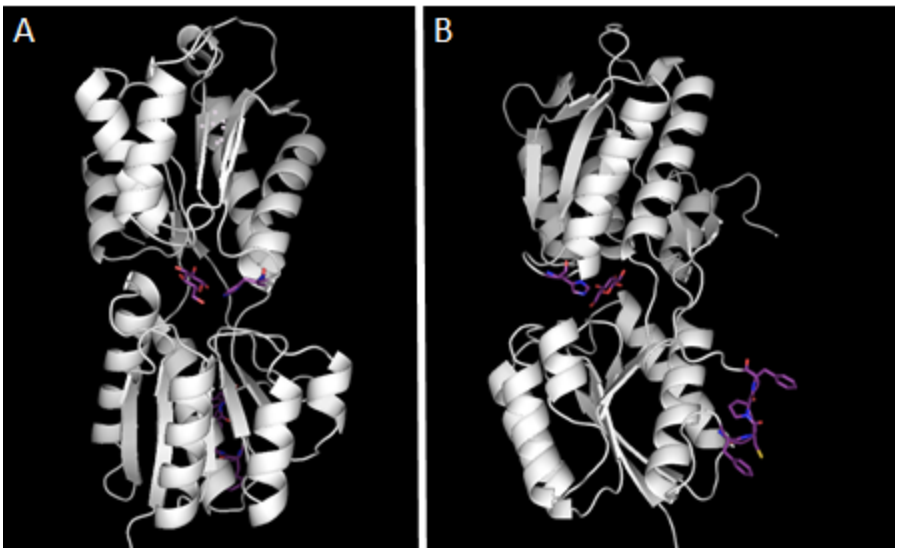

Figure 55:: Crystallographic structure of GGBP_mut_H152C/A213R/L238S_DGTN280-283FCPF.
The pi-clamp motif FCPF was introduced in the N-terminal domain of helix 3 for the attachment of the FRET donor. The attachment site of the acceptor is located at position 152 within the binding pocket in the C-terminal domain. A) Front view into binding pocket of GGBP towards the hinge-region with lower N-terminal domain and upper C-terminal domain B) Anticlockwise rotation of structure by about 45° and C) View from above to C-terminal domain of GGBP with 45° rotation compared to A (hinge on the left). The pi-clamp, position 152, as well as the ligand are indicated in purple.

The formation of FCPF at these positions resulted in the two phenylalanine residues facing each other by surrounding the free thiol group of the cysteine residue. Consequently, the reverse motif FPCF at positions 280-283 resulted in a rotation of the first phenylalanine residue due to the dihedral angle of the proline-phenylalanine peptide bond. On the other hand, the cysteine residue was facing towards the helix inside the binding domain resulting in a bad accessibility for fluorophore attachment. The overall structure of the reverse motif and the

unparallel formation of the phenyl rings was considered as being hardly accessible for any fluorophore attachment. The distance between the pi-clamp motif and position 152 is the largest for GGBP_mut_H152C/A213R/L238S_DGTN280-283FCPF compared to the other mutations. The distance of the two cysteines increases significantly when GGBP is within its open state. This results in suitable FRET attachment positions overall. The fifth GGBP mutant, GGBP_mut_H152C/A213R/L238S_KIDN285-288FPCF, was built into the loop of the upper part of the N-terminal binding domain with the pi-clamp motif inserted at positions 285-288. The structure is shown in **figure 56**.

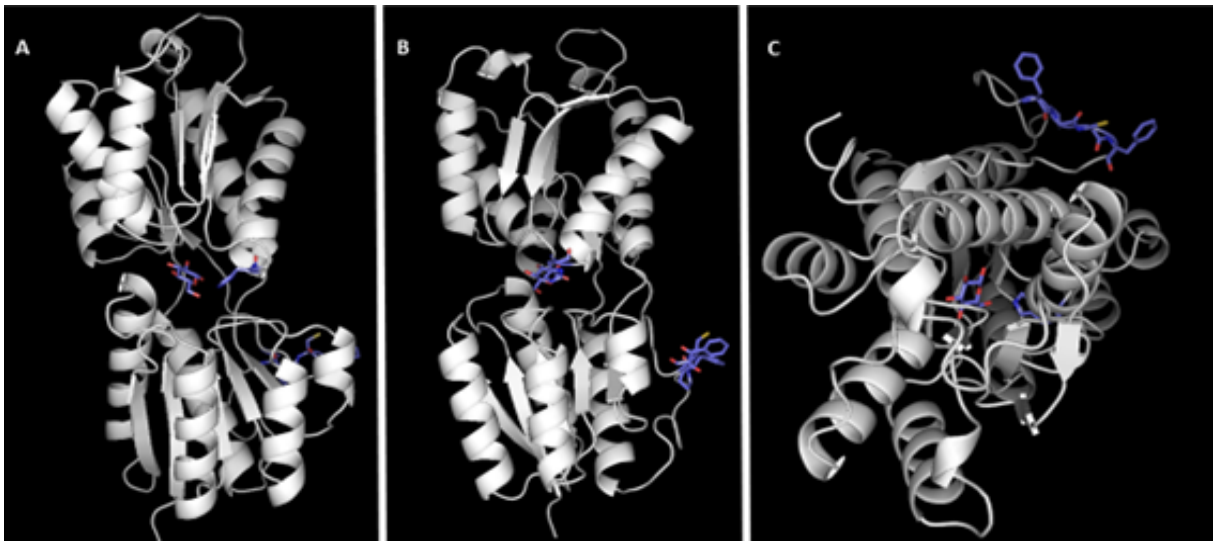

Figure 56: Crystallographic structure of GGBP_mut_H152C/A213R/L238S_KIDN285-288FPCF.
The pi-clamp motif FPCF was introduced at the flexible loop region in the N-terminal domain for the attachment of the FRET donor. The attachment site of the acceptor is located at position 152 within the binding pocket in the C-terminal domain. A) Front view into binding pocket of GGBP towards the hinge-region with lower N-terminal domain and upper C-terminal domain B) Clockwise rotation of structure by about 45° and C) View from above to C-terminal domain of GGBP with a 90° vertical rotation. The pi-clamp, position 152, as well as the ligand are indicated in purple.

The reverse pi-clamp at positions 285-288 shows a parallel orientation of both phenyl rings of the phenylalanine residues. The free thiol of the cysteine mutation is surrounded by the phenyl rings and is directed to the environment which allows activation of the thiol group and accessibility by labeling molecules. The free thiol of the pi-clamp motif FCPF sitting at position 286, however, was directed towards the inner helix 5 of the N-terminal domain. Although the phenyl residues show a parallel orientation in this configuration towards the thiol group, a free rotation of the cysteine does not seem to be possible to be able to activate the thiol group. Therefore, the reverse pi-clamp motif was generated. The distance from the pi-clamp cysteine to the cysteine at position 152 in this mutant is slightly shorter compared to GGBP_mut_H152C/A213R/L238S_KIDN285-288FPCF.

The DNA of the five mutant forms of GGBP that were presented in this chapter, were ordered, and synthesized at GeneArt GmbH, Germany. The mutant genes were cloned into the pET vector system by NdeI and XhoI, according to the protocols in chapter 7.2.1.

4.4 Cloning, Expression and Purification of GGBP variant with the encoded pi-clamp

The mutant genes were cloned into the expression vector and transformed into the bacterial expression strain and were sequenced. The correct sequences were validated (the sequencing data can be found in the back-up). A test expression of the five designed mutants was performed and the expression profile was analyzed by SDS-page. The results can be found in **figure 57**.

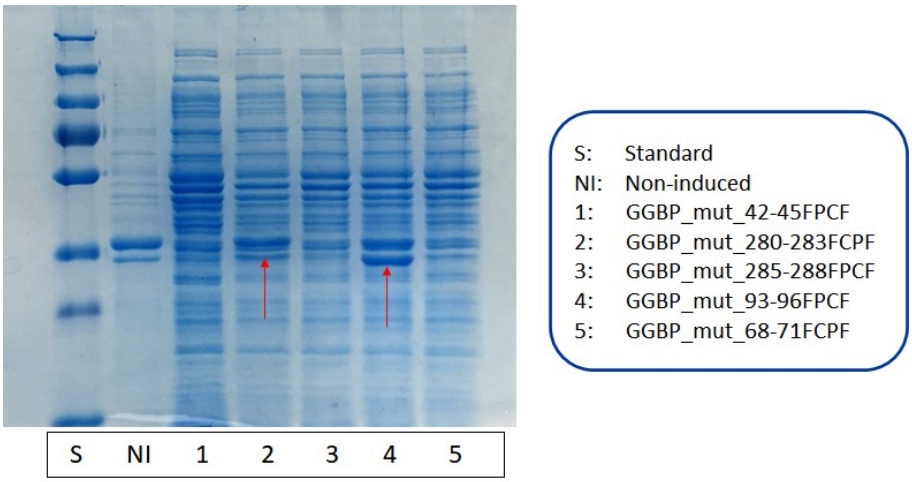

Figure 57: SDS-page profiling and test expression of designed GGBP pi-clamp mutants in 150 ml expression medium induced with 1mM IPTG. The mutants are named according to the pi-clamp mutation (short form).

The GGBP mutant protein with the pi-clamp coded at positions 93-96FPCF was clearly overexpressed. In addition, the variant with the pi-clamp motif located at positions 280-283FCPF was slightly overexpressed. The three variants with the pi-clamp located at positions 42-45FPCF, 68-71FCPF and 285-288FPCF were expressed, but not overexpressed compared to the non-induced variants. One of the non-induced mutants was used as a standard. Consequently, the test expression was repeated and scaled up to one liter of expression medium. The cultures were inoculated with 10 ml inoculum that was prepared before and stirred over night at 28°C. On the next day, the medium was centrifuged at 4 °C, washed, and the resulting pellets were shock frozen at -80°C (see protocol chapter 7.2.2) for further purification of the proteins of interest. The cells were disrupted to a crude cell extract, and the proteins were separated from the cell mass by centrifuging. Finally, proteins were concentrated onto the first column by a histidine trap column after which the his-tag proteins were eluted. In a second step, the eluted proteins were purified on a gel filtration column for further refinement. The His trap purifications are depicted in the following **figures 58-62**.

For the purifications, a 100% gradient from buffer A (low imidazole) to buffer B (high imidazole) was used. Buffer B contained 400mM of imidazole in phosphate buffer and was used as elution buffer. The variants which did not contain the pi-clamp, eluted at around 25% of buffer B. This served as a reference for the purification of the new variants. The SDS page of the induced

expression sample (I) of GGBP variant GGBP_mut_ H152C/A213R/L238S_QNDQ42-45FPCF (**figure 58**) showed high overexpression of the protein of interest. Fraction 2 and 3 eluted at concentrations below 20% of buffer B without containing the protein of interest. With fraction 5, the protein finally started eluting and was contained in 4 different fractions increasing from fraction 5 to 8. The fractioning was stopped after the UV signal reached 20mAU threshold. It must be noted that the impurities of fraction 4-8 are unusually high and several smaller proteins did elute together with the protein of interest. The protein band is marked in red.

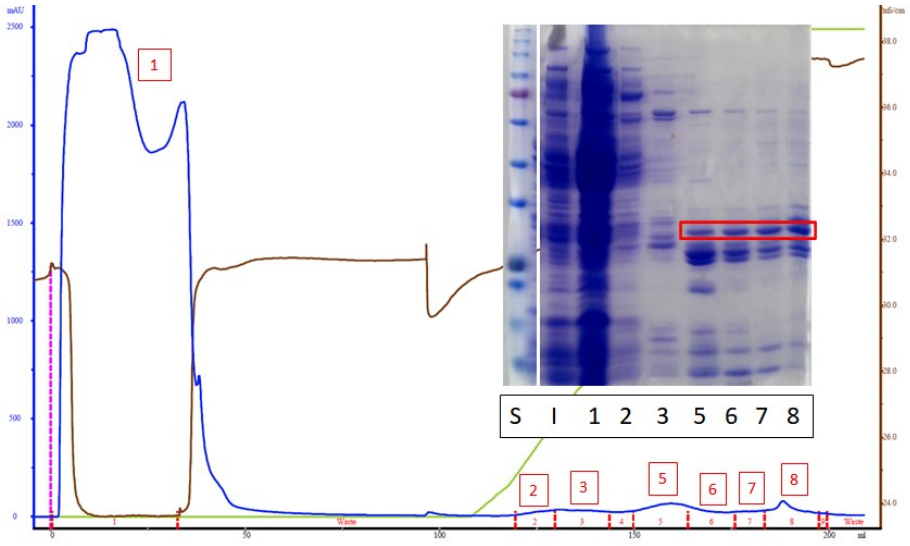

Figure 58: Purification of GGBP_mut_H152C/A213R/L238S_QNDQ42-45FPCF from one liter expression culture. The expression in BL21 (DE3) was induced with 1 mM of IPTG. The protein fractions (1-3, 4-8) were collected and analyzed by SDS gel electrophoresis. Samples of a protein standard (S) and an induced (I) expression were added. The purification analysis is done with the UNICORN 5 software from GE Healthcare. (blue: UV-signal, brown: conductivity, green: solvent gradient of buffer A and B, pink: injection, red: fractions)

GGBP_mut_H152C/A213R/L238S_VDPA68-71FCPF showed a high overall expression rate of total protein amount which is indicated in sample 1 in **figure 59**. The proteins were loaded onto the His Trap column and were washed with low imidazole buffer. At 25% of buffer B the protein eluted in fraction 3, 4, and 5. The conductivity was increasing according to the increase in imidazole concentration. The peaks in all fractions are overlapping and as indicated by fraction 3-6, a lot of smaller as well as larger proteins eluted in the same fraction. The expression and purification were done simultaneously with the purification of variant 42-45FPCF which is described above. When comparing these purifications with the chromatogram of GGBP_mut_H152C/A213R/L238S_EPSR93-96FPCF (see figure 60) which was recorded in another week, all protein containing fractions show exceptionally low impurities. It raised the concern that the condition of the column or the buffer was inaccurate which led to increased impurities in the single fractions. The reasons that might have occurred will be discussed in detail in chapter 4.10. However, figure 59 clearly indicates the presence of the overexpressed protein in the fractions. The final concentration obtained was 5 mg/ml.

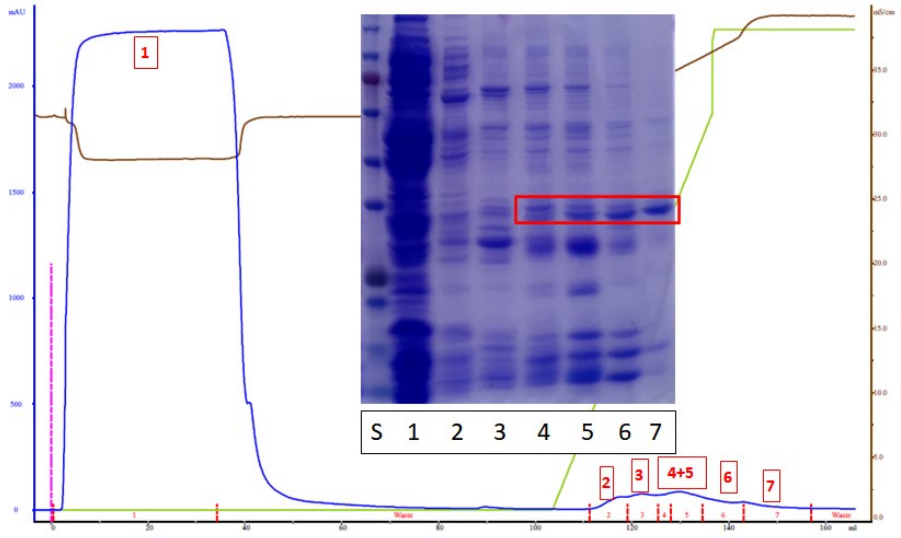

Figure 59: Purification of GGBP_mut_H152C/A213R/L238S_VDPA68-71FCPF from one liter expression culture. The expression in BL21 (DE3) was induced with 1 mM of IPTG. The protein fractions (1-7) were collected and analyzed by SDS gel electrophoresis. A sample of a protein standard (S) was added. The purification analysis is done with the UNICORN 5 software from GE Healthcare. (blue: UV-signal, brown: conductivity, green: solvent gradient of buffer A and B, pink: injection, red: fractions)

The purification of GGBP_mut_H152C/A213R/L238S_EPSR93-96FPCF is shown in **figure 60**. The non-induced expression sample (NI) shows already an overexpression of the protein of interest with a low total protein concentration. This phenomenon was also observed for the variants of GGBP that were labeled with environmental sensitive dyes showing an active promoter of the pET vector system in E. coli. The induced sample (I) shows similar amounts of overexpressed protein as well as an increased amount of total protein concentration. The total protein concentration of the fractions was measured by a Bradford assay and the samples were applied at equal concentration onto the SDS page.

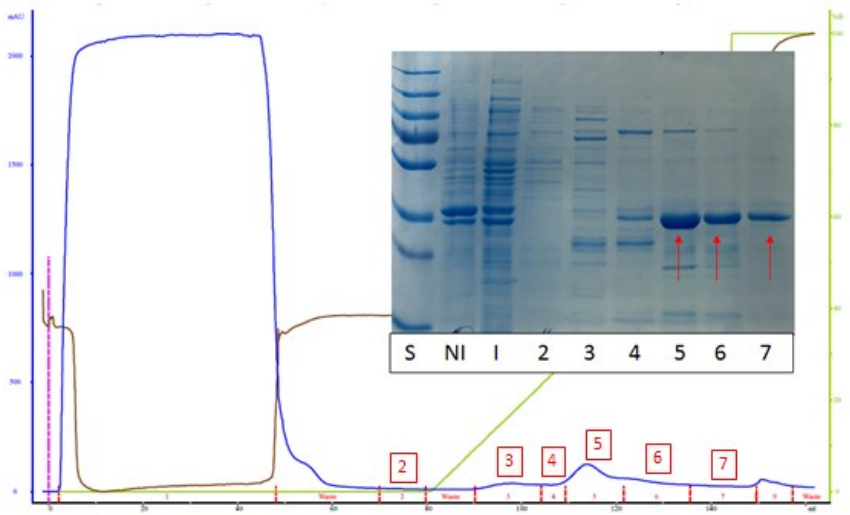

Figure 60: Purification of GGBP_mut_H152C/A213R/L238S_EPSR93-96FPCF from one litre expression culture. The expression in BL21 (DE3) was induced with 1 mM of IPTG. The protein fractions (2-7) were collected and analyzed by SDS gel electrophoresis. Samples of a protein standard (S), of a non-induced and an induced (I) expression were added. The purification analysis is done with the UNICORN 5 software from GE Healthcare. (blue: UV-signal, brown: conductivity, green: solvent gradient of buffer A and B, pink: injection, red: fractions)

The protein elutes in the fractions 5, 6, and 7and has a mass of 8 mg in total when combining the fractions. Fraction 5 was further concentrated to 1.6 mg/ml for subsequent labeling with a FRET donor and acceptor pair (chapter 4.7 and following).

GGBP_mut_H152C/A213R/L238S_DGTN280-283FCPF was expressed and purified on the same day and under similar conditions like GGBP_mut_H152C/A213R/L238S_DGTN280-283FCPF as mentioned above. The non-induced sample (NI) shows a low overexpression of the protein of interest as well as a low overexpression and a higher total protein amount when induced with 400 mM IPTG (**see figure 61**). The protein elutes in fractions 4 and 5 with 6 mg of total mass and a concentration of 0.4 mg/ml. After concentrating, the protein had a concentration of 3.3 mg/ml which was used for subsequent labeling of FRET pairs.

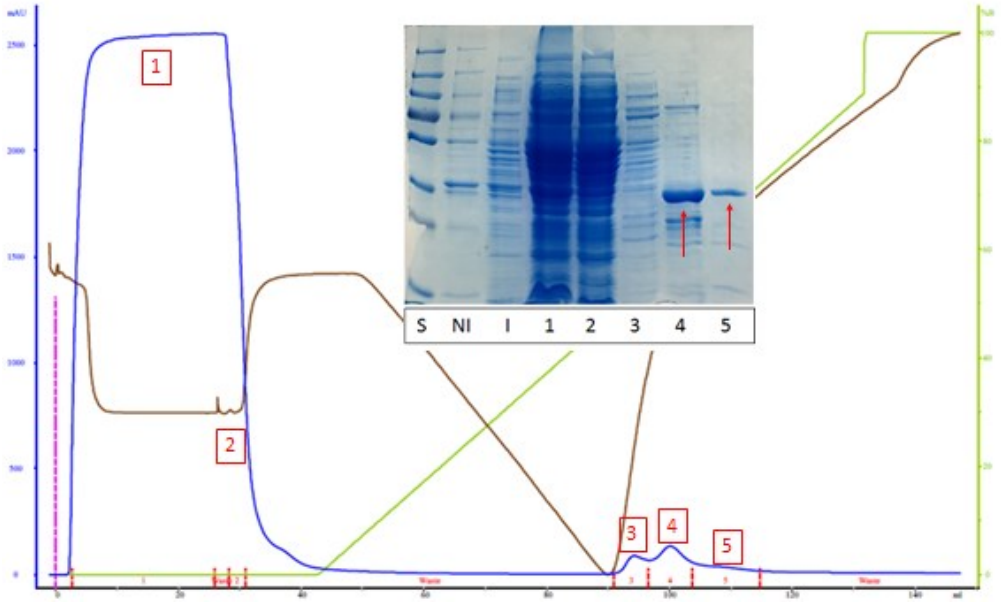

Figure 61: Purification of GGBP_mut_H152C/A213R/L238S_DGTN280-283FCPF from one liter expression culture. The expression in BL21 (DE3) was induced with 1 mM of IPTG. The protein fractions (1-5) were collected and analyzed by SDS gel electrophoresis. Samples of a protein standard (S), of a non-induced and an induced (I) expression were added. The purification analysis is done with the UNICORN 5 software from GE Healthcare. (blue: UV-signal, brown: conductivity, green: solvent gradient of buffer A and B, pink: injection, red: fractions)

GGBP_mut_H152C/A213R/L238S_KIDN285-288FPCF was expressed and purified on the same day and under similar conditions. The induced expression sample (I) shows a noticeably overexpression of the protein. The protein of interest was found in fraction 5 (0.57 mg/ml) and 6 (0,12 mg/ml). However, the impurities found in the two fractions were relatively high which mostly account for the higher protein concentration in fraction 5. In fraction 2 and 3, which were eluted at concentrations of around 25%-30% of butter B, small amounts of protein were already found. This supports the assumption that either the column or the buffer system was defective on that day of purification. Interestingly, the protein peak was not eluting between 25-40% of buffer B, so the gradient was set to 100% for a complete elution to avoid further dilution of the protein of interest. Consequently, the complex protein mixtures eluted in 1 large peak.

The results can be found in **figure 62**.

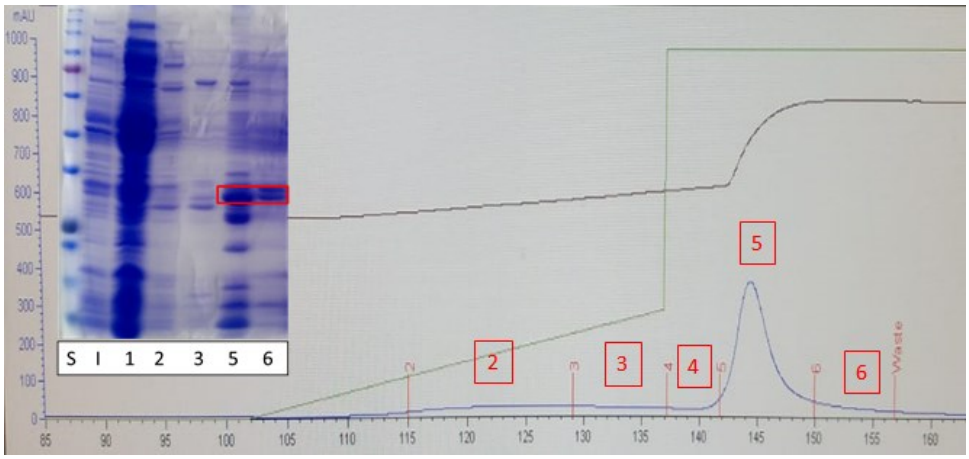

Figure 62: Purification of GGBP_mut_H152C/A213R/L238S_KIDN285-288FPCF from one liter expression culture. The expression in BL21 (DE3) was induced with 1 mM of IPTG. The protein fractions (1-5) were collected and analyzed by SDS gel electrophoresis. Samples of a protein standard (S), of a non-induced and an induced (I) expression were added. The purification analysis is done with the UNICORN 5 software from GE Healthcare. (blue: UV-signal, brown: conductivity, green: solvent gradient of buffer A and B, pink: injection, red: fractions)

In summary, 2 out of 5 expressions worked very well with an acceptable purity for further labeling experiments (in short: GGBP_mut_93-96FPCF & GGBP_mut_280-283FCPF). The other three purification results were used to find potential errors within the workflow on the respective day, but nevertheless, an overexpressed protein of interest was found in all expressions, however at lower concentrations. Due to a lack of time, the purification of GGBP_mut_H152C/A213R/L238S_DGTN280-283FCPF and the other two variants (GGBp_mut_42-45FPCF) with impurities could not be repeated and optimized.

4.5 Synthesis of 5/6-Carboxyfluoresceine in conjugation with a perfluoro-biphenyl linker as pi-clamp reactive FRET donor molecule

It was shown that the π-clamp peptide motif Phe-Cys-Pro-Phe reacts selectively with perfluoro aromatic compounds.(115) A pi-stacking orientation of two phenylalanine rings enhances the activation of the cysteine group which will readily react with these compounds. Perfluoro aromatic compounds do not conjugate to any other cysteine residue within a protein without prior activation of the latter. The pi-clamp motif has been used in the antibody drug conjugate field as well as in the attachment of single fluorophore molecules, but it has never been used in the labeling of a protein with two fluorescent molecules. So far it has been only possible to introduce FRET pairs at specific sites by either enzyme mediated conjugations, mostly limited to the C- or N-terminal endings of a protein sequence, or, click ligation chemistry which needs relatively harsh reaction conditions that a protein would only hardly tolerate (overview of labeling techniques see chapter 1.9.1). The pi-clamp, however, can be encoded directly into

the site of interest and reacts with perfluoro aromatic compounds under very mild conditions. It must be noted that commercially available fluorophores with a perfluoro arylated linker do simply not exist yet, so a custom synthesis had to been done. Dr. Xinlai Cheng from the Wölfl group developed a synthesis route for a perfluoro arylated fluorophore (5/6-Carboxyfluorescein derivative) that could be attached to amino-reactive NHS-esters. The synthetic pathway is shown in **figure 63**.

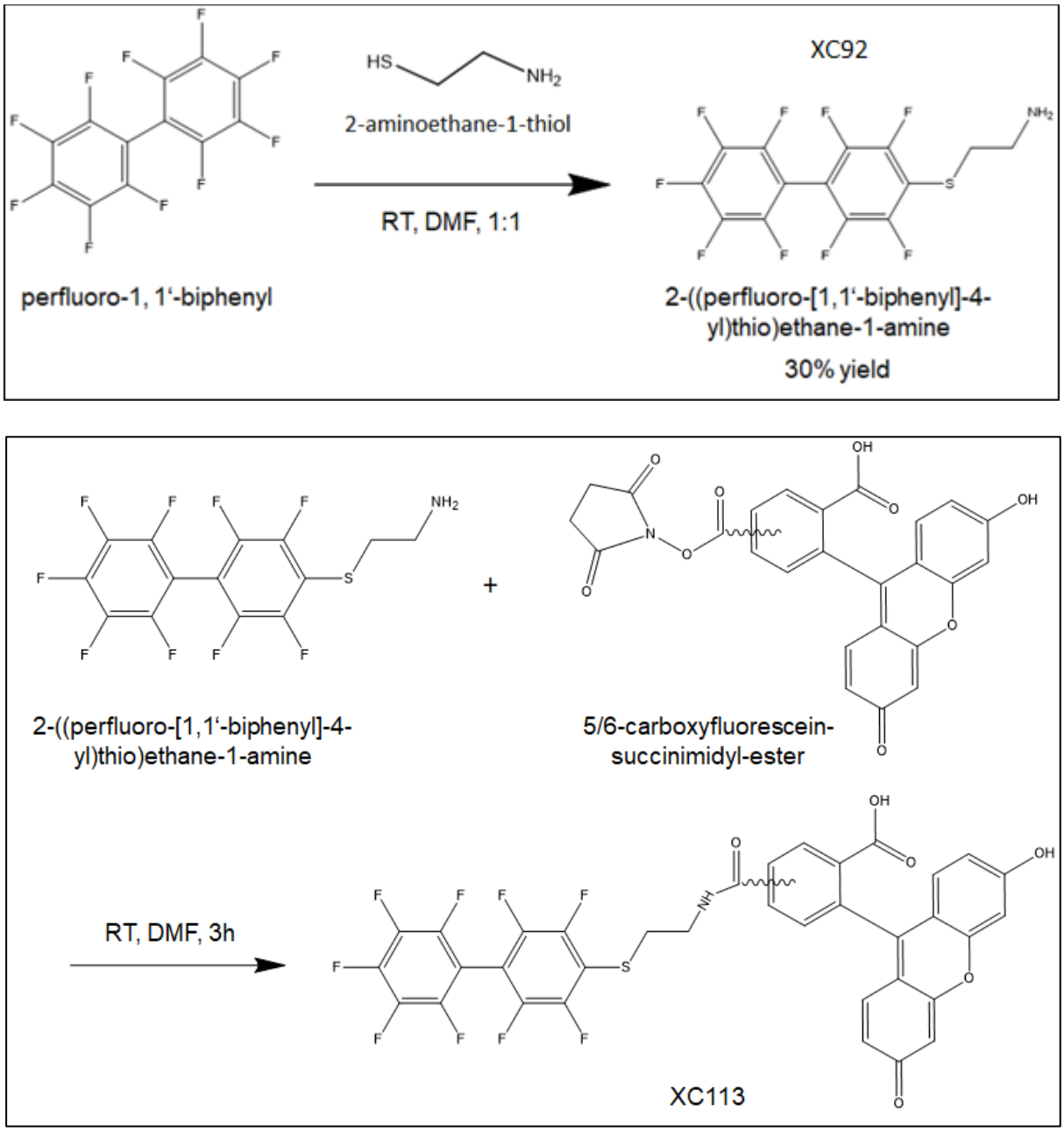

Figure 63: Synthesis route of XC113 (perfluoro arylated 5/6-carboxyfluorescein) as donor molecule in FRET labeling of proteins. The synthesis was developed and carried out by Dr. Xinlai Cheng with permission to publish in this work.

Perfluoro-1, 1'-biphenyl was modified with 2-aminoethane-1-thiol to obtain a functionalised perfluoro arylated linker with an amino function. The reaction educts were added to a reaction

vessel at equal molarities and stirred at room temperature for a few hours in DMF. The product was obtained at a 30% yield. In a second step, the purified 2-((perfluoro-[1,1'-biphenyl]-4-yl) thio) ethane-1-amine was added to the commercially available fluorophore 5/6-carboxyfluorescein-succinimidyl-ester (molar ratio of 1:1) and stirred for 3 hours at room temperature. The compound XC113 was obtained. Finally, the reaction product was purified and validated by ^{1}H-NMR.

4.6 ^{1}H-NMR chemical analysis of XC113 and its synthesis precursors

The linker molecule (2-((perfluoro-[1,1'-biphenyl]-4-yl) thio) ethane-1-amine) and the 5/6-carboxyfluorescein sample were investigated with ^{1}H-NMR. The NMR spectrum of the linker molecule is shown in **figure 64**. The free hydrogen atoms at position 1 and 2 are indicated at a chemical shift of δ=2.91 ppm and δ=3.11 ppm as a doublet of doublet, marked in red. The hydrogen atoms bound to the amino group show one singlet at δ=2.25 ppm, also marked in red.

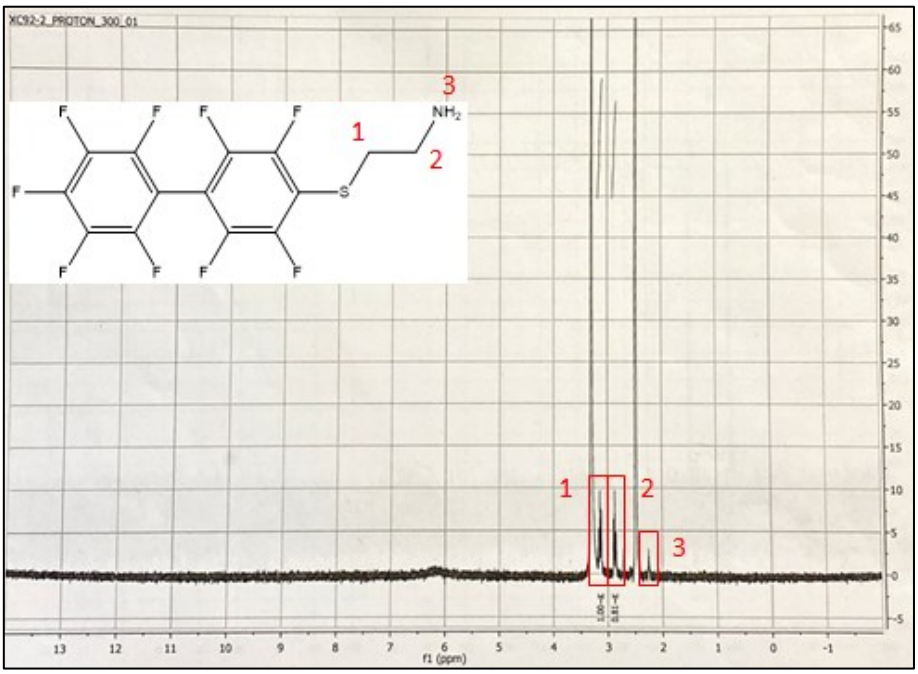

Figure 64: 1H-NMR spectrum of compound XC92 (perfluoro aryl linker molecule).
^{1}H NMR: δ 2.25 ppm (1H, s), 2.91 ppm (2H, dd), 3.11 ppm (2H, dd). This compound was synthesized by Dr. Xinlai Cheng from AG Wölfl. The NMR spectrum was carried out by the NMR department of the IPMB Heidelberg.

As a reference, 5/6-carboxy-fluorescein-NHS was characterized. The ^{1}H-NMR spectrum of this compound shows a singlet at δ=2.2 ppm for the 4 hydrogens that are part of the succinimidyl linker group. The three hydrogens 4, 5, and 6 at the carboxy-benzene group are indicated at a chemical shift between 7.55-8.5 ppm with one singlet and one doublet signal. The hydrogen 14 at the carboxyl group shows a singlet at δ=10.15 ppm. The six hydrogens from the xanthene

body of fluorescein (7, 8, 9, 10, 11, 12) show two singlets and two doublets of doublets. The large peak at δ=3.4 ppm indicated the solvent (DMF). The results can be found in **figure 65**.

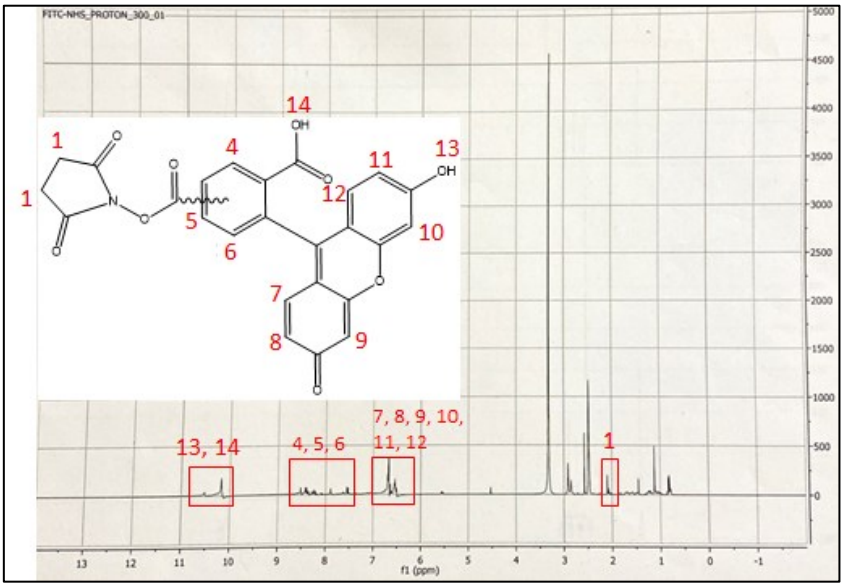

Figure 65: 1H-NMR spectrum of 5/6-Carboxyfluorescein-succinimidyl (NHS).
^{1}H NMR: δ 2.2 ppm (4H, dd, *J* = 13.7, 8.1), 6.5-7.0 ppm (6H, s, d), 7.55-8.50 ppm (3H, s, d), 10.15 (1H, s), 10.55 ppm (1H, s). The compound was purchased by ThermoFisher GmbH. The NMR spectrum was carried out by the NMR department of the IPMB Heidelberg.

XC113 is compared with the ^{1}H-NMR spectra from XC92 and 5/6-carboxyfluorescein-NHS. **Figure 66** indicates the formation of compound XC113 from XC92 and 5/6-carboxy-fluorescein-succinimidyl (NHS). The main difference between 5/6-carboxyfluorescein-NHS and XC113 is the four additional hydrogens of the linker and the newly formed amide function.

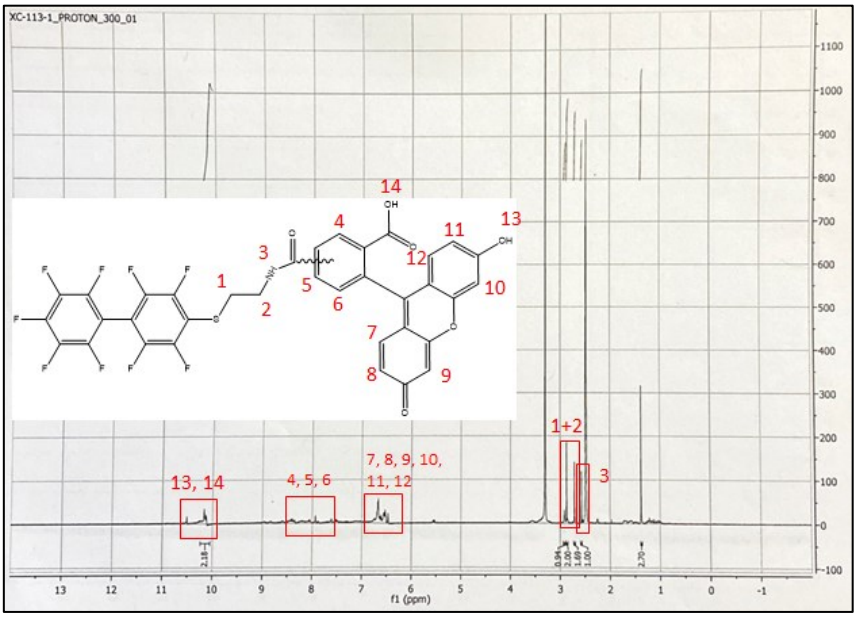

Figure 66:1H-NMR spectrum of compound XC113 (perfluoro arylated 5/6-carboxyfluoresceine derivative).
^{1}H NMR: δ= 2.2 ppm (4H, dd, *J* = 13.7, 8.1), 2.61-2.91 ppm (3H, dd, s), 6.5-7.0 ppm (6H, s, d), 7.55-8.50 ppm (3H, s, d), 10.15 ppm (1H, s), 10.55 ppm (1H, s). This compound was synthesized by Dr. Xinlai Cheng from AG Wölfl. The NMR spectrum was carried out by the NMR department of the IPMB Heidelberg.

The four additional hydrogen atoms from the linker at position 1 and 2 are indicated at δ=2.91 ppm (doublet of doublets) as presented in **figure 64**. The singlet signal of the amino function of the linker which has been transformed to an amide bond in XC113 got shifted from one singlet (2H) at δ=2.25 ppm to one singlet at δ=2.61.

4.7 Spectral characterization of XC113 and suitable FRET pair combinations

Excitation and emission spectra were recorded from the fluorophore XC113 as well as from two Dyomics dyes DY 557 and DY 585 to identify a suitable FRET acceptor molecule for XC113. Figure 67 shows the results. XC113 demonstrated a 35% absorbance rate upon excitation at 450 nm where DY557 shows no absorption. Furthermore, XC113 demostrated a 50% absorption rate upon excitation at 455 nm where DY 585 shows no absorption rate.

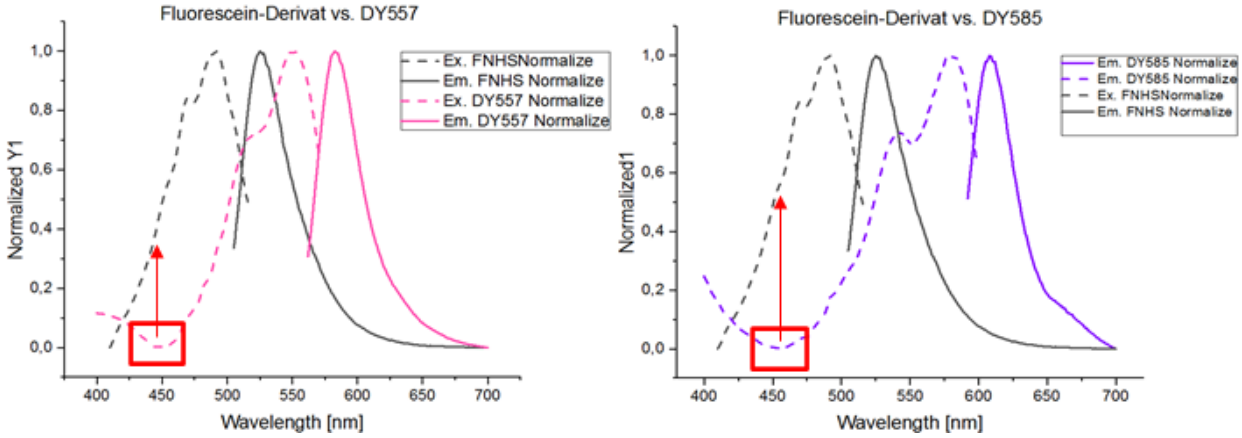

Figure 67: Excitation and emission overlap spectra of perfluoro arylated 5/6-Carboxyfluorescein as FRET donor and DY557 and DY585 as FRET acceptors.
DY585 shows a larger FRET stokes shift with an excitation at 450 nm (higher FRET efficiency by excitation at 50 % of the donor excitation maximum compared to 35% for DY557)

Consequently, DY 585 has been chosen as FRET acceptor molecule as higher energy transfer rates are expected.

Figure 5 shows the characteristic fluorescence excitation and emission maxima for XC113 which have to be considered when chosing the right FRET combinations.

Table 5: Excitation and emission maxima of the 5/6-carboxy-fluorescein derivatives in DMSO and DPBS pH 7.4 as well as of the Perfluoroarylated 5/6 carboxy-fluorescein with and without attachment to GGBP.

	Ex. max.	Em. max.
5-/6-Carboxyfluorescein-NHS (DMSO)	470 nm	560 nm
5-/6-Carboxyfluorescein-NHS (DPBS)	492 nm	515 nm
XC113 (DPBS)	492 nm	532 nm
GGBP-XC113 (DPBS)	492 nm	525 nm

4.8 Labelling of GGBP pi-clamp variants XC113 and DY585

In the first labeling step, the pi-clamp cysteine is selectively coupled to XC113 at pH 8.0, the excess of free dye is separated by gel filtration (PD-10 column) and absorption spectra are recorded. For the degree of labeling the correction factor for XC113 at 280 nm was determined as well as the extinction coefficient from the literature of 5/6-Fluorescein: ε=81.000 M^{-1} x cm^{-1}, ex max 492nm) was used. The extinction coefficient of the GGBP protein was determined by Lambert-Beer law: 32.673 M^{-1} x cm^{-1}.

Degree of Labeling (GGBP_mut_280-283FCPF-XC113):

$$C_{280} = \frac{0{,}17354}{0{,}31755} = 0{,}546$$

$$Prot.conc.\,(M) = \frac{(0{,}17354 - (0{,}31755 * 0{,}546))}{32.673\ (M^{-1} * cm^{-1})} * 101 = 7{,}35x10^{-7}\ M$$

$$\frac{moles\ dye}{mol\ protein} = \frac{0{,}0655}{81.000(M^{-1} * cm^{-1}) * 7{,}35 * 10^{-9}\ (M)} * 101 = 1{,}09$$

The second label is attached at pH 7.4, treated equally and the degree of labeling is determined. A correction factor of both dyes has to be calculated at 280 nm.

Degree of labeling (GGBP_mut_280-283FCPF-XC113-DY585):

$$C_{280} = \frac{0{,}1266}{0{,}5533} = 0{,}229$$

$$C_{280} = 0{,}229 + 0{,}546 = 0{,}779$$

$$Prot.conc.\,(M) = \frac{(0{,}1216 - (0{,}0466 * 0{,}779))}{32.673\ (M^{-1} * cm^{-1})} = 2{,}61x10^{-6}\ M$$

$$\frac{moles\ dye}{mol\ protein} = \frac{0{,}0466}{120.000(M^{-1} * cm^{-1}) * 2{,}61x10^{-6}\ (M)} = 0{,}15$$

As a result, the perfluoro compound XC113 binds to the pi-clamp in GGBP_mut280-283FCPF at a ratio of 1,09:1 (dye: protein). DY585, however, only attached to an extend of 15% to the mutant. Other labeling experiments with different mutants showed attachment rates of up to 50%. The absorbance spectrum of GGBP_mut_H152C/A213R/L238S_DGTN280-283FCPF with both dyes XC113 and DY585 is shown in figure 68.

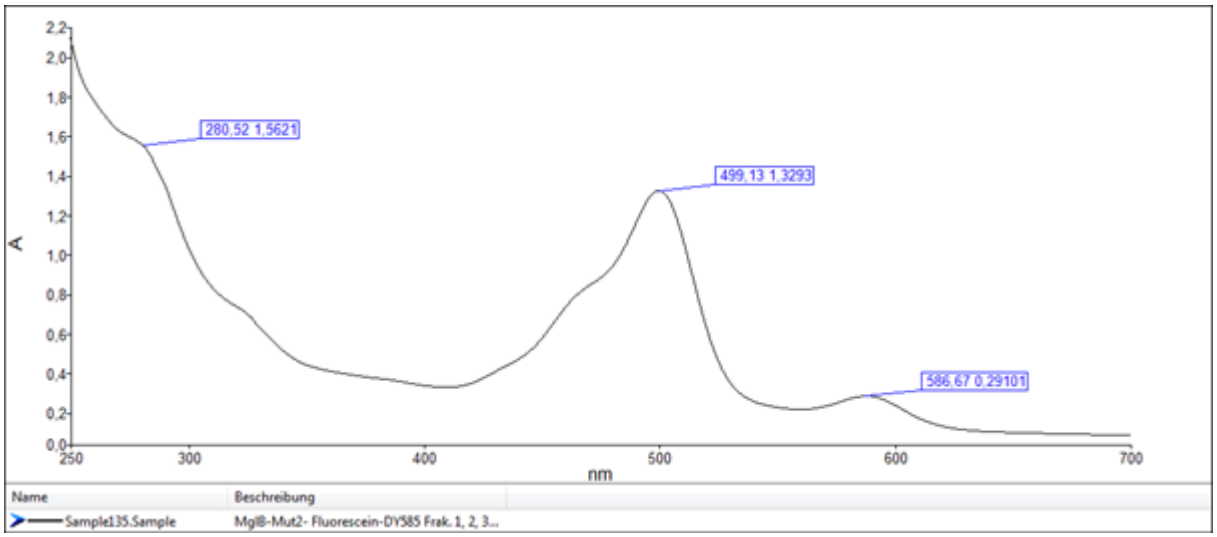

Figure 68: Absorption spectrum of GGBP_mut_ H152C/A213R/L238S_DGTN280-283FCPF-XC113-DY585.

4.9 Glucose Sensitivity of FRET labelled GGBP

The mutant GGBP_mut_H152C/A213R/L238S_DGTN280-283FCPF-XC113-DY585 was finally tested for different glucose concentrations. A fluorescence energy transfer of 18% could be detected by excitation at 455 nm and emission (602 nm). A linear correlation of R^2=0.9 towards glucose with a total fluorescence increase of 12% was obtained. The results are shown in **figure 69**. The fluorescence emission on the right indicates an environmental sensitive position 152 as well as a more constant emission from DY 585 at positions 280-283. The findings are discussed in the next chapter. Similar results were obtained for GGBP_mut_H152C/A213R/L238S_EPSR93-96FPCF (see figure 70).

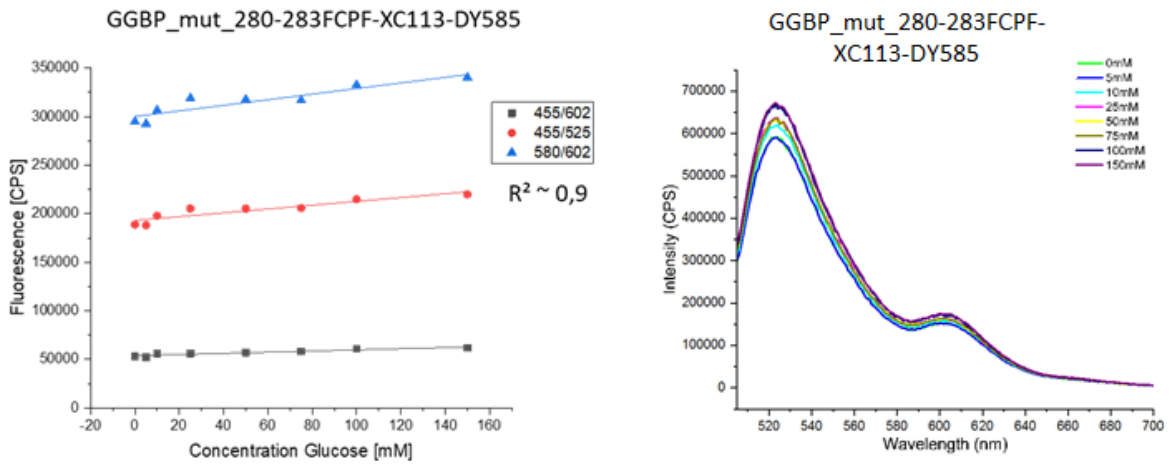

Figure 69: FRET-transfer of GGBP_mut_280-283FCPF-XC113-DY585 at varying glucose concentrations. The FRET transfer rate equals 18%. The fluorescence emission spectrum is shown on the right.

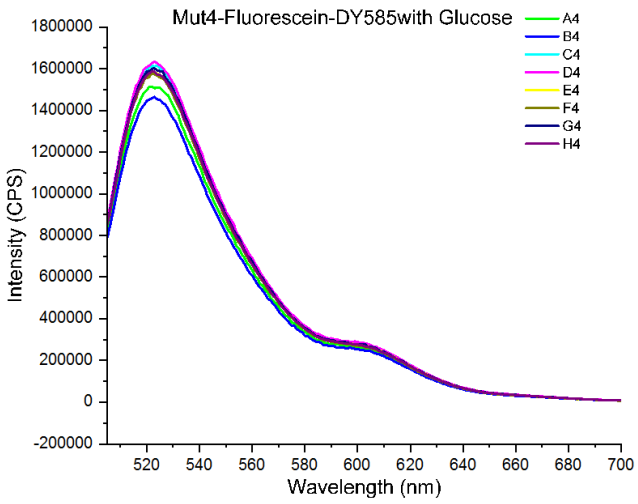

Figure 70: Fluorescence emission of GGBP_mut_H152C/A213R/L238S_EPSR93-96FPCF-XC113-DY585.

4.10 Discussion

In the results part 2, the development of ratiometric FRET biosensor recognition elements based on the glucose galactose binding protein (GGBP) in E. coli using the Pi-Clamp strategy of Pentelute et al, 2016 was reported for the first time. The Pi-clamp strategy involves a four amino acid sequence 'FCPF' that can be encoded into a gene and translated into a protein. The cysteine of this motif is surrounded by a locally tuned environment of two phenylalanine residues that active the free thiol group for nucleophilic attacking. Specific perfluoro arylated linker molecules can therefore react with the thiol group to form a thioether bond. These linker molecules This labeling strategy was previously used for the selective attachment of toxins to antibodies in the antibody-drug-conjugate research. This method offers a whole new horizon of selective coupling in optical biosensor developments.

As a first step, sequence alignments of various glucose binding proteins in different organisms were performed. This analysis showed that even amongst different organisms with various sequence similarities, the structural molecular domains of these proteins are highly conserved. The goal of the sequence alignments was to identify regions within GGBP that are neither part of an α-helix or β-sheet nor involved in direct or indirect stabilizing the ligand. Furthermore, the open source software Swiss Model was used to determine the quality of the overall model based on the crystal structure (2HPH, 0.92Å) of GGBP. The QMEAN scoring algorithm was identifying quality parameters such as torsion angles, solvation potential, interaction potential and solvent accessibility of the secondary structure. Due to the overall high stability of GGBP, the model had a particularly good quality. The following residues were considered as being

tolerant to mutations: amino acid regions from N-terminal to C-terminal: 11-14, 30-33, 41-44, 69-72, 93-96, 193-197, 147-150, 169-172, 181-184, 197-200, 225-238 and 274-308. However, region 11-14 as well as 181-184 were avoided because of a direct and indirect stabilization of glucose in the binding pocket. As a result, five mutation tolerating regions were identified were the pi-clamp motif was inserted. The following mutations were designed and expressed and purified on a His-taq affinity column on the Äkta purifier in Prof. Mack's lab.

1. GGBP_mut_H152C/A213R/L238S_QNDQ42-45FPCF
2. GGBP_mut_H152C/A213R/L238S_VDPA68-71FCPF
3. GGBP_mut_H152C/A213R/L238S_EPSR93-96FPCF
4. GGBP_mut_H152C/A213R/L238S_DGTN280-283FCPF
5. GGBP_mut_H152C/A213R/L238S_KIDN285-288FPCF

The proteins 3 and 4 were obtained in relatively high yield and with a high purity (10mg). However, the proteins 1, 2 and 5 could be only obtained at less quality, as many other proteins were eluting with the protein of interest. The potential problem could be that the specific column and/or the specific high imidazole buffer B were in a bad condition on that day. A reconstitution of the column could have solved the problem. Unfortunately, due to a limit of time, glucose sensitivity experiments have only been carried out with mutants 3 and 4 to minimize side effects of impurities in testing.

For the FRET labeling of GGBP, a perfluoro arylated linker molecule was synthesized by Dr. Xinlai Cheng from AG Wölfl which was attached to the commercially available 5/6-carboxy-fluorescein-NHS fluorophore. It must be noted that any other amino-reactive fluorophore could have been used. Fluorescein, however, is excited above 400 nm and was perfectly suitable as a fluorescent donor molecule. The final fluorophore XC113 was synthesized in a simple 2 step-synthesis. The linker molecule XC92 was obtained at a 30% yield after 3 hours stirring in DMF at room temperature. The 5/6-carboxy-fluorescein-NHS was coupled for another 3 hours at room temperature after purification. The purified samples were analyzed by ^{1}H-NMR and the successful synthesis could be confirmed by the formation of the singlet of the newly introduced amide function at δ=2.61 ppm (compared to δ=2.25 ppm of the amine function of the linker).

The Dyomics dyes DY 557 and DY 585 were analyzed for their suitability as FRET donor molecules. It was shown that DY 585 shows a higher absorbance (50% of its total fluorescence) at the wavelength were the absorbance of 5/6-carboxyfluorescein (donor) is zero. This is important, otherwise the acceptor molecule would be partially excited with the excitation of the donor molecule. This must be avoided to ensure a pure energy transfer of the donor molecule. DY 557 only showed a 35% absorbance, therefore DY 585 was the acceptor molecule of choice.

The pi-clamp selective dye XC113 was labeled to GGBP in a first reaction, then the reaction was stopped by a gel filtration step to remove excess dye. The absorbance of the dye was measured to determine the degree of labeling (DOL). As an example, for mutant 4, a DOL of 1.1:1 (dye: protein) was observed for XC113. In a second step, DY 585 was equally labeled to the donor-protein complex and was separated from excess dye after 3 hours. Here, a DOL of 0.15:1 (dye: protein) was obtained. In other experiments, degree of labeling rates of up to 50% were obtained for DY585. The reason for this could be the pH during labeling, as a pH of 8.0 is required for the perfluoro aryl-cysteine reaction. These conditions could explain the lowered DOL of DY 585 in the second labeling step.

Mutant 3 was then tested for glucose sensitivity at various glucose concentrations ranging from 1-150 mM. A fluorescence energy transfer from the donor to the acceptor molecule of 18% was observed (ex. 455 nm / em. 602 nm). A sensitivity towards glucose was observed from 1-150 mM with a total fluorescence intensity increase of 12%. This increase comes exclusively from the fluorescence emission intensity of XC113. The fluorescence emission of DY 585 stays constant over varying glucose concentrations. This indirectly proves the idea of the developed FRET sensor system to work accurately if the donor molecule XC113 would be exchanged by a potent fluorophore that has been studied in the environmentally sensitive section of this work, for example, Atto 465 or Atto 495. This assumption can be further confirmed by the fluorescence emission of Mutant 3 which also shows the 12 % fluorescence intensity increase at position 152 from XC113 upon binding of glucose and a slight increase of the fluorescence emission also at the acceptor molecule DY 585. This increase can be explained by the position that the acceptor molecule is attached to in this mutant, namely position 95. Position 95 is located on top of helix 4 at the N-terminal domain in vicinity to position 152 and the ligand binding pocket and is exposed to the environmental changes that influence all other fluorophores at position 152 as well. This means that mutant GGBP_mut_H152C/A213R/L238S_DGTN280-283FCPF should work as an effective ratiometric glucose biosensor recognition element if it is labeled with Atto 495 and DY 585.

5 Conclusion & Outlook

In this work, fluorescent environmentally sensitive as well as FRET-based glucose biosensor elements by using the glucose galactose binding protein in E. coli have successfully been developed. The best results for an environmentally sensitive sensing scheme could be obtained by the triple mutant GGBP_H152C/A213R/L238S for the Atto dyes Atto 465 and Atto 495, with 48% and 44% of maximal fluorescence intensity increase upon binding of 100mM glucose.

Furthermore, GGBP_mut_H152C/A213R/L238S_DGTN280-283FCPF was discovered and could prove the successful selective attachment of FRET donor and acceptor molecules by the pi-clamp strategy. In a future experiment, the efficiency could be highly improved by attaching an environmental sensitive dye to position 152 such as the discovered molecule Atto 495, and DY 585 to position 281 in the loop on the backside of the protein. Hence, a fully suitable ratiometric FRET biosensor element would be discovered.

6 Experimental Part

6.1 Material

6.1.1 Technical Equipment and Software

Cloning & expression:

- C1000 Thermal Cycler for PCR, Bio-Rad Laboratories GmbH, Munich, Germany
- agarose gel chamber Power Pac HC, 250V/3.0A/300W, Bio-Rad Laboratories GmbH
- universal hood with camera for analyzing ethidium bromide stained gels, Bio-Rad Laboratories GmbH
- Heraeus Multifuge X3 FR, Heraeus Fresco 21, Thermo Fisher Scientific
- Ecotron shaker incubator, Infors HT
- Heraeus Function Line incubator for cell plates
- MM300 swing rotor lysator, Retsch GmbH

Protein purification:

- pH-meter 761 Calimatic, Knick
- cellulose nitrate filter, 0.45µm, Sartorius Stedim Biotech GmbH, Göttingen
- Sonorex Super 10P digital, Bandelin GmbH
- constant cell disruption system, t-series hydraulic disrupter, LAUDA Eco silver RE620 cooling system, Low March, Daventry, Northants, NN11 4SD., United Kingdom
- Heraeus Multifuge X1R centrifuge for 15/50ml falcons, Thermo Fisher Scientific
- Avanti-J-30I ultra centrifuge with JA-30.50Ti Rotor, Beckman Coulter
- Beckman centrifuge vials
- IKA vortex 2, Vortexer

Absorption measurements:

- Nano Vue, micro protein/DNA absorption UV spectrometer, GE Healthcare
- UV/VIS plate reader Anthos Microsystems Germany, Software Mikro Win 2000 (Mikro-Tec GmbH)
- Lambda 35 UV/VIS cuvette spectrometer from Perkin-Elmer, Software Win Lab 6.0.3
- 96 well plates, polystyrol, Greiner Bio-One GmbH, Frickenhausen

Fluorescence measurements:

- Spectrofluorometer Fluorolog-3 from Horiba Jobin Yvon GmbH, cuvette and microplate reader, Software Origin
- QS High Precision Cell Quartz SUPRASIL® cuvette, 10x10mm from Hellma Analytics, Germany
- Micro Max 384 microwell plate reader for Fluorolog-3, Horiba Jobin Yvon GmbH
- Fluorohub single photon counting controller, Horiba Jobin Yvon GmbH

6.1.2 Chemicals

Chemicals	Application	Manufacturer
sodium chloride Lot: 0001056155	buffer, LB-medium	AppliChem ITW Reagents
potassium chloride	buffer	
Na2HPO4*2H2O Emprove® Bio	buffer	Merck KGaA, Darmstadt
NaH2PO4*H2O Emprove® Bio	buffer	Merck KGaA, Darmstadt
imidazole bio ultra ≥99.5%(GC) Lot # BCBN3257V	buffer	Sigma Life Science
ethidium bromide	agarose gel	Sigma-Aldrich
glass-beads acid-washed	cell lysis	Sigma-Aldrich
ampicillin sodium salt	antibiotic	Carl Roth
kanamycin-sulfate	antibiotic	Santa Cruz
agarose for molecular biology	agarose gel	Sigma Life Science
yeast extract for bacteriology	LB-medium	Carl Roth, Karlsruhe
trypton/pepton from casein, pancreatic digestion	LB-medium	Carl Roth, Karlsruhe
TEMED ≥98.5%	SDS-PAGE	Carl Roth, Karlsruhe
TRIS ≥99.9%	SDS-PAGE	Carl Roth, Karlsruhe
SDS ≥99%	SDS-PAGE	Carl Roth, Karlsruhe
APS 99%	SDS-PAGE	Grüssing GmbH
Brillant Blue R250	staining solution	Carl Roth, Karlsruhe
methanol	staining solution	VWR Chemicals, Radnor, USA
acetic acid ≥99,8%	destaining solution	Sigma-Aldrich
2-propanol 99,9%	destaining solution	Zentrallager INF 367
glycine	running buffer	Labochem international
ß-mercaptoethanol ≥99%	loading buffer	Sigma-Aldrich
bromphenolblue	loading buffer	Sigma-Aldrich
glycerine ≥99,5%, waterfree	loading buffer	Carl Roth, Karlsruhe

6.1.3 Bacteria strains, plasmids, restriction enzymes

Strain	Genotype	Manufacturer
E.coli BL21(DE3) Singles™ chemical competent bacteria	F^-, ompT, hsd $S_B(r_B^-m_B^-)$, gal, dcm (DE3)	Merck Novagen, EMD Millipore, Temecula, USA
E.coli TOP-10 cloning strain	F^-, mcrA, D(mrr-hsdRMS-mcrBC) 80lacZM15, lacX74 recA1, araD139 (ara-leu)7697, galU, galK, rpsL(Str^R), endA1 λ^-	AG Mack
E.coli DH5α cloning strain	F^-, φ80d/lacZΔM15, recA1, endA1, gyrA96, thi^-, hsdR17 (r_K^- m_K^+), supE44, relA1, deoR, Δ(lacZYA-argF) U169	AG Wölfl/AG Mack

Enzymes and Plasmids:

NdeI	restriction enzyme	New England Biolabs
XhoI	restriction enzyme	New England Biolabs
EcoRI	restriction enzyme	New England Biolabs
pET24a(+)	E.coli expression plasmid, kanamycin resistance, C-terminal His-Taq	Merck KGaA, Darmstadt
pET28a(+)	E.coli expression plasmid, kanamycin resistance, N-terminal His-Taq	Merck KGaA, Darmstadt
pET24a(MglBwt)	E.coli expression plasmid with MglB-wt-gene	this work
pET24a(MglB-H152C/A213R/L238S)	E.coli expression plasmid with MglB-mutant-gene	this work
pET24a (MglB-H152C/A213R/L238S)-(42-45FPCF)	E.coli expression plasmid with MglB-mutant and pi-Clamp mutation	this work
pET24a (MglB-H152C/A213R/L238S)-(68-71FCPF)	E.coli expression plasmid with MglB-mutant and pi-Clamp mutation	this work
pET24a (MglB-H152C/A213R/L238S)-(93-96FPCF)	E.coli expression plasmid with MglB-mutant and pi-Clamp mutation	this work
pET24a (MglB-H152C/A213R/L238S)-(280-283FCPF)	E.coli expression plasmid with MglB-mutant and pi-Clamp mutation	this work

pET24a (MglB-H152C/A213R/L238S)-(285-288FPCF)	E.coli expression plasmid with MglB-mutant and pi-Clamp mutation	this work

Kits and Standards:

auto induction system 1	pET expression systems (E.coli)	Merck Millipore
Bradford protein assay solution	determining protein concentrations from 0,1-0,5mg/ml	Bio-Rad Laboratories, Munich
rotiphorese gel 30	acrylamide	Carl Roth, Karlsruhe
GeneRuler®, 1kb	Gene size standard	ThermoFisher
PageRuler®	Protein size standard	Thermofisher

Sequence Alignments

>sequence Insert MglB-3Mut_mut42-45FPCF:
CATATGAATAAGAAGGTGTTAACCCTGTCTGCTGTGATGGCCAGCATGTTATTCGGTGCCGCTGCACACGCTGCTGATAC
TCGCATTGGTGTAACAATCTATAAGTACGACGATAACTTTATGTCTGTAGTGCGCAAGGCTATTGAGCAAGATGCGAAAG
CCGCGCCAGATGTTCAGCTGCTGATGAATGATTCTTTCCCCTGTTTCTCCAAGCAGAACGATCAGATCGACGTATTGCTG
GCGAAAGGGGTGAAGGCACTGGCAATCAACCTGGTTGACCCGGCAGCTGCGGGTACGGTGATTGAGAAAGCGCGTGGGCA
AAACGTGCCGGTGGTTTTCTTCAACAAAGAACCGTCTCGTAAGGCGCTGGATAGCTACGACAAAGCCTACTACGTTGGCA
CTGACTCCAAAGAGTCCGGCATTATTCAAGGCGATTTGATTGCTAAACACTGGGCGGCGAATCAGGGTTGGGATCTGAAC
AAAGACGGTCAGATTCAGTTCGTACTGCTGAAAGGTGAACCGGGCTGCCCGGATGCAGAAGCACGTACCACTTACGTGAT
TAAAGAATTGAACGATAAAGGCATCAAAACTGAACAGTTACAGTTAGATACCGCAATGTGGGACACCGCTCAGGCGAAAG
ATAAGATGGACGCCTGGCTGTCTGGCCCGAACGCCAACAAAATCGAAGTGGTTATCGCCAACAACGATCGCATGGCAATG
GGCGCGGTTGAAGCGCTGAAAGCACACAACAAGTCCAGCATTCCGGTGTTTGGCGTCGATGCGAGCCCAGAAGCGCTGGC
GCTGGTGAAATCCGGTGCACTGGCGGGCACCGTACTGAACGATGCTAACAACCAGGCGAAAGCGACCTTTGATCTGGCGA
AAAACCTGGCCGATGGTAAAGGTGCGGCTGATGGCACCAACTGGAAAATCGACAACAAAGTGGTCCGCGTACCTTATGTT
GGCGTAGATAAAGACAACCTGGCTGAATTCAGCAAGAAACTCGAG

>sequence Insert MglB-3Mut_mut68-71FCPF:
CATATGAATAAGAAGGTGTTAACCCTGTCTGCTGTGATGGCCAGCATGTTATTCGGTGCCGCTGCACACGCTGCTGATAC
TCGCATTGGTGTAACAATCTATAAGTACGACGATAACTTTATGTCTGTAGTGCGCAAGGCTATTGAGCAAGATGCGAAAG
CCGCGCCAGATGTTCAGCTGCTGATGAATGATTCTCAGAATGACCAGTCCAAGCAGAACGATCAGATCGACGTATTGCTG
GCGAAAGGGGTGAAGGCACTGGCAATCAACCTGTTTTGCCCATTCGCTGCGGGTACGGTGATTGAGAAAGCGCGTGGGCA
AAACGTGCCGGTGGTTTTCTTCAACAAAGAACCGTCTCGTAAGGCGCTGGATAGCTACGACAAAGCCTACTACGTTGGCA
CTGACTCCAAAGAGTCCGGCATTATTCAAGGCGATTTGATTGCTAAACACTGGGCGGCGAATCAGGGTTGGGATCTGAAC
AAAGACGGTCAGATTCAGTTCGTACTGCTGAAAGGTGAACCGGGCTGCCCGGATGCAGAAGCACGTACCACTTACGTGAT
TAAAGAATTGAACGATAAAGGCATCAAAACTGAACAGTTACAGTTAGATACCGCAATGTGGGACACCGCTCAGGCGAAAG
ATAAGATGGACGCCTGGCTGTCTGGCCCGAACGCCAACAAAATCGAAGTGGTTATCGCCAACAACGATCGCATGGCAATG
GGCGCGGTTGAAGCGCTGAAAGCACACAACAAGTCCAGCATTCCGGTGTTTGGCGTCGATGCGAGCCCAGAAGCGCTGGC
GCTGGTGAAATCCGGTGCACTGGCGGGCACCGTACTGAACGATGCTAACAACCAGGCGAAAGCGACCTTTGATCTGGCGA
AAAACCTGGCCGATGGTAAAGGTGCGGCTGATGGCACCAACTGGAAAATCGACAACAAAGTGGTCCGCGTACCTTATGTT
GGCGTAGATAAAGACAACCTGGCTGAATTCAGCAAGAAACTCGAG

>sequence Insert MglB-3Mut_mut93-96FPCF:
CATATGAATAAGAAGGTGTTAACCCTGTCTGCTGTGATGGCCAGCATGTTATTCGGTGCCGCTGCACACGCTGCTGATAC
TCGCATTGGTGTAACAATCTATAAGTACGACGATAACTTTATGTCTGTAGTGCGCAAGGCTATTGAGCAAGATGCGAAAG
CCGCGCCAGATGTTCAGCTGCTGATGAATGATTCTCAGAATGACCAGTCCAAGCAGAACGATCAGATCGACGTATTGCTG
GCGAAAGGGGTGAAGGCACTGGCAATCAACCTGGTTGACCCGGCAGCTGCGGGTACGGTGATTGAGAAAGCGCGTGGGCA
AAACGTGCCGGTGGTTTTCTTCAACAAATTCCCGTGTTTCAAGGCGCTGGATAGCTACGACAAAGCCTACTACGTTGGCA
CTGACTCCAAAGAGTCCGGCATTATTCAAGGCGATTTGATTGCTAAACACTGGGCGGCGAATCAGGGTTGGGATCTGAAC
AAAGACGGTCAGATTCAGTTCGTACTGCTGAAAGGTGAACCGGGCTGCCCGGATGCAGAAGCACGTACCACTTACGTGAT
TAAAGAATTGAACGATAAAGGCATCAAAACTGAACAGTTACAGTTAGATACCGCAATGTGGGACACCGCTCAGGCGAAAG
ATAAGATGGACGCCTGGCTGTCTGGCCCGAACGCCAACAAAATCGAAGTGGTTATCGCCAACAACGATCGCATGGCAATG
GGCGCGGTTGAAGCGCTGAAAGCACACAACAAGTCCAGCATTCCGGTGTTTGGCGTCGATGCGAGCCCAGAAGCGCTGGC

GCTGGTGAAATCCGGTGCACTGGCGGGCACCGTACTGAACGATGCTAACAACCAGGCGAAAGCGACCTTTGATCTGGCGA
AAAACCTGGCCGATGGTAAAGGTGCGGCTGATGGCACCAACTGGAAAATCGACAACAAAGTGGTCCGCGTACCTTATGTT
GGCGTAGATAAAGACAACCTGGCTGAATTCAGCAAGAAACTCGAG

>sequence Insert MglB-3Mut_mut280-283FCPF:
CATATGAATAAGAAGGTGTTAACCCTGTCTGCTGTGATGGCCAGCATGTTATTCGGTGCCGCTGCACACGCTGCTGATAC
TCGCATTGGTGTAACAATCTATAAGTACGACGATAACTTTATGTCTGTAGTGCGCAAGGCTATTGAGCAAGATGCGAAAG
CCGCGCCAGATGTTCAGCTGCTGATGAATGATTCTCAGAATGACCAGTCCAAGCAGAACGATCAGATCGACGTATTGCTG
GCGAAAGGGGTGAAGGCACTGGCAATCAACCTGGTTGACCCGGCAGCTGCGGGTACGGTGATTGAGAAAGCGCGTGGGCA
AAACGTGCCGGTGGTTTTCTTCAACAAAGAACCGTCTCGTAAGGCGCTGGATAGCTACGACAAAGCCTACTACGTTGGCA
CTGACTCCAAAGAGTCCGGCATTATTCAAGGCGATTTGATTGCTAAACACTGGGCGGCGAATCAGGGTTGGGATCTGAAC
AAAGACGGTCAGATTCAGTTCGTACTGCTGAAAGGTGAACCGGGCTGCCCGGATGCAGAAGCACGTACCACTTACGTGAT
TAAAGAATTGAACGATAAAGGCATCAAAACTGAACAGTTACAGTTAGATACCGCAATGTGGGACACCGCTCAGGCGAAAG
ATAAGATGGACGCCTGGCTGTCTGGCCCGAACGCCAACAAAATCGAAGTGGTTATCGCCAACAACGATCGCATGGCAATG
GGCGCGGTTGAAGCGCTGAAAGCACACAACAAGTCCAGCATTCCGGTGTTTGGCGTCGATGCGAGCCCAGAAGCGCTGGC
GCTGGTGAAATCCGGTGCACTGGCGGGCACCGTACTGAACGATGCTAACAACCAGGCGAAAGCGACCTTTGATCTGGCGA
AAAACCTGGCCGATGGTAAAGGTGCGGCTTTTTGCCCATTCTGGAAAATCGACAACAAAGTGGTCCGCGTACCTTATGTT
GGCGTAGATAAAGACAACCTGGCTGAATTCAGCAAGAAACTCGAG

>sequence Insert MglB-3Mut_mut285-288FPCF:
CATATGAATAAGAAGGTGTTAACCCTGTCTGCTGTGATGGCCAGCATGTTATTCGGTGCCGCTGCACACGCTGCTGATAC
TCGCATTGGTGTAACAATCTATAAGTACGACGATAACTTTATGTCTGTAGTGCGCAAGGCTATTGAGCAAGATGCGAAAG
CCGCGCCAGATGTTCAGCTGCTGATGAATGATTCTCAGAATGACCAGTCCAAGCAGAACGATCAGATCGACGTATTGCTG
GCGAAAGGGGTGAAGGCACTGGCAATCAACCTGGTTGACCCGGCAGCTGCGGGTACGGTGATTGAGAAAGCGCGTGGGCA
AAACGTGCCGGTGGTTTTCTTCAACAAAGAACCGTCTCGTAAGGCGCTGGATAGCTACGACAAAGCCTACTACGTTGGCA
CTGACTCCAAAGAGTCCGGCATTATTCAAGGCGATTTGATTGCTAAACACTGGGCGGCGAATCAGGGTTGGGATCTGAAC
AAAGACGGTCAGATTCAGTTCGTACTGCTGAAAGGTGAACCGGGCTGCCCGGATGCAGAAGCACGTACCACTTACGTGAT
TAAAGAATTGAACGATAAAGGCATCAAAACTGAACAGTTACAGTTAGATACCGCAATGTGGGACACCGCTCAGGCGAAAG
ATAAGATGGACGCCTGGCTGTCTGGCCCGAACGCCAACAAAATCGAAGTGGTTATCGCCAACAACGATCGCATGGCAATG
GGCGCGGTTGAAGCGCTGAAAGCACACAACAAGTCCAGCATTCCGGTGTTTGGCGTCGATGCGAGCCCAGAAGCGCTGGC
GCTGGTGAAATCCGGTGCACTGGCGGGCACCGTACTGAACGATGCTAACAACCAGGCGAAAGCGACCTTTGATCTGGCGA
AAAACCTGGCCGATGGTAAAGGTGCGGCTGATGGCACCAACTGGTTTCCCTGCTTCAAAGTGGTCCGCGTACCTTATGTT
GGCGTAGATAAAGACAACCTGGCTGAATTCAGCAAGAAACTCGAG

6.2 Methods and Protocols

6.2.1 Cloning

The coding gene of the wildtype Glucose-Galactose binding protein was amplified by PCR from the Eserichia coli strain K-12 M1655 which was a kind gift from Prof. Dr. Mathias Mack, Microbiology lab, university of applied science Mannheim. The coding DNA fragment was amplified using two designed primers each of which contains a restriction site, for the enzymes XhoI and NdeI, respectively.

PCR protocol

Master Mix	PCR reaction
5 µl Pfu buffer	*40 µl Master Mix*
1 µl dNTP	*5 µl Primer 1 (10 µM)*
1 µl Polymerase	*5 µl Primer 2 (10 µM)*
1 µl DNA (~10 ng/µl)	
32 µl water	
40 µl total volume	***50 µl total volume***

Digestion protocol for pET vector and amplified PCR product

vector	purified PCR product
2 µl Fast Digest buffer 10x	*3 µl Fast Digest buffer 10x*
10 µl vector DNA (up to 1µg)	*10 µl DNA (~10 ng/µl)*
1µl XhoI	*1 µl XhoI*
1µl NdeI	*1 µl NdeI*
13 µl H_2O	*15 µl H_2O*
1 µl Fast-AP (Alkaline phosphatase)	
20 µl total volume	***30 µl total volume***

Ligation protocol

The ligation mixture is incubated for 10 – 60 min at room temperature, alternatively over night at 16 °C.

Ligation of digested vector and PCR product
3 µl linear vector (20-100 ng)
5 µl insert DNA fragment (molar ratio DNA:vector 5:1)

2 µl T4 DNA ligase buffer (1 unit) 10x
0,2 µl T4 DNA ligase 5x
9,8 µl H2O
20 µl total volume

Transformation protocol & mini preparation of cloning and expression strains

For the transformation (DNA insertion into a vector) of the cloned DNA, 50 µl of chemical competent bacterial cells are thawed on ice for 5 min. 1-5 µl DNA (equals 5-10 ng) are added, carefully mixed and spun down. After incubated for 30 min on ice, the mixture is heat shocked at 42 °C for 30 sec and put back on ice for 2 min. 250 µl sterile super optimal broth medium with catabolite repression medium (SOC medium) are heated up to 37 °C before added to the mixture and incubated in an Eppendorf vial shaker (225 rpm) for an hour at the same temperature. For a single construct, 20 µl and 200 µl of the transformed bacteria are evenly distributed onto agar plates with respective antibiotic (50µg/ml). The agar plates are incubated in an incubator at 37 °C overnight. Single colonies are picked with pipette tips each of which is transferred into ca. 10 ml of 2x YT medium with respective antibiotic. A new agar plate can be prepared accordingly for storage. The vessel is incubated in a shaker incubator at 37 °C overnight. On day 2, 4 ml of inoculated culture medium is transferred into an Eppendorf tube and spun down at 8000 rpm for 2 min. The supernatant is removed, and the pellet is resuspended in 250 µl of resuspending buffer containing RNAse. 250 µl lysis buffer are added and carefully inverted 4-6 times (not longer than 5 min incubation!). 350 µl neutralization buffer is added and carefully inverted. The debris is centrifuged at 8000 rpm for 5 min. The suspension is placed onto a small column and centrifuged for 1 min. The supernatant is removed and 500 µl of washing buffer is added, followed by an additional centrifugation step. The washing procedure is repeated for one more time. The column is emptied by 2 min centrifugation. Finally, 50 µl of elution buffer is added, followed by a spun down for 1 min at 8000 rpm. A control digestion can assure that ligation and transformation were successful. Afterwards, the purified DNA is sent to a sequencing service with the respective forward and reverse vector primer.

Control digestion of the construct in pET24a
2 µl Green buffer 10x (gel electrophoresis)
2 µl mini-prep DNA (~50 ng/µl)
1µl XhoI
1µl NdeI
14 µl H_2O

20 µl total volume

6.2.2 Expression

For the expression of the E.coli derived mutants, the expression strain BL21 (DE3) was used to obtain the highest expression levels for recombinant proteins. Chemically competent cells (Ca2+) were purchased from Merck KGaA with the genotype F^-, ompT, hsd $S_B(r_B^-m_B^-)$, gal, dcm (DE3) to enhance the transformation probability. The induction of the BL21(DE3) system was based on the small molecule IPTG The transformation protocol for BL21 (DE3) follows the same protocol as described in section 3.3. including transformation, mini-preparation, gel-electrophoresis, and sequencing. The resulting mutant strains are finally stored on 10% glycerol at -80°C.

For a small-scale expression, LB broth medium is used under sterile conditions. The stored mutant strains are thawed on ice for 5 min and a tube of 10 ml LB-broth medium solution is inoculated after the determination of the OD600. The respective antibiotic is added. The expression is stirred over night at 28°C. For a large-scale expression, 1 liter of culture medium is inoculated with a pre-culture of 25 ml. The expression is induced at an OD600 of 1 and also stirred over night at 28°C.

6.2.3 Expression Profiling by SDS-PAGE

After the expression of the desired plasmid the expression profile is checked by SDS-PAGE, a method where proteins can be separated in an electric field according to their molecular mass. SDS-PAGE is based on a polyacrylamide gel electrophoresis that uses sodium dodecyl sulfate as a detergent to denature proteins.

Gel preparation

The resolution gels prepared in this work contained either 10% or 12% Acrylamide. The stacking gel usually contains 4% of Acrylamide. The components for the resolution gel are mixed, APS and TEMED are added to start the radical polymerization. The mixture is poured immediately into an appropriate chamber until a set mark and the gel can polymerize for 45 min. Water is poured on top of it to prevent drying. The stacking gel mixture is prepared accordingly, the water is carefully removed, and the mixture is poured and a comb is placed on top. The prepared gel can polymerize for another 30 min. If necessary the gels can be stored one week in buffer at 4°C. The according protocols are depicted in **Table 1.**

Table 6: Stacking and Resolution Gel Preparation

Components	Amount for 15ml of Gel
Bis-Acrylamid (30%)	5.00 ml
SDS (10%)	150 µl
ddH2O	6.03 ml
TRIS (1,5M, pH 8,8)	3.75 ml
APS (10%)	75 µl
TEMED	7.5µl

Sample Preparation

4 ml of a fresh bacterial culture are pelleted. The cells are resuspended in PBS pH 7.4 and transferred into a fresh Eppendorf tube containing 1 g of glass beads. The cells are lysed in a Mix Mill for 10min at 30 units per second. The cell debris is pelleted at 10.000 rpm for 10 min and the supernatant is collected. The concentration of the total protein amount is determined by a Bradford Assay and a concentration of 0.5 mg/ml is used for staining. To denature the proteins, 10µl of a 5x loading buffer is mixed with 40µl of the supernatant. The solution is heated up to 95°C for 5 min until it can be loaded on the gel. A protein marker is used as an external standard to identify protein bands according to their size.

Table 7: 5x loading buffer pH 6.8

Components	Amount
SDS (20%)	2,5 ml
glycerine	3,0 ml
TRIS	0.242 g
ß-mercaptoethanol	2,5 ml
bromphenolblue	add for staining

Running mode

The electrophoresis is performed in an electrophoresis cell at 100V for the first 15 min and then increased to 150V for additional 45-60 min. Finally, the gel is carefully removed from the plate and is placed in water for 10 min. Then it is stained by Coomassie-Staining for 2-3 hours. The gel is rinsed with water and transferred into a destaining solution for 15 min. This procedure is repeated 2-3 times until the protein bands are clearly visible. If necessary, the gel can be destained overnight and stored in water.

Table 8: Coomassie-Blue Staining Solution

Components	Amount
Methanol	500 ml
Acetic Acid	100 ml
Coomassie-Brillant-Blue	2.5 g
ddH_2O	ad 1000ml

Table 9: Destaining Solution of Coomassie-Stained Gels

Components	Amount per 1 liter
Aqua dest.	500 ml
2-propanol	400 ml
Acetic acid	100 ml

6.2.4 Protein Purification

The expressed proteins in this work were purified with the automated system Äkta Purifier (GE Healthcare).

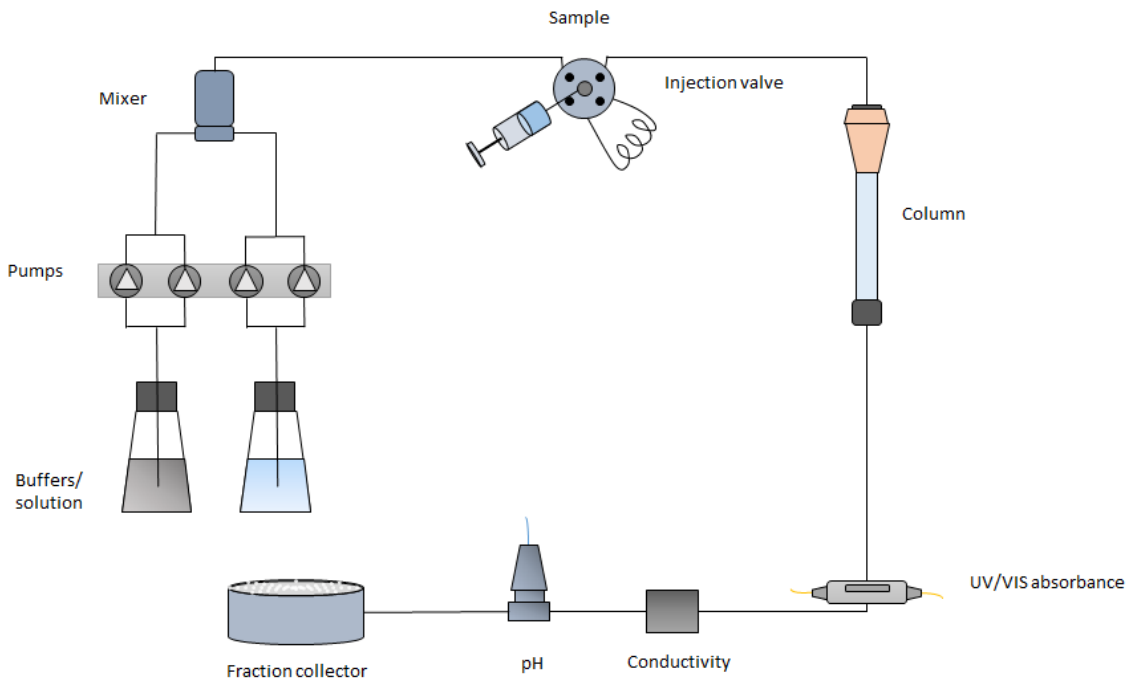

The HiPrep 26/10 Desalting column from GE Healthcare is a convenient, easy-to-use column prepacked with Sephadex G-25 for desalting and buffer exchange. The matrix of this column

is a hydrophilic cross-linked dextran with a particle size distribution of 17-132 µm and a high operational pH stability between 2 and 13. Chemical stability is provided in commonly used buffers such as 0.2 M NaOH, 1 M acetic acid, 8 M urea, 6 M guanidine HCl, 1 % SDS, 24 % ethanol, 30 % propanol and 30 % acetonitrile. For sample preparation it is recommended not to use more than 70mg/ml of globular protein and not more than 15ml of sample volume to achieve the best resolution. Before applying the crude sample onto the column either a filtration step is required with a filter pore size of maximum 0.45 µm or the sample is centrifuged at 10.000 x g for 10 min. The following buffers where used for purification and for storage. Buffer exchange was done by gel filtration.

Table 10: Buffer Compositions for His-Taq Purification (Affinity Chromatography)

Components	Concentration	Amount per 1 Liter
Buffer A (pH 7.4)		
$Na_2HPO_4 * 2\ H_2O$	25 mM	4.45 g
$NaH_2PO_4 * 2\ H_2O$	25 mM	3.90 g
NaCl	300 mM	17.6 g
Imidazole	20 mM	1.36 g
Buffer B (pH 7.4)		
$Na_2HPO_4 * 2\ H_2O$	25 mM	4.45 g
$NaH_2PO_4 * 2\ H_2O$	25 mM	3.90 g
NaCl	300 mM	17.6 g
Imidazole	400 mM	27.2 g

Table 11: Storage Buffer Compositions Dulbecco's PBS pH 7.4

Components	Concentration	Amount per 1 Liter
$Na_2HPO_4 * 2\ H_2O$	8 mM	1.15 g
KH_2PO_4	1.47 mM	0.20 g
NaCl	138 mM	8.00 g
KCl	2.67 mM	0.20 g
$CaCl_2$	0.9 mM	0.10 g

An overview of orthogonal purification methods is shown in **figure 70**. In this work, step 1 ans 2 were used only. The other two methods (IEX and HIC) are used for polishing.

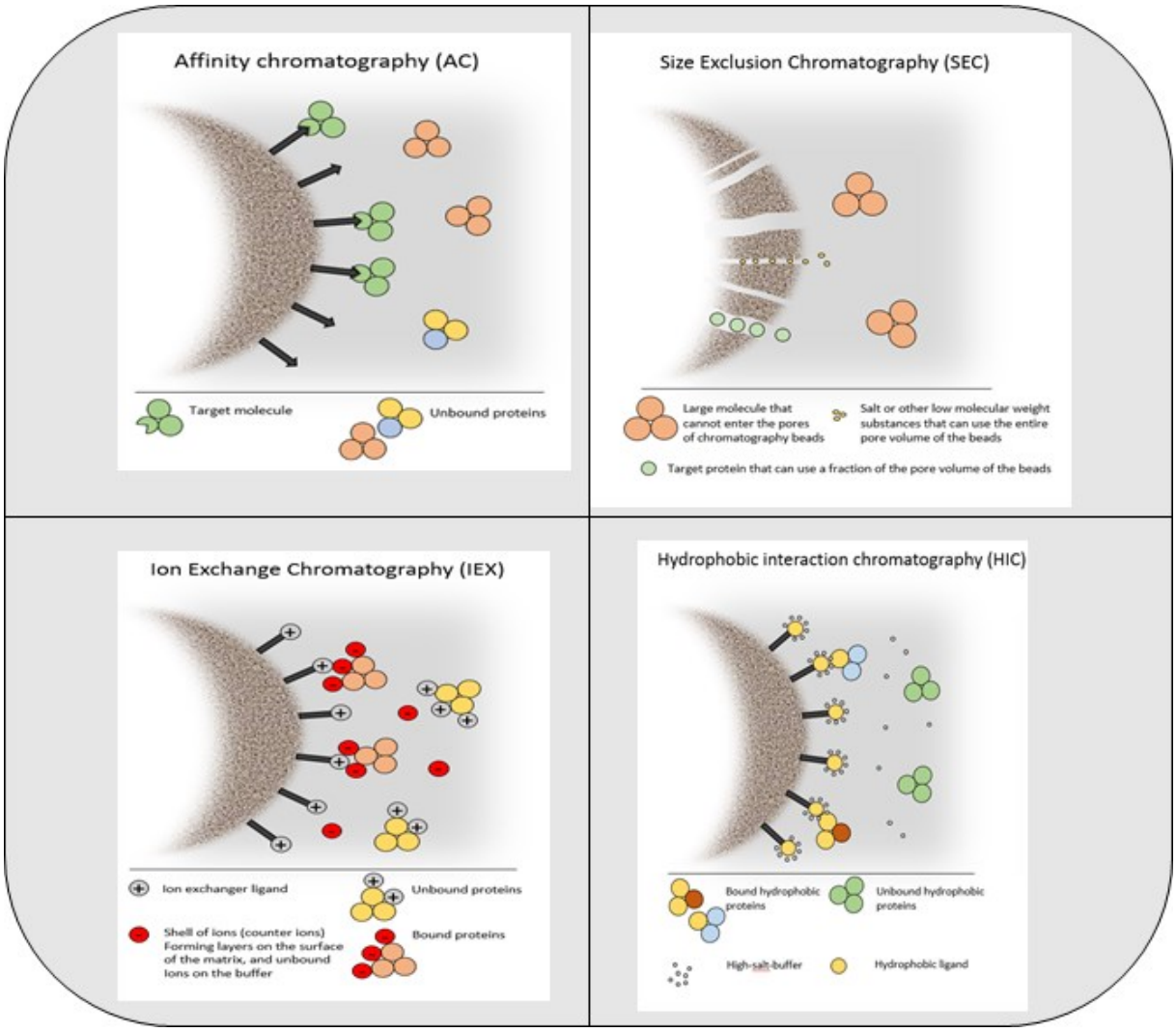

Figure 71: Overview of orthogonal protein purification methods

6.2.5 Labeling of Solvatochromic Thiol-Reactive Fluorophores

The labeling of the single cystein residue 152 within GGBP_mut_H152C/A213R/L238S was achieved by a standard maleimide coupling procedure. The different environmentally sensitive maleimide-functionalized dyes were commercially purchased and dissolved in either Acetonitrile (BADAN) or DMSO (rest of compounds) in a concentration of 1 mg/100 µl (0,01 ug/µl) and were stored at +5 °C. The final concentration of the stored proteins was determined by the Bradford assay. Five mg of protein were incubated for 20 min with a 50-fold molar excess of the mild, disulfide bond reducing agent Tris-(2-carboxyethyl) phosphine (abbrev.: TCEP). Consequently, a 3-fold molar excess of functionalized dye was added, and the mixture was incubated for 3 hours at room temperature while shaking or overnight without shaking at +5 °C. For BADAN, a 1,3 molar excess was sufficient for an adequate labeling efficiency of 1:1 (dye: protein). The reaction was stopped by a gel filtration process which was either done by a desalting purification on the Äkta purifier system (see figure 16) with the HiPrep 26/10 column or by PD-10 flow-through column for smaller samples below 5 mg of protein.

TCEP as a reducing agent of thiol groups in proteins

In proteins, reactive thiols are present as functional groups in cysteine residues and normally form disulfide bridges under oxidative conditions. Therefore, they must be reduced prior to their reaction with thiol-reactive dyes. Reducing agents as 2-mercaptoethanol (β-mercaptoethanol) or dithiothreitol (DTT) are relatively strong and can directly reduce disulfides. Then both must be removed by dialysis or gel filtration before labelling with thiol-reactive dyes as they contain thiols itself which risks the reformation of the protein disulfide. An alternative reagent, tris-(2-carboxyethyl) phosphine (TCEP) is more convenient as it has not to be removed before the reaction and can therefore avoid disulfide reformation due to its phosphine structure.

6.2.6 Labeling Purification

The purification of the dye-labeled proteins is either done by flow-through gel filtration with PD-10 columns or by gel filtration with the HiPrep 26/10 Desalting Column from GE Healthcare suitable for the Äkta system. The matrix of the PD-10 column is identical to the matrix used in the HiPrep 26/10 Desalting Column with a particle size distribution of 38-235 µm. The operational and chemical stabilities are therefore similar as described in Chapter 3.4.

6.2.7 Protein Determination with Bradford Reagent

In this work, the Protein Determination Assay from Bio-Rad Laboratories GmbH is used. The Bio-Rad protein assay is a simple colorimetric assay for measuring total protein concentration and is based on the Bradford dye-binding method (Bradford 1976). Based on the colour change of Coomassie brilliant blue G-250 dye in response to various concentrations of protein — the dye binds to primarily basic (especially arginine) and aromatic amino acid residues. The assay is carried out as followed:
One part of the dye reagent concentrate is diluted with four parts of double-deionized water. The diluted reagent is filtered through a Whatman Filter (or equivalent) to remove particulates. Protein standards are prepared between 0.05 mg/ml and 0.5 mg/ml which correspond to the linear range of the assay. Samples are diluted accordingly. 10 µl of each standard and sample solution are added to a well in a microtiter plate. 200 µl of diluted reagent are then added to each well of sample. The samples are mixed thoroughly using a microplate mixer. The reaction is incubated at room temperature for at least 5 minutes but no longer than 1 hour as the absorbance will increase over time. The plate is then measured at 595 nm. The protein samples were tested in triplicates.

6.2.8 Labeling Efficiency (DOL)

XC113 is incubated with GGBP variants for 3h at an increased pH of 8.0. the reaction is stopped by gel filtration and separation of free dye via PD-10 flow through columns. The sample is concentrated, and absorption spectra are measured. The absorption spectra help to determine the labeling efficiency. The labeling efficiency, also called degree of labeling is an important measure to control labeling reactions. It also gives an information about non-specific binding of fluorescent dyes which display hydrophobic properties and tend to bind non-covalently to proteins. In assays on a single molecular level, non-specific binding should be avoided to enhance the overall sensitivity. The labeling efficiencies were determined as followed.

a) Calculation of protein molarity in solution

$$Protein\ concentration\ (M) = \frac{\mathrm{A280} - (Amax * CF)}{\varepsilon} * dilution\ factor$$

A_{280}: Absorbance at 280nm

A_{max}: Absorption at local maximum measured

CF: Correction factor

ε: molar extinction coefficient

b) Calculation of degree of labeling

$$Moles\ dye\ per\ mol\ protein = \frac{A\ max\ of\ labeled\ protein}{\varepsilon' * protein\ concentration\ (M)} * dilution\ factor$$

The absorbance at 280nm is used to determine the protein concentration. A correction factor must be determined as a conjugated dye will also likely absorb at 280nm. The molar extinction coefficient of the glucose-galactose binding protein was determined by a concentration determination by Bradford assay and determination of the Lambert-Beer law in a diluted solution (< 0,1 M):

$$A = \varepsilon * c * d$$

6.2.9 **F**örster-**R**esonance-**E**nergy-**T**ransfer Determination

The fluorescence energy transfer was determined by measuring at the excitation and emission maxima wavelengths of the donor (455nm/525nm) and the acceptor (580nm/ 602nm) and in addition at the excitation wavelength of the donor and at the emission wavelength of the acceptor (455nm/602nm). The latter can only be a FRET transfer signal. Then the spectra of donor and FRET are compared to each other and a FRET rate is determined.

6.2.10 Synthesis

The synthesis route of XC92 (Perfluoroarylated linker) which is sensitive to the i-clamp motif in proteins, and XC113, a carboxyfluorescein-derivative, is explained in detail in the result part 2 (chapter 4.5). The synthetic educts and products have been analysed by ^{1}H-NMR and have been compared to the NMR spectrum of XC113.

List of Abbreviations

BSA	bovine serum albumin
DTT	dithiothreitol
E. coli	Eserichia coli
FRET	(Förster-)resonance energy transfer
GMP	good manufacturing process
GBP	glucose binding protein
GGBP	glucose-galactose binding protein in E. coli
MglB	gene that encodes for GGBP
ssDNA	single-stranded deoxyribonucleic acid
RNA	ribonucleic acid
FAD/FADH	Flavin adenine dinucleotide
NADP+/NADPH	Nicotinamide adenine dinucleotide
IPTG	isopropyl β-D-1-thiogalactopyranoside
TCEP	tris-(2-carboxyethyl) phosphine

List of Tables

Table 1: Analyte-receptor interactions of a biosensor. 4
Table 2:Endosteric, peristeric and allosteric binding sites of GGBP for the attachment of environmentally sensitive fluorophores were identified. 14
Table 3: Comparison of optical glucose recognition elements based on enzymes, boronic acids and glucose-binding proteins for their features such as stability, sensitivity, reagentless sensing ability, formation of cell-toxic by-products, ratiometric and small volume measurement capability. 16
Table 4: BLAST entries of sequence alignment (figure 49) of different bacterial glucose ABC transporter proteins 64
Table 5: Excitation and emission maxima of the 5/6-carboxy-fluorescein derivatives in DMSO and DPBS pH 7.4 as well as of the Perfluoroarylated 5/6 carboxy-fluorescein with and without attachment to GGBP. 81
Table 6: Stacking and Resolution Gel Preparation 96
Table 7: 5x loading buffer pH 6.8 96
Table 8: Coomassie-Blue Staining Solution 97
Table 9: Destaining Solution of Coomassie-Stained Gels 97
Table 10: Buffer Compositions for His-Taq Purification (Affinity Chromatography) 98
Table 11: Storage Buffer Compositions Dulbecco's PBS pH 7.4 98

List of Figures

Figure 1: Process analytical technologies. 2
Figure 2: Schematic draw of a biosensor. 4
Figure 3: Biosensor classifications. 5
Figure 4: Chemical reaction of the enzyme glucose oxidase. 6
Figure 5: Schematic representation of different glucose sensor generations based on the enzymes such as glucose oxidase or glucose dehydrogenase. 7
Figure 6: Chemical structure of quinine. 17
Figure 7: Jablonski diagram. 18
Figure 8: Maleimids as reactive functional groups for the selective labeling of proteins. 22
Figure 9: Schematic principle of a FRET-labeled Glucose binding protein. 24
Figure 10: Pi-clamp as depicted from and described by Zhang et al., 2016.(115) 26
Figure 11: Reaction mechanism of the nucleophilic aromatic substitution (S_NAr) reaction of a perfluoro arylated thiol with the pi-clamp motif FCPF compared to GCPG. 27
Figure 12: Fluorescence overlap of FRET donor and FRET acceptor molecule. 28
Figure 13: Control digestion of the wildtype and mutant gene encoding for GGBP_wt and GGBP_mutant. 32
Figure 14: Test expression of 50ml inoculation media with triple mutant to screen for optimal expression conditions. 33
Figure 15: Purification of GGBP_wt using a 5ml His-Trap column from GE Healthcare on the Äkta purifier system. 35
Figure 16: Gel filtration of GGBP_mut_H152C/A213R/L238S-BADAN after labeling. 36
Figure 17: Molecular structure of BADAN (6-Bromoacetyl-2-Dimethylaminonaphthalene). 37
Figure 18: Excitation and emission spectra of 6-Bromoacetyl-2-Dimethylaminonaphthalene (BADAN) in acetonitrile and DPBS pH 7.4. 38
Figure 19: Excitation and emission spectra of 6-Bromoacetyl-2-Dimethylaminonaphthalene (BADAN) covalently bound to the triple mutation GGBP-H152C/A213R/L238S are compared to the excitation and emission profile of unlabelled BADAN. 38
Figure 20: Polar-sensitivity BADAN: Fluorescence emission spectra of BADAN in different concentration ratios of acetonitrile and DPBS pH 7.4 (in accordance with literature). 39
Figure 21: Fluorescence emission spectra of GGBP-H152C/A213R/L238S-BADAN in response to different glucose concentrations between 0mM and 200 mM Glucose at pH

7.4. Excitation of all spectra was at 397 nm. The fluorescence increases by 190% on addition of 200 mM glucose. The emission maximum is slightly red shifted by 4 nm. 40
Figure 22: The fluorescence of GGBP-H152C/A213R/L238S-BADAN shows a linear correlation between 2.5 mM and 100 mM. 40
Figure 23: Glucose dependency of GGBP-H152C/A213R/L238S-BADAN between 1 µM and 1 M. 41
Figure 24: Excitation and emission spectra from DYV11 in DMSO and DPBS pH 7.4 at concentrations of 1 ng/ml. 42
Figure 25: Excitation and emission spectra from DYV11 covalently bound to the triple mutation GGBP-H152C/A213R/L238S are compared to the excitation and emission profile of unlabelled DYV11. 43
Figure 26: Polar-sensitivity DY V11: Fluorescence emission spectra of DY V11 in different concentration ratios of DMSO and DPBS pH 7.4. 44
Figure 27: Glucose dependency of the fluorescence intensity of GGBP-H152C/A213R/L238S-DY V11 between 2.5 mM and 100 mM. 44
Figure 28: Excitation and emission spectra from DY 610 in DMSO and DPBS pH 7.4 at concentrations of 1 ng/ml. DY 610 was kindly provided from Dyomics GmbH, Jena, Germany. 45
Figure 29: Excitation and emission spectra from DY 610 covalently bound to the triple mutation GGBP-H152C/A213R/L238S are compared to the excitation and emission profile of unlabelled DY 610. DY 610 was kindly provided from Dyomics GmbH, Jena, Germany. 46
Figure 30: Polar sensitivity DY 610: Fluorescence emission spectra of DY610 in different concentration ratios of DMSO and DPBS pH 7.4. 47
Figure 31: Glucose dependency of the fluorescence intensity of GGBP-H152C/A213R/L238S-DY 610 between 2.5 mM and 100 mM. 47
Figure 32: Glucose dependency of GGBP-H152C/A213R/L238S-DY 610 between 1 µM and 100 mM. 48
Figure 33: Excitation and emission spectra from DY 490 in DMSO and DPBS pH 7.4 at concentrations of 1 ng/ml. DY V11 was kindly provided from Dyomics GmbH, Jena, Germany. 49
Figure 34: Excitation and emission spectra from DY 490 covalently bound to the triple mutation GGBP-H152C/A213R/L238S are compared to the excitation and emission profile of unlabelled DY 490. 49
Figure 35: Polar sensitivity of DY 490: Fluorescence emission spectra of DY490 in different concentration ratios of DMSO and DPBS pH 7.4. 50

Figure 36: Glucose dependency of the fluorescence intensity of GGBP-H152C/A213R/L238S-DY 490 between 2.5 mM and 100 mM. 51
Figure 37: Excitation and emission spectra from the coumarin derivative compound Atto 425 dissolved in DMSO and DPBS pH 7.4 at concentrations of 1 ng/ml. 52
Figure 38: Comparison of excitation and emission spectra from Atto 425 and GGBP-H152C/A213R/L238S-Atto425. 52
Figure 39: Polar sensitivity of Atto 425: Fluorescence emission spectra of Atto 425 in different concentration ratios of DMSO and DPBS pH 7.4. All spectra were excited at 419 nm (exc. max. of Atto 425 in DMSO). 53
Figure 40: Glucose dependency of the fluorescence intensity of GGBP-H152C/A213R/L238S-Atto 425 between 2.5 mM and 75 mM. 54
Figure 41: Excitation and emission spectra from the Acridine-orange derivative compound Atto 465 dissolved in DMSO and DPBS pH 7.4 at concentrations of 1 ng/ml. 54
Figure 42: Comparison of excitation and emission spectra from Atto 465 and GGBP-H152C/A213R/L238S-Atto465. 55
Figure 43: Polar sensitivity of Atto 465: Fluorescence emission spectra of Atto 465 in different concentration ratios of DMSO and DPBS pH 7.4. All spectra were excited at 450 nm (exc. max. of Atto 425 in DMSO. This graph was accomplished by our intern Laura Freitag under my supervision. 56
Figure 44: Glucose dependency of the fluorescence intensity of GGBP-H152C/A213R/L238S-Atto 465 between 2.5 mM and 75 mM. 57
Figure 45: Excitation and emission spectra from the Acriflavine-orange derivative compound Atto 495 dissolved in DMSO and DPBS pH 7.4 at concentrations of 1 ng/ml. This graph was accomplished by our intern Laura Freitag under my supervision. 57
Figure 46: Comparison of excitation and emission spectra from Atto 495 and GGBP-H152C/A213R/L238S-Atto495. 58
Figure 47: Polar-sensitivity Atto 495: Fluorescence emission spectra of Atto 495 in different concentration ratios of DMSO and DPBS pH 7.4. All spectra were excited at 495 nm (exc. max. of Atto 495 in DPBS pH 7.4. 59
Figure 48: Glucose dependency of the fluorescence intensity of GGBP-H152C/A213R/L238S-Atto495between 2.5 mM and 100 mM. 60
Figure 49: Multiple sequence alignment of glucose ABC transporters in different bacterial organisms. The structural motifs are obtained from the crystal structure (UniProt ID: P0AEE5) of E.coli (light pink: signal peptide, pink: α-helix, yellow: β-sheet, blue: calcium binding site, dark grey: similarity between amino acids) 65

Figure 50: Quality assessment of generated mutants (GGBP_mut_H152C/A213R/L238S_QNDQ42-45FPCF as example). The calculations are based on QMEAN scoring function, Ramachandran Plot, upper right: Z-score (model prediction compared to other models in databank), quality of the model, as normalised QMEAN score (y-axis), in comparison to the scores obtained for high-resolution crystal structures 66
Figure 51: Ligand binding site of the wild-type glucose-galactose binding protein (GGBPwt) with its natural ligand glucose. 67
Figure 52: Crystallographic structure of GGBP_mut_H152C/A213R/L238S_QNDQ42-45FPCF. 68
Figure 53: Crystallographic structure of GGBP_mut_H152C/A213R/L238S_VDPA68-71FCPF. 69
Figure 54: Crystallographic structure of GGBP_mut_H152C/A213R/L238S_EPSR93-96FPCF. 70
Figure 55:: Crystallographic structure of GGBP_mut_H152C/A213R/L238S_DGTN280-283FCPF. 71
Figure 56: Crystallographic structure of GGBP_mut_H152C/A213R/L238S_KIDN285-288FPCF. 72
Figure 57: SDS-page profiling and test expression of designed GGBP pi-clamp mutants in 150 ml expression medium induced with 1mM IPTG. The mutants are named according to the pi-clamp mutation (short form). 73
Figure 58: Purification of GGBP_mut_H152C/A213R/L238S_QNDQ42-45FPCF from one liter expression culture. 74
Figure 59: Purification of GGBP_mut_H152C/A213R/L238S_VDPA68-71FCPF from one liter expression culture. 75
Figure 60: Purification of GGBP_mut_H152C/A213R/L238S_EPSR93-96FPCF from one litre expression culture. 75
Figure 61: Purification of GGBP_mut_H152C/A213R/L238S_DGTN280-283FCPF from one liter expression culture. 76
Figure 62: Purification of GGBP_mut_H152C/A213R/L238S_KIDN285-288FPCF from one liter expression culture. 77
Figure 63: Synthesis route of XC113 (perfluoro arylated 5/6-carboxyfluorescein) as donor molecule in FRET labeling of proteins. The synthesis was developed and carried out by Dr. Xinlai Cheng with permission to publish in this work. 78
Figure 64: 1H-NMR spectrum of compound XC92 (perfluoro aryl linker molecule). 79
Figure 65: 1H-NMR spectrum of 5/6-Carboxyfluorescein-succinimidyl (NHS). 80

Figure 66:1H-NMR spectrum of compound XC113 (perfluoro arylated 5/6-carboxyfluoresceine derivative). 80
Figure 67: Excitation and emission overlap spectra of perfluoro arylated 5/6-Carboxyfluorescein as FRET donor and DY557 and DY585 as FRET acceptors. 81
Figure 68: Absorption spectrum of GGBP_mut_ H152C/A213R/L238S_DGTN280-283FCPF-XC113-DY585. 83
Figure 69: FRET-transfer of GGBP_mut_280-283FCPF-XC113-DY585 at varying glucose concentrations. 83
Figure 70: Fluorescence emission of GGBP_mut_H152C/A213R/L238S_EPSR93-96FPCF-XC113-DY585. 84
Figure 71: Overview of orthogonal protein purification methods 99

List of Publications

1. Lücke J, Bädeker, M., Hildinger, M. Medizinische Biotechnologie in Deutschland 2017. BCG, editor2017.
2. e.V. VFA. Zugelassene gentechnische Arzneimittel in Deutschland 2018 [25.05.2018].
3. Celik M. Quality by design, process analytical technology, GMP and regulatory affairs. Pharmaceutical development and technology. 2018;23(6):553.
4. Riley BS, Li X. Quality by design and process analytical technology for sterile products--where are we now? AAPS PharmSciTech. 2011;12(1):114-8.
5. Administration FUSFaD. Guidance for Industry PAT — A Framework for Innovative Pharmaceutical Development, Manufacturing, and Quality Assurance. Webpage FDA. 2004.
6. Lee S, Brorson K. Emerging Technology as a Key Enabler for Modernizing Pharmaceutical Manufacturing. PDA Journal of Pharmaceutical Science and Technology. 2017;71(2):66-7.
7. Zhao L, Fu HY, Zhou WC, Hu WS. Advances in process monitoring tools for cell culture bioprocesses. Eng Life Sci. 2015;15(5):459-68.
8. Tric M, Lederle M, Neuner L, Dolgowjasow I, Wiedemann P, Wolfl S, et al. Optical biosensor optimized for continuous in-line glucose monitoring in animal cell culture. Analytical and bioanalytical chemistry. 2017;409(24):5711-21.
9. Lederle M, Tric M, Packi C, Werner T, Wiedemann P. An Optical Biosensor for Continuous Glucose Monitoring in Animal Cell Cultures. Methods in molecular biology. 2020;2095:319-33.
10. Weegman BP, Nash P, Carlson AL, Voltzke KJ, Geng Z, Jahani M, et al. Nutrient Regulation by Continuous Feeding Removes Limitations on Cell Yield in the Large-Scale Expansion of Mammalian Cell Spheroids. 2013;8(10):e76611.
11. Reuveny S, Velez D, Macmillan JD, Miller L. Factors affecting cell growth and monoclonal antibody production in stirred reactors. Journal of immunological methods. 1986;86(1):53-9.
12. Steiner MS, Duerkop A, Wolfbeis OS. Optical methods for sensing glucose. Chemical Society reviews. 2011;40(9):4805-39.
13. Ang KH, Tamborlane WV, Weinzimer SA. Combining glucose monitoring and insulin delivery into a single device: current progress and ongoing challenges of the artificial pancreas. Expert Opin Drug Del. 2015;12(10):1579-82.
14. Clark LC, Jr., Lyons C. Electrode systems for continuous monitoring in cardiovascular surgery. Annals of the New York Academy of Sciences. 1962;102:29-45.
15. Boyne MS, Silver DM, Kaplan J, Saudek CD. Timing of changes in interstitial and venous blood glucose measured with a continuous subcutaneous glucose sensor. Diabetes. 2003;52(11):2790-4.
16. Mohan AMV, Windmiller JR, Mishra RK, Wang J. Continuous minimally-invasive alcohol monitoring using microneedle sensor arrays. Biosensors & bioelectronics. 2017;91:574-9.
17. Valdes-Ramirez G, Li YC, Kim J, Jia WZ, Bandodkar AJ, Nunez-Flores R, et al. Microneedle-based self-powered glucose sensor. Electrochem Commun. 2014;47:58-62.
18. Heller A, Feldman B. Electrochemical glucose sensors and their applications in diabetes management. Chemical reviews. 2008;108(7):2482-505.
19. Ferri S, Kojima K, Sode K. Review of glucose oxidases and glucose dehydrogenases: a bird's eye view of glucose sensing enzymes. Journal of diabetes science and technology. 2011;5(5):1068-76.
20. Ahlstrom J, Cadio MA, Liedtke S, Mert A, inventors; Roche Diabetes Care Inc, assignee. Glucose meter. US2014.
21. Shults MC, Rhodes RK, Updike SJ, Brauker JH, inventors; DexCom Inc assignee. Low oxygen in vivo analyte sensor US2006.

22. Sierra JF, Galban J, Castillo JR. Determination of glucose in blood based on the intrinsic fluorescence of glucose oxidase. Analytical chemistry. 1997;69(8):1471-6.
23. Trettnak W, Wolfbeis OS. Fully Reversible Fibre-Optic Glucose Biosensor Based on the Intrinsic Fluorescence of Glucose-Oxidase. Analytica chimica acta. 1989;221(2):195-203.
24. Hussain F, Birch DJ, Pickup JC. Glucose sensing based on the intrinsic fluorescence of sol-gel immobilized yeast hexokinase. Analytical biochemistry. 2005;339(1):137-43.
25. Narayanaswamy R, Sevilla F. An Optical Fiber Probe for the Determination of Glucose Based on Immobilized Glucose-Dehydrogenase. Anal Lett. 1988;21(7):1165-75.
26. D'Auria S, DiCesare N, Staiano M, Gryczynski Z, Rossi M, Lakowicz JR. A novel fluorescence competitive assay for glucose determinations by using a thermostable glucokinase from the thermophilic microorganism Bacillus stearothermophilus. Analytical biochemistry. 2002;303(2):138-44.
27. Singh S, Gupta BD. Fabrication and characterization of a surface plasmon resonance based fiber optic sensor using gel entrapment technique for the detection of low glucose concentration. Sensor Actuat B-Chem. 2013;177:589-95.
28. Endo H, Yonemori Y, Musiya K, Maita M, Shibuya T, Ren H, et al. A needle-type optical enzyme sensor system for determining glucose levels in fish blood. Analytica chimica acta. 2006;573-574:117-24.
29. Pasic A, Koehler H, Schaupp L, Pieber TR, Klimant I. Fiber-optic flow-through sensor for online monitoring of glucose. Analytical and bioanalytical chemistry. 2006;386(5):1293-302.
30. A. Pasic HK, I. Klimant and L. Schaupp. Miniaturized fiber-optic hybrid sensor for continuous glucose monitoring in subcutaneous tissue. Sens Actuators B. 2007;122:60–8.
31. Wu M, Lin Z, Durkop A, Wolfbeis OS. Time-resolved enzymatic determination of glucose using a fluorescent europium probe for hydrogen peroxide. Analytical and bioanalytical chemistry. 2004;380(4):619-26.
32. O. S. Wolfbeis MSaAD. Reversible optical sensor membrane for hydrogen peroxide using an immobilized fluorescent probe, and its application to a glucose biosensor. Microchim Acta. 2003;143:221–7.
33. W. Trettnak MJPLaOSW. Fibre-optic glucose sensor with a pH optrode as the transducer. Biosensors. 1989;4:15-26.
34. Robinson JWAaGA, inventorSensor for optical assay1993.
35. Sierra JF, Galban J, de Marcos S, Castillo JR. Fluorimetric-enzymatic determination of glucose based on labelled glucose oxidase. Analytica chimica acta. 1998;368(1-2):97-104.
36. Sanz V, Galban J, de Marcos S, Castillo JR. Fluorometric sensors based on chemically modified enzymes Glucose determination in drinks. Talanta. 2003;60(2-3):415-23.
37. Duong HD, Il Rhee J. Use of CdSe/ZnS core-shell quantum dots as energy transfer donors in sensing glucose. Talanta. 2007;73(5):899-905.
38. Aruga R. Borate-polyol complexes in aqueous solution: determination of enthalpies by thermometric titrimetry. Talanta. 1985;32(6):517-9.
39. Wu X, Chen XX, Jiang YB. Recent advances in boronic acid-based optical chemosensors. The Analyst. 2017;142(9):1403-14.
40. Fang G, Wang H, Bian Z, Sun J, Liu A, Fang H, et al. Recent development of boronic acid-based fluorescent sensors. RSC Advances. 2018;8(51):29400-27.
41. Ballerstadt R, Schultz JS. A fluorescence affinity hollow fiber sensor for continuous transdermal glucose monitoring. Analytical chemistry. 2000;72(17):4185-92.
42. Ballerstadt R, Polak A, Beuhler A, Frye J. In vitro long-term performance study of a near-infrared fluorescence affinity sensor for glucose monitoring. Biosensors & bioelectronics. 2004;19(8):905-14.

43. Schultz JS, Mansouri S, Goldstein IJ. Affinity sensor: a new technique for developing implantable sensors for glucose and other metabolites. Diabetes care. 1982;5(3):245-53.
44. Mansouri S, Schultz JS. A Miniature Optical Glucose Sensor Based on Affinity Binding. Bio-Technol. 1984;2(10):885-90.
45. J. S. Schultz TUSoArbtDoH, inventorOptical sensor for blood plasma constituents1980.
46. Meadows DL, Schultz JS. Design, Manufacture and Characterization of an Optical-Fiber Glucose Affinity Sensor-Based on an Homogeneous Fluorescence Energy-Transfer Assay System. Analytica chimica acta. 1993;280(1):21-30.
47. Russell RJ, Pishko MV, Gefrides CC, McShane MJ, Cote GL. A fluorescence-based glucose biosensor using concanavalin A and dextran encapsulated in a poly(ethylene glycol) hydrogel. Analytical chemistry. 1999;71(15):3126-32.
48. Tolosa L, Szmacinski H, Rao G, Lakowicz JR. Lifetime-based sensing of glucose using energy transfer with a long lifetime donor. Analytical biochemistry. 1997;250(1):102-8.
49. G. L. Cote´ MVP, K. Sirkar, R. Russell and R. R. Anderson, The Texas A&M University System, The General Hospital Corporation, inventorCompositions and methods for analyte detection2002.
50. W. March NA, inventorApparatus for measuring blood glucose concentrations2002.
51. Zhang J, Roll D, Geddes CD, Lakowicz JR. Aggregation of silver nanoparticle-dextran adducts with concanavalin A and competitive complexation with glucose. Journal of Physical Chemistry B. 2004;108(32):12210-4.
52. Aslan K, Lakowicz JR, Geddes CD. Nanogold-plasmon-resonance-based glucose sensing. Analytical biochemistry. 2004;330(1):145-55.
53. Aslan K, Lakowicz JR, Geddes CD. Nanogold plasmon resonance-based glucose sensing. 2. Wavelength-ratiometric resonance light scattering. Analytical chemistry. 2005;77(7):2007-14.
54. D'Auria S, Herman P, Rossi M, Lakowicz JR. The fluorescence emission of the apo-glucose oxidase from Aspergillus niger as probe to estimate glucose concentrations. Biochemical and biophysical research communications. 1999;263(2):550-3.
55. J. R. Lakowitz and S. D'auria RotUoM, Baltimore, inventor Inactive enzymes as non-consuming sensors2001.
56. Chinnayelka S, McShane MJ. Resonance energy transfer nanobiosensors based on affinity binding between apo-enzyme and its substrate. Biomacromolecules. 2004;5(5):1657-61.
57. Chinnayelka S, McShane MJ. Microcapsule biosensors using competitive binding resonance energy transfer assays based on apoenzymes. Analytical chemistry. 2005;77(17):5501-11.
58. Chinnayelka S, McShane MJ. Glucose sensors based on microcapsules containing an Orange/Red competitive binding resonance energy transfer assay. Diabetes technology & therapeutics. 2006;8(3):269-78.
59. S. Chinnayelka HZaMJM. Near-Infrared Resonance Energy Transfer Glucose Biosensors in Hybrid Microcapsule Carriers. J Sensors. 2008;2008:1-11.
60. Fukami-Kobayashi K, Tateno Y, Nishikawa K. Domain dislocation: a change of core structure in periplasmic binding proteins in their evolutionary history. Journal of molecular biology. 1999;286(1):279-90.
61. Felder CB, Graul RC, Lee AY, Merkle HP, Sadee W. The Venus flytrap of periplasmic binding proteins: an ancient protein module present in multiple drug receptors. AAPS PharmSci. 1999;1(2):E2.
62. Anraku Y. Transport of sugars and amino acids in bacteria. 3. Studies on the restoration of active transport. The Journal of biological chemistry. 1968;243(11):3128-35.

63. Anraku Y. Transport of sugars and amino acids in bacteria. II. Properties of galactose- and leucine-binding proteins. The Journal of biological chemistry. 1968;243(11):3123-7.
64. Anraku Y. Transport of sugars and amino acids in bacteria. I. Purification and specificity of the galactose- and leucine-binding proteins. The Journal of biological chemistry. 1968;243(11):3116-22.
65. Vyas MN, Vyas NK, Quiocho FA. Crystallographic analysis of the epimeric and anomeric specificity of the periplasmic transport/chemosensory protein receptor for D-glucose and D-galactose. Biochemistry. 1994;33(16):4762-8.
66. Vyas NK, Vyas MN, Quiocho FA. Sugar and signal-transducer binding sites of the Escherichia coli galactose chemoreceptor protein. Science. 1988;242(4883):1290-5.
67. Vyas NK, Vyas MN, Quiocho FA. A novel calcium binding site in the galactose-binding protein of bacterial transport and chemotaxis. Nature. 1987;327(6123):635-8.
68. Vyas NK, Vyas MN, Quiocho FA. The 3 A resolution structure of a D-galactose-binding protein for transport and chemotaxis in Escherichia coli. Proceedings of the National Academy of Sciences of the United States of America. 1983;80(7):1792-6.
69. Shilton BH, Flocco MM, Nilsson M, Mowbray SL. Conformational changes of three periplasmic receptors for bacterial chemotaxis and transport: the maltose-, glucose/galactose- and ribose-binding proteins. Journal of molecular biology. 1996;264(2):350-63.
70. Borrok MJ, Kiessling LL, Forest KT. Conformational changes of glucose/galactose-binding protein illuminated by open, unliganded, and ultra-high-resolution ligand-bound structures. Protein science : a publication of the Protein Society. 2007;16(6):1032-41.
71. Wang ZM, Luecke H, Yao NH, Quiocho FA. A low energy short hydrogen bond in very high resolution structures of protein receptor phosphate complexes. Nature structural biology. 1997;4(7):519-22.
72. Bitzer RS, Barbosa AG, da Silva CO, Nascimento MA. On the generalized valence bond description of the anomeric and exo-anomeric effects: an ab initio conformational study of 2-methoxytetrahydropyran. Carbohydr Res. 2005;340(13):2171-84.
73. Quiocho FA, Ledvina PS. Atomic structure and specificity of bacterial periplasmic receptors for active transport and chemotaxis: variation of common themes. 1996;20(1):17-25.
74. Magnusson U, Chaudhuri BN, Ko J, Park C, Jones TA, Mowbray SL. Hinge-bending motion of D-allose-binding protein from Escherichia coli: three open conformations. The Journal of biological chemistry. 2002;277(16):14077-84.
75. Stepanenko OV, Stepanenko OV, Povarova OI, Fonin AV, Kuznetsova IM, Turoverov KK, et al. New insight into protein-ligand interactions. The case of the D-galactose/D-glucose-binding protein from Escherichia coli. The journal of physical chemistry B. 2011;115(12):2765-73.
76. Khan F, Gnudi L, Pickup JC. Fluorescence-based sensing of glucose using engineered glucose/galactose-binding protein: a comparison of fluorescence resonance energy transfer and environmentally sensitive dye labelling strategies. Biochemical and biophysical research communications. 2008;365(1):102-6.
77. Stepanenko OV, Fonin AV, Stepanenko OV, Morozova KS, Verkhusha VV, Kuznetsova IM, et al. New insight in protein-ligand interactions. 2. Stability and properties of two mutant forms of the D-galactose/D-glucose-binding protein from E. coli. The journal of physical chemistry B. 2011;115(29):9022-32.
78. Scognamiglio V, Scire A, Aurilia V, Staiano M, Crescenzo R, Palmucci C, et al. A strategic fluorescence labeling of D-galactose/D-glucose-binding protein from Escherichia coli helps to shed light on the protein structural stability and dynamics. Journal of proteome research. 2007;6(11):4119-26.
79. Sakaguchi-Mikami A, Taneoka A, Yamoto R, Ferri S, Sode K. Engineering of ligand specificity of periplasmic binding protein for glucose sensing. Biotechnology letters. 2008;30(8):1453-60.

80. Dattelbaum JD, Lakowicz JR. Optical determination of glutamine using a genetically engineered protein. Analytical biochemistry. 2001;291(1):89-95.
81. Tolosa L, Gryczynski I, Eichhorn LR, Dattelbaum JD, Castellano FN, Rao G, et al. Glucose sensor for low-cost lifetime-based sensing using a genetically engineered protein. Analytical biochemistry. 1999;267(1):114-20.
82. Salins LL, Ware RA, Ensor CM, Daunert S. A novel reagentless sensing system for measuring glucose based on the galactose/glucose-binding protein. Analytical biochemistry. 2001;294(1):19-26.
83. Hellinga HW, Marvin JS. Protein engineering and the development of generic biosensors. Trends in biotechnology. 1998;16(4):183-9.
84. Gilardi G, Zhou LQ, Hibbert L, Cass AE. Engineering the maltose binding protein for reagentless fluorescence sensing. Analytical chemistry. 1994;66(21):3840-7.
85. Brune M, Hunter JL, Corrie JE, Webb MR. Direct, real-time measurement of rapid inorganic phosphate release using a novel fluorescent probe and its application to actomyosin subfragment 1 ATPase. Biochemistry. 1994;33(27):8262-71.
86. de Lorimier RM, Smith JJ, Dwyer MA, Looger LL, Sali KM, Paavola CD, et al. Construction of a fluorescent biosensor family. Protein science : a publication of the Protein Society. 2002;11(11):2655-75.
87. Marvin JS, Hellinga HW. Engineering biosensors by introducing fluorescent allosteric signal transducers: Construction of a novel glucose sensor. Journal of the American Chemical Society. 1998;120(1):7-11.
88. Tian Y, Cuneo MJ, Changela A, Hocker B, Beese LS, Hellinga HW. Structure-based design of robust glucose biosensors using a Thermotoga maritima periplasmic glucose-binding protein. Protein science : a publication of the Protein Society. 2007;16(10):2240-50.
89. Hsieh HV, Pfeiffer ZA, Amiss TJ, Sherman DB, Pitner JB. Direct detection of glucose by surface plasmon resonance with bacterial glucose/galactose-binding protein. Biosensors & bioelectronics. 2004;19(7):653-60.
90. Amiss TJ, Sherman DB, Nycz CM, Andaluz SA, Pitner JB. Engineering and rapid selection of a low-affinity glucose/galactose-binding protein for a glucose biosensor. Protein science : a publication of the Protein Society. 2007;16(11):2350-9.
91. Khan F, Saxl TE, Pickup JC. Fluorescence intensity- and lifetime-based glucose sensing using an engineered high-Kd mutant of glucose/galactose-binding protein. Analytical biochemistry. 2010;399(1):39-43.
92. Pickup JC, Khan F, Zhi ZL, Coulter J, Birch DJ. Fluorescence intensity- and lifetime-based glucose sensing using glucose/galactose-binding protein. Journal of diabetes science and technology. 2013;7(1):62-71.
93. Saxl T, Khan F, Ferla M, Birch D, Pickup J. A fluorescence lifetime-based fibre-optic glucose sensor using glucose/galactose-binding protein. The Analyst. 2011;136(5):968-72.
94. Khan F, Pickup JC. Near-infrared fluorescence glucose sensing based on glucose/galactose-binding protein coupled to 651-Blue Oxazine. Biochemical and biophysical research communications. 2013;438(3):488-92.
95. Ge X, Tolosa L, Rao G. Dual-labeled glucose binding protein for ratiometric measurements of glucose. Analytical chemistry. 2004;76(5):1403-10.
96. Hsieh HV, Sherman DB, Andaluz SA, Amiss TJ, Pitner JB. Fluorescence resonance energy transfer glucose sensor from site-specific dual labeling of glucose/galactose binding protein using ligand protection. Journal of diabetes science and technology. 2012;6(6):1286-95.
97. Gifford R. Continuous glucose monitoring: 40 years, what we've learned and what's next. Chemphyschem : a European journal of chemical physics and physical chemistry. 2013;14(10):2032-44.
98. Dehennis A, Mortellaro MA, Ioacara S. Multisite Study of an Implanted Continuous Glucose Sensor Over 90 Days in Patients With Diabetes Mellitus. Journal of diabetes science and technology. 2015;9(5):951-6.

99. Lakowicz JR. Principles of Fluorescence Spectroscopy: Springer Science & Business Media, LLC; 2006. 923 p.
100. Toseland CP. Fluorescent labeling and modification of proteins. Journal of chemical biology. 2013;6(3):85-95.
101. Hansen RE, Winther JR. An introduction to methods for analyzing thiols and disulfides: Reactions, reagents, and practical considerations. Analytical biochemistry. 2009;394(2):147-58.
102. Wolfbeis OS. Probes, sensors, and labels: why is real progress slow? Angewandte Chemie. 2013;52(38):9864-5.
103. Sletten EM, Bertozzi CR. Bioorthogonal chemistry: fishing for selectivity in a sea of functionality. Angewandte Chemie. 2009;48(38):6974-98.
104. Sahoo H. Fluorescent labeling techniques in biomolecules: a flashback. RSC Advances. 2012;2(18):7017.
105. Blackman ML, Royzen M, Fox JM. Tetrazine ligation: fast bioconjugation based on inverse-electron-demand Diels-Alder reactivity. Journal of the American Chemical Society. 2008;130(41):13518-9.
106. Ravasco J, Coelho JAS. Predictive Multivariate Models for Bioorthogonal Inverse-Electron Demand Diels-Alder Reactions. Journal of the American Chemical Society. 2020;142(9):4235-41.
107. Saxon E, Bertozzi CR. Cell surface engineering by a modified Staudinger reaction. Science. 2000;287(5460):2007-10.
108. Keppler A, Gendreizig S, Gronemeyer T, Pick H, Vogel H, Johnsson K. A general method for the covalent labeling of fusion proteins with small molecules in vivo. Nature biotechnology. 2003;21(1):86-9.
109. Gautier A, Juillerat A, Heinis C, Corrêa IR, Kindermann M, Beaufils F, et al. An Engineered Protein Tag for Multiprotein Labeling in Living Cells. Chemistry & biology. 2008;15(2):128-36.
110. Fang Q, Kanugula S, Pegg AE. Function of Domains of Human O 6 - Alkylguanine-DNA Alkyltransferase †. 2005;44(46):15396-405.
111. Daniels DS, Mol CD, Arvai AS, Kanugula S, Pegg AE, Tainer JA. Active and alkylated human AGT structures: a novel zinc site, inhibitor and extrahelical base binding. Embo Journal. 2000;19(7):1719-30.
112. Adams SR, Campbell RE, Gross LA, Martin BR, Walkup GK, Yao Y, et al. New Biarsenical Ligands and Tetracysteine Motifs for Protein Labeling in Vitro and in Vivo: Synthesis and Biological Applications. Journal of the American Chemical Society. 2002;124(21):6063-76.
113. Korpela J. AVIDIN, A HIGH-AFFINITY BIOTIN-BINDING PROTEIN, AS A TOOL AND SUBJECT OF BIOLOGICAL-RESEARCH. Medical Biology. 1984;62(1):5-26.
114. Johnson IS, M.T.Z. The molecular probes handbook. 2010;11. edition:1060.
115. Zhang C, Welborn M, Zhu T, Yang NJ, Santos MS, Van Voorhis T, et al. Pi-Clamp-mediated cysteine conjugation. Nature chemistry. 2016;8(2):120-8.
116. Tharp JM, Liu WR. The "pi-Clamp" Offers a New Strategy for Site-Selective Protein Modification. Chembiochem : a European journal of chemical biology. 2016;17(10):883-5.
117. Zhang C, Spokoyny AM, Zou Y, Simon MD, Pentelute BL. Enzymatic "click" ligation: selective cysteine modification in polypeptides enabled by promiscuous glutathione S-transferase. Angewandte Chemie. 2013;52(52):14001-5.
118. EMBL-EBI P, SIB. UniProt Knowledgebase - SwissProt. https://wwwuniprotorg/. 2002-2020.
119. rcsb pdb (protein databank). https://wwwrcsborg/. 2020.
120. Cuneo MJ, Hellinga, H.W. 2HPH - High resolution structure of E. coli glucose/galactose binding protein bound with glucose. rcsb pdb database. 2007;https://www.rcsb.org/structure/2HPH.
121. Borrok MJ, Kiessling, L.L., Forest, K.T. Apo Open Form of Glucose/Galactose Binding Protein. Protein science : a publication of the Protein Society. 2006(16):1032-41.

122. Brunger AT, Strop P, Vrljic M, Chu S, Weninger KR. Three-dimensional molecular modeling with single molecule FRET. 2011;173(3):497-505.
123. Förster T. Zwischenmolekulare Energiewanderung und Fluoreszenz. Annalen der Physik. 1948;437(1-2):55-75.
124. Abrusán G, Marsh JA. Alpha Helices Are More Robust to Mutations than Beta Strands. PLoS computational biology. 2016;12(12):e1005242.
125. Benkert P, Tosatto SC, Schomburg D. QMEAN: A comprehensive scoring function for model quality assessment. Proteins. 2008;71(1):261-77.
126. Ramachandran GN, Ramakrishnan C, Sasisekharan V. Stereochemistry of polypeptide chain configurations. Journal of molecular biology. 1963;7:95-9.

Acknowledgement

I very much enjoyed my PhD at the Institute for Analytical Chemistry at the Hochschule Mannheim and the IPMB Heidelberg to work such an interesting and joint collaboration project of Prof. Werner and Prof. Wölfl.

My sincere thanks go to **Prof. Werner** for being my supervisor and mentor over the past few years and for always giving me the freedom to explore, ideate and try out things around the topic of biosensing. He was encouraging me to explore my joy for innovation from the beginning.

My gratitude also goes to **Prof. Wölfl** who I feel priviledged to call my doctor father and mentor who was always welcoming me in his lab and group meetings and supporting me through my entire PhD journey.

I would also like to thank **Prof. Fricker** from the institute of pharmaceutical technology (Uni HD) and **Prof. Mack** (institute of Microbiology, HS Mannheim) for taking over the role of being members of my TAC committee and taking over the responsibility of being my examiners. A special thank goes to Prof. Mack for providing me the opportunity to work in his lab on all microbiology and protein purification experiments.

More special thanks go to:

Prof. Wiedemann, for always being a great mentor and for supporting me in all questions of cell- and microbiology.

Dr. Xinlai Cheng from the IPMB Heidelberg for the synthesis of XC113 and XC 92, a very crucial part of my PhD work and for the always fruitful discussions about chemistry!

Dr. Rolf Lutz, Sandra Martini and Martina Galvan from my graduate school (HBIGS Heidelberg)

Prof. D'Auria from university of Naples for providing me with the MglB plasmid

Dr. Lehmann from Dyomics GmbH who was kindly providing the environmental sensitive dyes

I would like to thank all my colleagues from the Hochschule Mannheim who are not just colleagues but also became friends:

My lab partner **Mircea** whom I had a lot of fun time with in the lab, as well as **Mario**, our dear friend and colleague who had passed away before he was able to submit his PhD thesis. I cannot put my grief into words and I would like to dedicate this thesis to him. I will never forget the great times we all had together.

The assistants in our lab **Gaby, Silvia, Anne, Kristian**, and of course **Prof. Weber**

My students **Tatjana Roth, Laura Freitag and Patricia Sutter** for being your supervisor throughout your bachelors and for your support in all figures and graphs that you were creating.

My friends & colleagues from MIB: **Carmen, Ben, Ahmed, Rodrigo, Valentino, Andreas & the assistants** for supporting and always welcoming me in your lab.

The complete student classes of 2015 to 2018 who I had the honor to teach inorganic and analytical chemistry at the Hochschule Mannheim

A special thanks for an unforgettable time and great support in the lab at the IPMB Heidelberg:

Biljana, Saskia, Suzan, Fadi, Jannick, Sawsan, Anna, Si Sang, Xinlai, Rodrigo, Ali, Yasi, Anastasia, Mohamed, Paraschiva, Sharouz, Hamed & all azubis & all I forgot to mention

All my HBIGS colleagues, especially Melanie!

And the best come last of course…

My deep gratitude goes to my whole **family (core and extended)** who always pushed me being the first member of the whole family that gets awarded with a PhD and who were also the ones who became so nervous if I would ever finish my thesis. This is for all of you!

My deepest gratitude goes to my **parents, Andrea & Harald** who I look up to, who supported me in every possible way to achieve my goals and live my dreams. Without them I would not stand where I am today.

And the absolute best comes last…

…my love, **Steffen**, thank you for always being there, for supporting me whatever I do, for being there when I had bad days and for always enjoying with me the good ones. The best is yet to come!

Thank you all!